2023

Development of A Hydrometallurgical Process for the Extraction of Cobalt, Manganese, and Nickel from Acid Mine Drainage Treatment Byproduct

Alejandro Agudelo Mira
West Virginia University, aa00109@mix.wvu.edu

DEVELOPMENT OF A HYDROMETALLURGICAL PROCESS FOR THE EXTRACTION OF COBALT, MANGANESE, AND NICKEL FROM ACID MINE DRAINAGE TREATMENT BYPRODUCT.

Alejandro Agudelo Mira

Thesis submitted.

To the Benjamin M. Statler College of Engineering and Mineral Resources

at West Virginia University

in partial fulfillment of the requirements for the degree of

Master of Science in

Mining Engineering

Qingqing Huang, Ph.D., chair

Deniz Talan, Ph.D.

Vladislav Kecojevic, Ph.D.

Hassan Amini, Ph.D.

Department of Mining Engineering

Morgantown, West Virginia

2023

Keywords: Acid Mine Drainage, Critical Minerals, Leaching, Oxidative Precipitation, Solvent Extraction, Stripping, Dissolution.

ABSTRACT

DEVELOPMENT OF A HYDROMETALLURGICAL PROCESS FOR THE EXTRACTION OF COBALT, MANGANESE, AND NICKEL FROM ACID MINE DRAINAGE TREATMENT BYPRODUCT

ALEJANDRO AGUDELO

Critical minerals (CMs) are defined as crucial elements for the country's economy due to the development of new cutting-edge applications and the risk of an eventual disruption in their supply chain. The unique chemical and physical properties of the CMs have made these elements decisive in the growth of industries such as telecommunications, army, medicine, Aerospace, etc. In 2022, the US Geological Survey established a list of 50 CMs, including manganese, cobalt, nickel, aluminum, magnesium, and others. Of the total of CMs, 26 are 100% imported from outside the United States (Venditti, 2022).

Driven by the ever-increasing demand for critical minerals (CMs) and the need to diversify their supply chains, extensive research efforts have been devoted to extracting CMs from various secondary sources, such as fossil fuel (coal ash and refuse), mining tailings, refuse piles, water produced by oil and gas industry, electronic waste (E-waste), and acid mine drainage (AMD), among which acid mine drainage and its treatment byproducts proved to be a viable source. Characterization studies of different AMD and sludge materials indicate the occurrence of CMs containing rare earth elements (REEs), cobalt, manganese, nickel, zinc, aluminum, magnesium, etc. In this context, our research aimed to develop an optimized hydrometallurgical process for extracting multiple individual CM concentrates, including cobalt, manganese, and nickel, from acid mine drainage treatment byproducts.

The feedstock used throughout is an REE solvent extraction raffinate loaded with cobalt, manganese, and nickel, with grades corresponding to 38.3 mg/L, 370.7 mg/L, and 69.4 mg/L, respectively, as well as impurity metals such as 3643.1 mg/L of aluminum, 2161.4 mg/L of magnesium, 224.1 mg/L of calcium, and 159.2 mg/L of iron. A hydrometallurgical process developed at the laboratory scale consists of an initial sodium hydroxide precipitation using 2M NaOH until reaching a pH value equal to 5. The approach targeted the upstream removal of impurities such as aluminum and iron and was established by performing stagewise precipitation from an initial pH of 2 to a final value of 12. The optimum pH values were identified by taking samples at each pH setpoint and analyzing the tradeoff between CM recovery and impurity removal. Afterward, a solution with a higher concentration of CMs and lower impurity content was subjected to a new precipitation process with 2M NaOH until reaching pH 10 to generate a precipitated product rich in CMs. The precipitated solids obtained at the pH range of 5 to 10 were

treated to separate cobalt and nickel from manganese. The procedure carried out in this stage was a nitric acid washing (HNO3), which was performed under controlled conditions of temperature, time, volume, etc. Two products were obtained in this stage: a dissolved solution with an extractable concentration of cobalt and nickel (393 mg/L and 619.9 mg/L, respectively) and a solid product with a manganese purity of 47.9% by weight. To continue separating cobalt and nickel from remaining impurities, such as magnesium, a new stagewise precipitation with sodium sulfide (Na2S) at 1M was performed to determine the separation feasibility of different elements in the solution. At this stage, three separation steps were determined to generate three solid products: the solid precipitated at the pH range of 1-5 with 5.1 wt.% of cobalt and 8 wt.% of nickel, solids precipitated at pH 5-10 with 20.15 wt.% of manganese, and the solid product at pH 10-12 with 27.49 wt.% of magnesium. Other separation approaches were also evaluated in this study to assess the possibility of separating cobalt from nickel, including oxidative precipitation and solvent extraction. As a result of all these combined studies, the highest cobalt and nickel purity of 9.92 wt.% and 14 wt. % were generated, respectively, in addition to the manganese (47.9 wt. %) and magnesium (27.49 wt. %) products obtained from the developed process.

ACKNOWLEDGMENTS

I would like to take this section to express my deep appreciation for the following individuals and organizations for their invaluable support, guidance, and encouragement through my academic journey at West Virginia University pursuing my master's degree.

First, I want to express my heartfelt appreciation to my advisor Dr. Qingqing Huang. The trust placed in me to be part of your research group has been a fundamental factor in my personal and professional growth. Her proficiency, dedication, patience, guidance, and constant support were indispensable to pursuing my academic and research interests. The insightful feedback and constructive criticism made me find new perspectives on my research path, discover new alternatives to solve all the issues faced, and get more expertise in my research field. I am deeply thankful for the valuable skills and knowledge I have obtained during the past two years under her mentoring. I would also like to extend my gratitude to my professor Oscar Jaime Restrepo Baena who has been my mentor since my undergraduate in Colombia; his passion for teaching and engagement with his students to reach their academic and professional goals were crucial in the decision to pursue my master's degree. His support through the process, patience, expertise, and shared experiences was essential from the beginning to the end of my graduate journey.

Besides, I would like to extend my gratitude to the mining department for the support and guidance during my journey at WVU; to the Department Chair Dr. Vladislav Kecojevic for his advice and patience during this process, and a deep appreciation to Genette Chapman and Karen Centofanti for their help in every matter related to my academic and research path. To Dr. Deniz Talan for all the support when I arrived at the university and the valuable knowledge and skills gained from her. A special mention to the research team members Zeynep Cicek, Görkem Geçimli, and Victor Oluwaseun Famobuwa for all the discussions and brainstorming sessions that help us to get new ideas and ways to improve our research. In addition, I thank all the guys in the office for the friendship given during this time and all the associated professors that were involved in my academic performance. In addition, I extend my gratitude to the US Department of the Interior for their support and financial backing of this research endeavor.

Also, I want to thank my friends Rosbel Jimenez, Juan Valencia, and Victor Valencia with whom I started this journey; we have been together during this time, sharing new experiences and supporting ourselves in our personal, professional, and academic life. I also want to mention all the friends made in Morgantown, Daniel, Carlos, Eduardo, Francisco, Sofia, Irene, Joao, etc. whom I shared valuable experiences with during this shared time.

Last but not least, I deeply express my enormous appreciation to my parents Rodrigo Agudelo and Dennise Mira, my brother Juan David Agudelo, and my whole family in Colombia. All their effort, dedication, and support during my life made it possible to reach the goals I have proposed myself giving me the motivation and strength to wake up every day and do my best to fulfill all my responsibilities and duties at my workplace and school. Thank you very much for everything; this achievement is not just mine but yours.

TABLE OF CONTENTS

LIST OF FIGURES

LIST OF TABLES

1. INTRODUCTION

Modern society is experiencing transitions involving new technological developments to supply the merging needs of environmental regulations, economic aspects, and social development. These transitions demand the use of materials whose chemical and physical characteristics are needed to manufacture goods and services that are able to fulfill the new demands imposed by the current society (M.Hayes & McCullough, 2018). These materials are denominated as critical minerals (CMs) by the U.S Geological Survey (USGS) because they are crucial elements for the economy and national security of the United States and are vulnerable to facing an eventual disruption in the supply chain. The first list of CMs was released in 2018 with a total of 35 elements and was updated in 2022, including 15 new elements to have a total of 50 elements by 2022.The classification of CMs is a dynamic list based on mineral resource potential, consumption, production, disposal, and interaction of the elements with the environment, which allows us to understand the importance and necessity of the elements in the global supply chain, establish the dependency across the different economic sectors, and forecast and evaluate the potential disruptions in the supply chain (Burton, 2022).

Some elements in the critical minerals list, such as cobalt, manganese, nickel, zinc, aluminum, lithium, and magnesium, are highly used in many applications in the different economic sectors and are crucial in energy transitions. Superalloys, stainless steel, galvanized steel, rechargeable batteries, EV batteries, catalytic converters, coatings, etc., are some industrial applications where CMs are utilized to manufacture different components needed to guarantee the sustainability and development of the economy in the country. In 2022, 26 of the 50 critical minerals established by the United States government were 100% imported from other countries such as China, the Democratic Republic of Congo, Australia, Indonesia, South Africa, and Canada. (Venditti, 2022), with China being the main producer of REEs (62.9%) and lithium (54.5%), the Democratic Republic of Congo of cobalt (71.4%), Indonesia of nickel (29.6%), and South Africa of manganese (>30%) (Burton, 2022) (Barbanell, 2023). Different factors, including limited end-of-life recycling and increasing global production, have elevated the threat of a disruption in the supply chain of the CMs, generating a stronger dependency on foreign sources, but at the same time, creating the necessity to increase the local production by developing new extraction technologies and looking for alternative sources to produce these elements (Nassar & Fortier, 2021).

Manganese, cobalt, and nickel are critical minerals playing an essential role in the electrification initiatives and electric storage, aiming at the global transition to a low-carbon economy and scientific developments. Cobalt has a high risk in its production supply due to the primary extraction as a by-product in the processing of copper and nickel from different ore types (Savinova, et al., 2023). On the other side, nickel has been experiencing increasing demand in the last few years. However, at the same time, the mining and export policies in Indonesia and the Philippines and COVID-19 have created uncertainty in the global supply chain of nickel (Xingxing Wang, 2022). Besides, for Mn, two concerns were identified as the main risks in the supply chain: one of them is the incomplete recovery of the element from the end-of-life products and slag, and

the other one is the increased geography concentration of the locations where the ore is produced (Xin Sun, 2020). Researchers have been seeking new alternatives to mitigate the impact of these risks by improving the extraction methods and identifying new alternatives, such as acid mine drainage (AMD), which has demonstrated its potential as a feasible resource.

1.1 Objectives of the research.

The research aimed at the recovery of critical minerals (CMs), including manganese, cobalt, and nickel, from the solvent extraction raffinate solution generated during the extraction of rear earth elements (REEs) present in acid mine drainage (AMD) treatment sludge. By using hydrometallurgical techniques on a laboratory scale, a laboratory process was developed to produce enriched manganese, cobalt, and nickel concentrates and achieve the targeted selective recovery. In addition, analytical techniques like Inductively coupled plasma mass spectrometry (ICP-MS) and characterization methods such as Scanning electron microscope and energy dispersive x-ray spectrometry(SEM-EDX), X-ray powder diffraction (XRD) were utilized to assist with such a process development. The motivation for developing this research is the increasing demand for critical minerals in the global market and the need to reduce the supply dependency on foreign sources. Moreover, by treating AMD sources generated by the mining industry, which represent an environmental hazard, AMDs could be turned into a valuable resource for the extraction of critical minerals. The specific objectives targeted for this research include:

1. Identify the residual stream in the REE solvent extraction process to select the most promising feedstock for CM extraction by understanding their respective behaviors during the extraction.

2. Develop a laboratory-scale hydrometallurgical process to extract manganese, cobalt, and nickel from AMD sources optimally.

3. Add a new body of knowledge to the ongoing research to improve the extraction processes of critical minerals over time.

2. LITERATURE REVIEW

2.1 Critical minerals

The global modern economy demands the use of different elements with specific characteristics for the development of high technologies and industrial applications (Karol Zglinicki, 2021). Literature definitions classified these elements as critical, pivotal, or strategic minerals because they are deemed vital commodities for the economy and national security of the countries; added to this, these elements are only available in specific zones of the earth and eventually could suffer disruptions in the supply chain (Hofstra, et al., 2021). The most popular term to refer to these elements is Critical minerals (CMs), which, according to the US Geological Survey (USGS), are a total of 50 elements.

The first list of critical minerals was released by the US Geological Survey in 2018 and was determined by using economic, geological, and mining databases to evaluate the criticality of each element in order to reduce the vulnerability of the supply chain of these elements (Burton, 2022). The first list was formed by 35 elements including aluminum, antimony, arsenic, barite, beryllium, bismuth, cesium, chromium, cobalt, fluorspar, gallium, germanium, graphite, hafnium, helium, indium, lithium, magnesium, manganese, niobium, platinum group metals, potash, the rare earth elements group, rhenium, rubidium, scandium, strontium, tantalum, tellurium, tin, titanium, tungsten, uranium, vanadium, and zirconium (Petty, 2018).

In 2022, the critical mineral list was updated based on the new economic trends and the participation of stakeholders involved in the production and trading of these elements. Overall, the new list was determined by implementing the following methodology: 1) a quantitative assessment of the supply risk when adequate data was accessible, 2) a partially quantitative evaluation of whether the supply chain had a sole vulnerability, and 3) a qualitative assessment applied in cases where alternative evaluations were not feasible (Applegate, 2022). The new list included 15 new elements such as dysprosium, erbium, europium, gadolinium, holmium, iridium, lanthanum, lutetium, neodymium, nickel, samarium, terbium, thulium, ytterbium, and yttrium. According to Steven M. Fortier, the USGS National Minerals Information Center director, the critical minerals are not static, and they will have new additions or removals of elements in the list over time (Burton, 2022).

The distribution of CMs in the periodic table is shown in the figure below. The elements in red boxes represent the total number of CMs, the elements in yellow boxes are the CMs coextracted in the process, and the green ones are the elements targeted by this research.

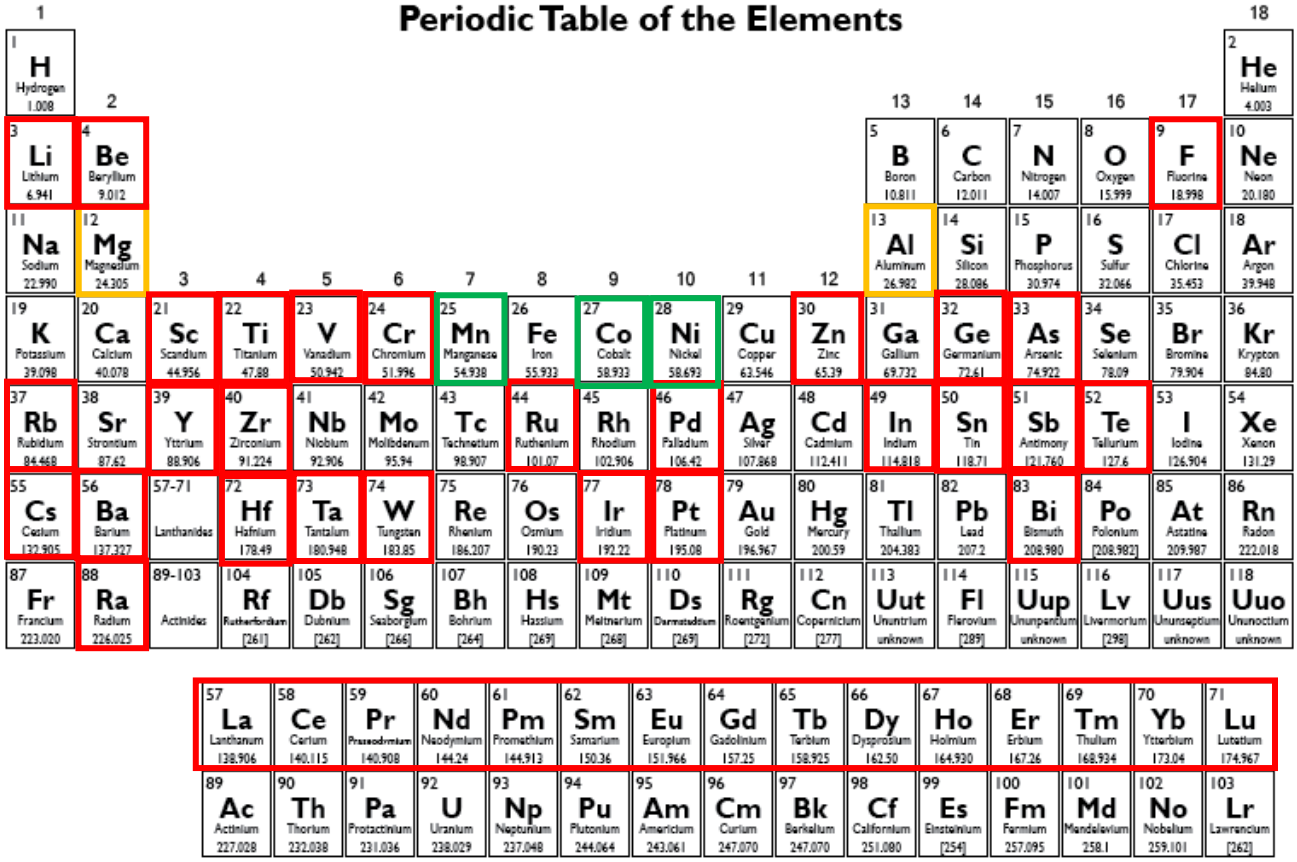

Figure 1. Distribution of critical minerals in the periodic table.

The critical elements aimed for this research are distributed in the periodic table in three different groups. The main elements cobalt (Co), manganese (Mn), and nickel (Ni) are located in block d between groups III and VII and are known as transition metals due to their similarities in atomic structures and chemical and physical characteristics. The term transition metals was established by the transition among three orbitals beginning from the inner electron layer with 8 electrons to a layer of 18 electrons and an external layer with 32 electrons. Related to their properties, transition metals are known to exhibit multiple positive oxidation states, low ionization energies, good electrical and thermal conduction, good catalysts, high boiling, and melting points, have a metallic appearance, and form alloys (Helmenstine, 2022).

Aluminum (Al) is located in group XIII, in the middle of the transition metals and the metalloids; this group is classified as a post-transition metal. This definition was established in 1940, but it has not been accepted so far because of the ambiguity of the term; the most accepted definition for those elements was the one proposed by Huheey and Keiter, which deemed these elements as metals close to the no-metals border (Zheng, et al., 2022). In general, post-transition elements

differ from transition metals in their physical and chemical characteristics due to the fact that they tend to form covalent bonds, which make them softer, brittle, and with lower boiling and melting points.

On the other hand, magnesium (Mg) is an alkaline earth metal occupying place number 12 in the periodic table; the alkaline earth metals are located in group III before the transition metals. This group is formed by other 5 elements, including beryllium (Be), calcium (Ca), strontium (Sr), barium (Ba), and radium (Ra). Alkaline earth metals share many of the properties of the metals, but they have low electron affinity and low electronegativity; as alkali metals are located at the left in group II, their properties depend on how easily the elements lose electrons. Some common characteristics of the alkaline earth elements are relatively low density, low melting and boiling points, good malleability and ductility, the formation of divalent cations, and high reactivity. As a result, these elements are not found free in the environment (Helmenstine, 2023).

2.2 Critical minerals applications

Depending on their physical and chemical properties, the critical minerals listed above are used in numerous industrial applications, such as superalloys, stainless steel, galvanized steel, rechargeable and electric vehicle batteries, catalytic converters, coatings, and more. These applications rely on CMs for the production of diverse components essential to ensure economic sustainability and advancement. The following table shows a summary of the main uses of the 50 critical minerals in 2022.

Table 1: Critical minerals list and uses (Venditti, 2022).

Mineral	Uses	Net imports
Aluminum	Power lines, construction, electronics	13%
Antimony	Lead-acid batteries, flame retardants	81%
Arsenic	Semi-conductors, lumber preservatives, pesticides	100%
Barite	Hydrocarbon production	75%
Beryllium	Alloying agent in aerospace, defense industries	11%
Bismuth	Medical, atomic research	94%
Cerium	Catalytic converters, ceramics, glass, metallurgy	100%
Cesium	Research, development	100%
Cobalt	Rechargeable batteries, superalloys	76%
Chromium	Stainless steel	75%
Dysprosium	Data storage devices, lasers	100%
Erbium	Fiber optics, optical amplifiers, lasers	100%
Europium	Phosphors, nuclear control rods	100%
Fluorspar	Manufacture of aluminum, cement, steel, gasoline	100%

Gadolinium	Medical imaging, steelmaking	100%
Gallium	Integrated circuits, LEDs	100%
Germanium	Fiber optics, night vision applications	50%
Graphite	Lubricants, batteries	100%
Holmium	Permanent magnets, nuclear control rods	100%
Hafnium	Nuclear control rods, alloys	Net exporter
Indium	Liquid crystal display screens	100%
Iridium	Coating of anodes for electrochemical processes	No data available
Lanthanum	Catalysts, ceramics, glass, polishing compounds	100%
Lutetium	Scintillators for medical imaging, cancer therapies	100%
Lithium	Rechargeable batteries	50%
Manganese	Steelmaking, batteries	100%
Magnesium	Alloys, electronics	50%
Neodymium	Rubber catalysts, medical, industrial lasers	100%
Niobium	Steel, superalloys	100%
Nickel	Stainless steel, rechargeable batteries	50%
Palladium	Catalytic converters	40%
Platinum	Catalytic converters	79%
Praseodymium	Permanent magnets, batteries, aerospace alloys	100%
Rubidium	Research, development in electronics	100%
Rhodium	Catalytic converters, electrical components	No data available
Ruthenium	Electrical contacts, chip resistors in computers	No data available
Samarium	Cancer treatment, absorber in nuclear reactors	100%
Scandium	Alloys, ceramics, fuel cells	100%
Tantalum	Electronic components, superalloys	100%
Terbium	Permanent magnets, fiber optics, lasers	100%
Tellurium	Solar cells, thermoelectric devices	95%
Thulium	Metal alloys, lasers	100%
Titanium	White pigment, metal alloys	88%
Tin	Coatings, alloys for steel	75%
Tungsten	Wear-resistant metals	50%
Vanadium	Alloying agent for iron and steel	96%
Ytterbium	Catalysts, scintillometers, lasers, metallurgy	100%
Yttrium	Ceramic, catalysts, lasers, metallurgy, phosphors	100%
Zinc	Metallurgy to produce galvanized steel	83%
Zirconium	High-temperature ceramics production	25%

As of 2022, a noteworthy aspect is that 26 out of the 50 critical minerals designated by the U.S. government are entirely imported from other nations, including China, the Democratic Republic of Congo, Australia, Indonesia, South Africa, and Canada, among others (Venditti, 2022). China assumes a primary role as the leading producer of rare earth elements (62.9%) and lithium (54.5%).

In comparison, the Democratic Republic of Congo is a dominant source of cobalt (71.4%), Indonesia supplies a significant portion of nickel (29.6%), and South Africa contributes substantially to manganese production (Burton, 2022) (Barbanell, 2023).

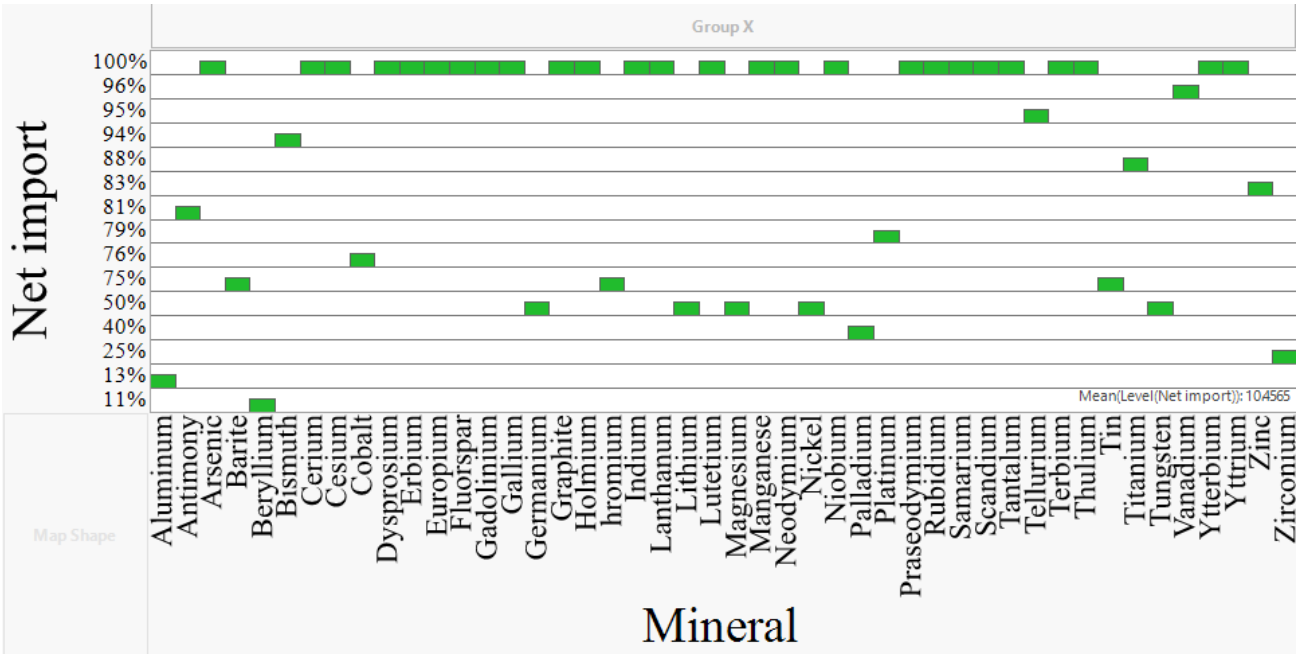

Figure 2. Net importation of critical minerals in the United States.

2.2.1 Cobalt

Cobalt is a transition metal located at the d block of the periodic table with an atomic number equivalent to 27 and Co as its atomic symbol; cobalt is located between iron and nickel which makes the elements share similar chemical and physical properties (Pourret & Faucon, 2016). Cobalt is a ferromagnetic hard metal with a bluish-white-silver color, which mainly occurs as arsenides, sulfides, and oxides. The only stable isotope of cobalt is ^{59}Co. However, 26 more radioactive isotopes are known, of which only ^{57}Co and ^{60}Co have importance in the industry. The element occurs in three valence states (0, +2, +3) where Co (0) is metallic cobalt, Co (II) is cobaltous, and Co (III) is cobaltic, with Co (II) being more stable than Co (III) (Kim & Gibb, 2006).

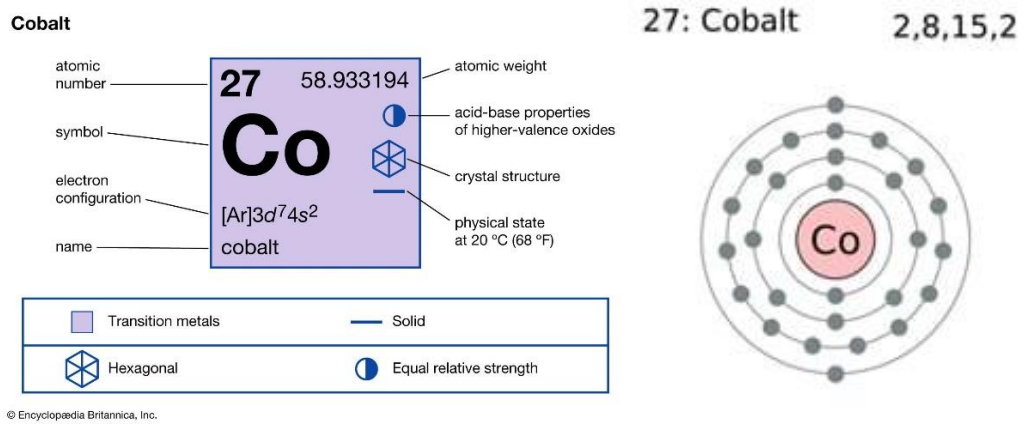

Figure 3. Atomic structure and periodic table nomenclature of cobalt (Brandt, 2023).

Below, a comprehensive table of cobalt properties is shown with the purpose of presenting a concise overview of the main chemical and physical characteristics of cobalt.

Table 2: Overview of the main properties of cobalt.

Properties			
Chemical		**Physical**	
Ionic radius	0.630 Å	**Density**	8.80 g/cm^3
Electronegativity	1.88	**Boiling point**	2927 °C
CAS number	7440-48-4	**Melting point**	1493 °C
Electrode potential	-0.280 V	**Atomic mass**	58.93 g/mol
X-ray absorption edge	1.608 Å		
Electrochemical equivalent	1.1 g/A/h		

Cobalt is highly used in different commercial, military, and industrial applications, which are strategic for the development of the United States. In the global context, the main use of cobalt is the generation of rechargeable battery electrodes. It is also used in superalloys to make parts of gas turbine engines, in the petroleum and chemical industries to make catalysts, drying agents in paints, varnished and inks. Added to this, cobalt is utilized in diamond tools, airbags for automobiles, coats for porcelain enamels, magnetic recording media, pigments and dyes, corrosion-resistant alloys, and steel fabrication (Shedd, 2023).

Cobalt is low in abundance on the Earth's crust, with an average content of 8 ppm, but it is possible to find it in soils with concentrations of 70 ppm. The global production of cobalt is mainly commanded by magmatic Ni-Cu deposits, nickel laterite deposits, and stratiform sediment-hosted copper deposits. According to the United Nations Framework Classification (UNFC), there are 151 cobalt deposits with a total of 1,342,649 tons of estimated resources. This resource classification is distributed in 114,638 tons of commercial extraction in current mining projects,

370,409 tons for potential projects, 111,107 tons of historic estimates compared with current reports, and 746,495 tons of non-compliant historical estimates (Horn, et al., 2021).

According to the London Metal Exchange (LME), which is the organization in charge of the trading of worldwide industrial metals, cobalt stocks in the United States have a downward tendency, with the stocks in June of 2023 3% less than the ones in May 2022. The price of cobalt had a similar behavior since 2022, with a spot price of 40 USD per pound approximately in June of 2022 and 15 USD per pound in June of 2023, equivalent to a reduction of 57% in the spot price of cobalt (Ewing, 2023). The following graph shows the tendency of the metal in terms of price and stocks in the United States for the last two years.

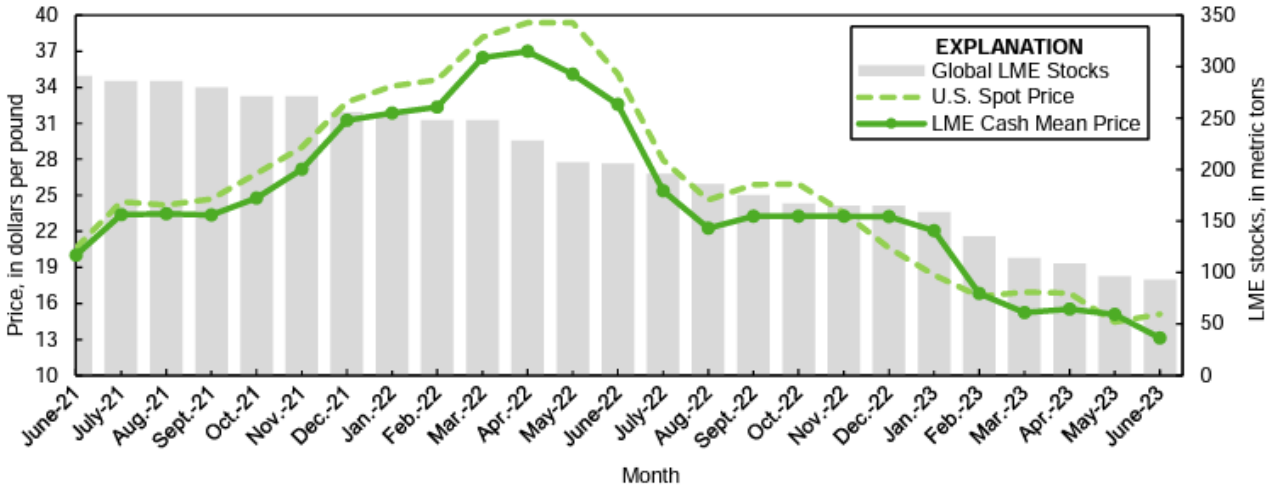

Figure 4. LME stocks and spot prices of cobalt in the United States for the last two years.

2.2.2 Manganese

Manganese is known as a transition metal in the d block of the periodic table, filling three orbitals; Manganese occupied position number 25 (atomic number) of the VIII group in the periodic table, and its nomenclature corresponds to Mn. Manganese is a hard gray-white metal comparable to iron in terms of physical and chemical properties, but it is harder and more brittle than iron. Mn is commonly found in +2 and +3 valences; however, it has access to higher valence levels equal to +4 and +7, which are found in complex manganese minerals. The only stable atom of manganese is ^{55}Mn. However, it has eleven more radioactive isotopes from ^{49}Mn to ^{58}Mn (Kuleshov, 2017). Table 3 provides a summary of the main properties of manganese, including chemical as well as physical properties of the element.

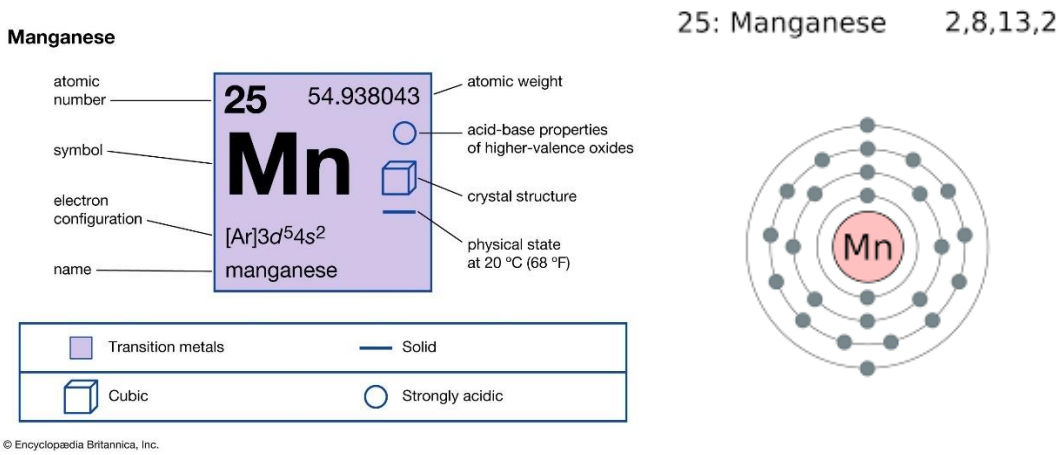

Figure 5. Atomic structure and periodic table nomenclature of manganese (Brandt, 2023).

Table 3: Overview of the main properties of manganese.

Properties			
Chemical		**Physical**	
Ionic radius	0.460 Å	**Density**	7.26 g/cm3
Electronegativity	1.55	**Boiling point**	2095 °C
CAS number	7439-96-5	**Melting point**	1244 °C
Electrode potential	-1.05 V	**Atomic mass**	54.94
X-ray absorption edge	1.896 Å		
Electrochemical equivalent	0.684 g/A/h		

Due to their deoxidizing, fixing, and alloying properties, manganese plays an important role in the manufacture of iron and steel; steelmaking activities in the country have a demand of around 90% of this metal due to the grades of ferromanganese and silicomanganese are an essential key in the industries such as machinery, transportation, and construction. Manganese is also highly used in aluminum alloys, dry cell batteries, plant fertilizers, colorants for bricks, and animal feed (Kim, 2023).

Manganese is considered the 10th most abundant element in the Earth's crust, with an average content of 1,060 ppm, and it is commonly found as oxides and hydroxides. In addition, manganese has occurrences in streams and groundwater, with values equal to 7 µg/L and <0.1 mg/L, respectively (Kuleshov, 2017). According to the United States Geological Survey (USGS), the reserves of manganese for 2022 correspond to 1,500,000 metric tons, with South Africa being the main source of the element, which accounts for 30% of the total reserves (USGS, 2022).

In June of 2023, the main import sources of the United States were South Africa exporting manganese ores with a grade between 20% and 47%, and Gabon, with an ore grade over 47%. In the last semester of 2023, the total imports were 74% less than the imports in 2022 in the same period. In June 2023, the US spot price of manganese ore with a grade of 36%-38% was $3.82 per metric ton and $4.75 for ore with a grade equal to 44%, representing a decrease of 26% and 35%, respectively, compared to the prices of May 2022 (Kim, 2023). The figures below illustrate the behavior of the prices and imports of manganese in the past few years.

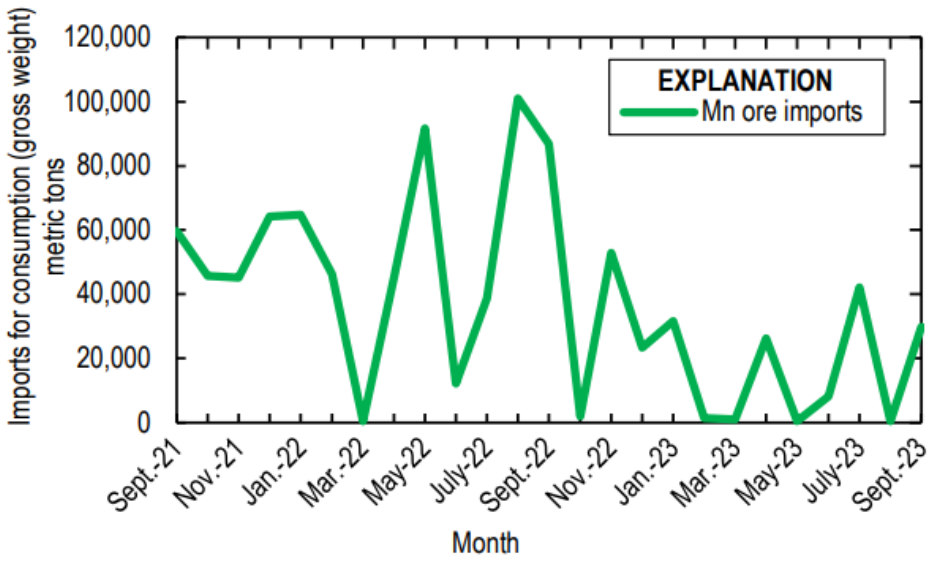

Figure 6. US imports of manganese in metric tons from 2021 to 2023 (Kim, 2023).

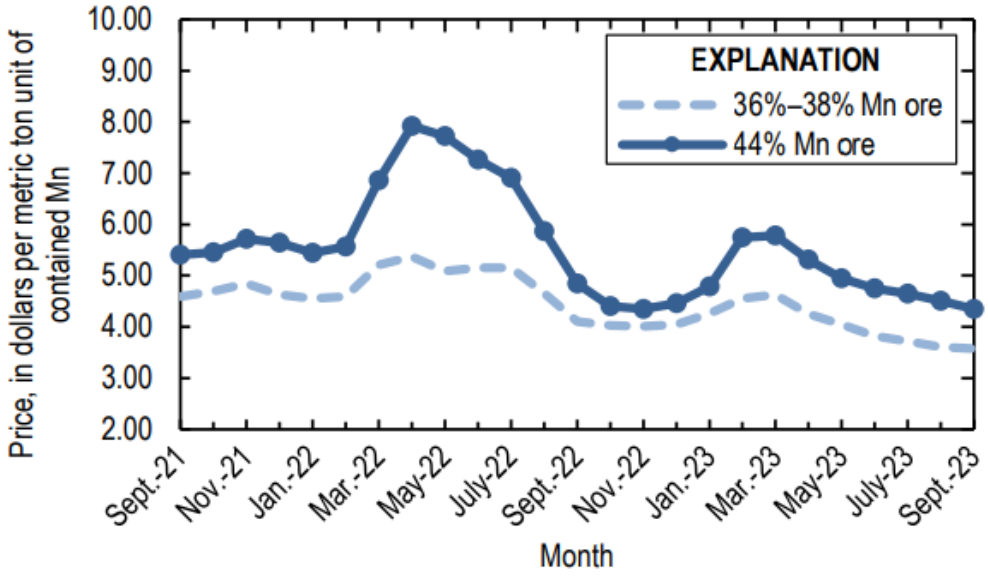

Figure 7. Price tendency of manganese ore in the United States (Kim, 2023).

2.2.3 Nickel

Like manganese and cobalt, nickel is a metal member of the transition series located in the d block of the periodic table with an atomic number equal to 28, and its symbol is Ni. In its metallic state nickel occurs as a silvery-white metal, but most of its compounds are green or blue. Under environmental conditions, the prevalent oxidation state in nickel is +2, but it also occurs with valences of -1, +1, +3, and +4. Related to the nickel isotopes, this element presents 5 stable isotopes corresponding to ^{58}Ni, ^{60}Ni, ^{61}Ni, ^{62}Ni, and ^{64}Ni, nineteen unstable isotopes of nickel are also known (M. Cempel, 2006). Table 4 provides a dual perspective of the chemical and physical properties of nickel, giving a concise overview of its main attributes.

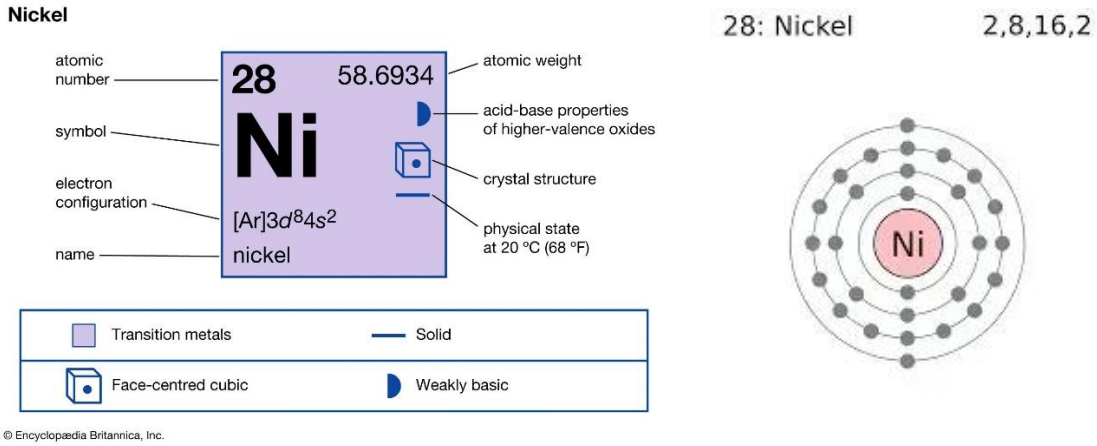

Figure 8. Atomic structure and periodic table nomenclature of nickel (Brandt, 2023).

Table 4: Overview of the main properties of nickel.

Properties			
Chemical		**Physical**	
Ionic radius	0.69 Å	**Density**	8.89 g/cm3
Electronegativity	1.91	**Boiling point**	2913 °C
CAS number	7440-02-0	**Melting point**	1453 °C
Electrode potential	-0.257 V	**Atomic mass**	58.71 g/mol
X-ray absorption edge	12.27 Å		
Electrochemical equivalent	1.095 g/A/h		

The primary use of nickel is the manufacture of refined metal. About 65% of nickel consumed in the Western world is utilized in the fabrication of austenitic steel, another 12% is used in the fabrication of superalloys, and the remaining 23% is distributed in rechargeable batteries, coinage, plating, foundry products, and catalysts. The aerospace industry is the main consumer of nickel superalloys in the fabrication of turbine blades and critical parts of jet engines; power generation

stations also use the superalloys to fabricate essential parts and covers for combustion turbines (McRae, 2023).

The content of nickel in the earth's crust can vary from 0.2 ppm to 750 ppm. It is considered the 24th most abundant element in the crust. The record indicates that there are currently 627 Ni deposits around the world with ground resources and reserves divided as follows: 148 resources and 86 reserves in laterite deposits, 248 resources and 93 reserves in magmatic sulfide deposits, 33 resources and 14 reserves in hydrothermal deposits, and 3 and 2 containing Ni-tailings. This data yields 350.2 million tons of nickel resources (Mudd & Jowitt, 2022).

2.3 CM sources and geological aspects.

2.3.1 Cobalt

The main extraction of cobalt is a by-product (98%) during the recovery processes of copper and nickel. The main source of cobalt production in the world is the Central African Copperbelt, the sole sedimentary rock-hosted stratiform zone known with substantial cobalt deposits. The primary extraction of cobalt output comes from nickel laterites and magmatic nickel-copper deposits. Besides, cobalt is present in several lead-zinc and copper regions with carbonate as the host material. It is also found with minor frequency in deposits in back-arc and rift environments linked to mafic-ultramafic rocks hosted by massive sulfide and siliciclastic sedimentary rocks. Metasedimentary cobalt-copper-gold deposits also present variable composition levels of cobalt (Hitzman, et al., 2017). Copper, nickel, and cobalt are elements that are commonly coextracted during the mining processes, whether in surface or underground mining.

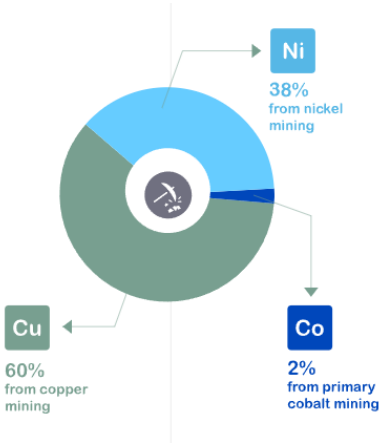

Figure 9. Cobalt extraction distribution as a byproduct of copper and nickel mining and from primary extraction (Cobalt-Institute, 2023).

The most common occurrence of nickel ores is sulfides and laterites. Laterites are known as weathered rocks with a high content of metals, specifically in limonite or serpentine forms. Both varieties of ore are found adjacent to each other, often with serpentine existing below the limonite due to the differential leaching by natural weathering processes. Nevertheless, the boundary between both of them is not clear under specific weathering conditions. Serpentines are composed of hydrated magnesium silicates with nickel and ferrous elements in their contents. On the other hand, limonite is formed by iron oxides containing mainly nickel and cobalt, and a minor content of magnesium (Hawkins, 1998). The economic concentrations of cobalt are found mainly in five geological settings, which are described below.

2.3.1.1 Sediment hosted

This type of deposit is the primary work for the extraction of copper with cobalt as a byproduct, which is the main source of cobalt extraction, with 50% of cobalt mined from these deposits. The ore minerals are commonly found in organic-rich pyritic shales and sandstone. Mineralized sediments are always found in the top of oxidized terrestrial clastic layers (Cobalt-Institute, 2023).

2.3.1.2 Hydrothermal and Volcanogenic

The key process in this type of deposit is the precipitation of hydrothermal fluids going through the host powered by volcanic activity. The ores are found in veins, faults, planes, fissures, cracks, or when the host rock is metasomatically replaced. Depending on the geological conditions and the makeup of the host rock, these deposits can vary with a vast variety of minerals and deposit types (Cobalt-Institute, 2023).

2.3.1.3 Laterite

Laterites are surficial deposits enriched in cobalt and nickel by the extreme weathering of ultramafic rocks in tropical and subtropical climates. The cobalt in sulfides and silicates within the host rock is deposited in the weathered layers as hydroxides and oxides close to the surface and silicate in the deeper layers. Deposits are typically 20 meters thick, and the main product is nickel with cobalt as a byproduct. The most common minerals are limonite, goethite, asbolite, erythrite, and garnierite (Cobalt-Institute, 2023).

2.3.1.4 Manganese nodules and cobalt-rich crust

Concretions rich in manganese, cobalt, and nickel can form around debris and organic material on the deep ocean bottom, commonly at a depth of 4 to 5.5 kilometers. The proximity to the mid-ocean ridge leads to the possibility of a volcanic source as minerals enrichment. These deposits are found as tightly packed sheets spread in hundreds of square kilometers with a cobalt content between 1% and 2.5 %. Nevertheless, due to deep-sea ecosystems being vulnerable, the extraction of the elements poses environmental challenges and regulatory considerations (Cobalt-Institute, 2023).

2.3.1.5 Magmatic sulfide

An immiscible liquid sulfide phase is generated by a mafic to ultramafic melt, which is enriched with nickel, cobalt, and platinum-group elements (PGE). As a result, these elements are scavenged from the leftover magma and deposited in distinct sulfide-rich strata. The most economically important magmatic deposits include Russia's Merensky Reef, Norilsk, Western Australia, Sudbury, Canada, Kambanda, and South Africa (Cobalt-Institute, 2023).

2.3.1.6 Alternative Cobalt Sources

Recovery of cobalt from the intermediate mining process has received a lot of attention. For instance, it is known that copper smelting companies perform reprocessing of slag heaps with significant amounts of cobalt. Although no significant commercial facilities have been established to treat these slags alone, they frequently make up a small proportion of the feed to different refining processes. Many chemical producers and cobalt refiners throughout the world treat intermediates such as hydrates and white alloys to create their standard products (Hawkins, 1998).

Cobalt, which, after being used in a specific application enters the cobalt cycle is considered a secondary source, including superalloys, catalysts, magnets, and cement carbides as the main categories in cobalt recycling. According to estimates, 22% of the cobalt used in superalloys ends up as scrap, generating large amounts of waste material that is sent to downgraded applications and refineries. Hard-metal waste recycling is crucial because it accounts for nearly a third of the industry’s cobalt usage. An additional 8% is utilized in lower-grade applications such as steel manufacturing. Chemical techniques and zinc processing are utilized to create cobalt powder to re-use in hard-metal production. The main source of scrap is the catalyst industry. Co-Mn catalyst is used to make polymers and textiles, and the waste material is calcined and added back into the process of making new catalysts. However, they required reprocessing to remove contaminants

like organic materials. Catalysts used in the hydrodesulfurization of crude oil have been studied for reprocessing but have not been deemed cost-effective (Hawkins, 1998).

2.3.2 Manganese

Manganese deposition increased as the changing tectonic behavior led to the stabilization of the cratons and oxygenation of the hydrosphere and atmosphere. During this time, the terrigenous input was responsible for the formation of large to super-large manganese deposits. Manganese deposition became dominant in the Mesozoic era and reached its pick in the Cenozoic; the main causes of this were the development of enormous shallow-water deposits and the concurrent deposits of manganese crusts and nodules in deep-sea areas (Roy, 1988). Redox-controlled processes are involved in the deposition and concentration of manganese in modern and prior geological and geochemical settings. Instead of shallow water domains, modern Mn deposition occurs predominately in deep-sea areas. In addition, hydrothermal activity has a significant contribution to manganese deposition in the ocean systems. Manganese is also widely dispersed from vent sites in near and far field dispersion; these distributions are governed by the flow rate of the solution, the residence time, and the temperature in the seawater (Roy, 1992). Pyrolusite, which mainly consists of MnO_2, is the most prevalent mineral; however, numerous other minerals, including rhodonite ($MnSiO_3$), pink rhodochrosite ($MnCO_3$), alabandite (MnS), and black manganite (MnO (OH)), are common minerals that contain manganese. The principal source of the rapidly rising demand for manganese as an alloying component is primarily driven by the aluminum market, followed by the steel industry. Primary and secondary battery industries are the main consumer of electrolyte manganese dioxide (EMD) and chemical manganese dioxide (CMD) (Zhang & Cheng, 2007).

Manganese oxide ore is the most significant Mn-bearing resource widely spread around the world and makes up about 70% of all manganese ore deposits (You, et al., 2015). By far, South Africa is the world's top producer of manganese, with approximately 19 million metric tons produced in 2021, followed by Gabon with 7 million metric tons. The worldwide production of manganese is equivalent to 49.5 million metric tons by 2021 (Garside, 2023).

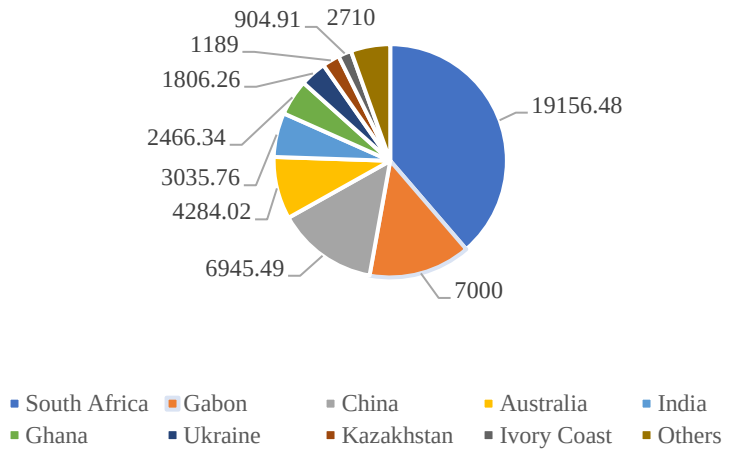

Figure 10. Manganese worldwide production in 2021 (values are in 1000 metric tons) (Garside, 2023).

2.3.2.1 Alternative manganese sources

Due to growing steel output, the annual demand for manganese has dramatically expanded in recent years. Manganese recovery from low-grade resources has received a lot of interest recently given that high-grade sources are gradually depleted (You, et al., 2015). Sources including the treatment of spent batteries and alkaline batteries are considered non-hazardous materials suitable for the recovery of elements such as manganese and nickel. This sort of battery cannot be recharged, which results in massive quantities of waste batteries that need to be recycled. Recycled batteries have an overall positive impact on the environment such as the reduced impact from global warming, ecotoxicity, abiotic depletion, and the avoidance of extracting manganese and zinc from primary sources (Sadeghi, et al., 2020). One method to recycle these batteries is the Batenus process which performs the extraction of manganese dioxide through metallurgical processes. This method was claimed to produce raw materials with remarkably high purity and low emissions. Manganese carbonate is the main product of this process, and it is used in the new batteries (Zhang & Cheng, 2007).

Another secondary source to extract manganese is the Mn-bearing sludges and slags. According to Zhang and Cheng (2007), a solution with a considerably low grade of manganese, cobalt, nickel, copper, zinc, chromium, etc., was used to extract manganese by applying different metallurgy techniques. Besides, scrap dry cells, electrolytic zinc anodic slime, and water treatment plant sludge were used as secondary sources to extract manganese (Zhang & Cheng, 2007).

2.3.3 Nickel

Almost all of the earth's terrestrial nickel resources are found in nickel laterites, which are the product of extensive weathering processes in ultramafic rocks on the earth's surface in humid climatic conditions. The breakdown of the primary minerals and the release of the chemical constituents into groundwater, leaching activities, residual concentrations of insoluble elements, and formation of the new mineralogy are all parts of the lateralization process. The combined effect of all these processes results in the formation of the laterite profile, a vertical succession of horizons with varying chemistry and mineralogy, where the differential mobility determines the overall structure in the weathering zone. The interaction of climatic and geological agents, including topography, tectonic, lithology, and drainage, have resulted in the variation of the laterite structures depending on the location. Nickel is enriched to ore grade by being incorporated into the structure by new minerals or the alteration of byproducts of primary minerals. Nickel laterites are formed by the lateritisation of ultramafic rocks or Mg-rich, with initial concentrations of nickel ranging from 0.2-0.4%. Such rocks are typically harzburgites, dunites, and peridotites found in ophiolite complexes, as well as, layered mafic-ultramafic rocks on cratonic platforms, and komatiites (Elias, 2002).

Magmatic sulfide deposits rich in nickel and copper with platinum group elements (PGE) are denominated as Ni-Cu ± PGE sulfide deposits, which are geographically and genetically connected to mafic and ultramafic rocks. Sulfide deposits take place when the mafic and ultramafic magmas become sulfide-saturated and segregate immiscible sulfide liquid after interaction with continental crustal rocks. Nickel-Cu sulfide deposits can appear as single or multiple lenses in mafic/ultramafic rocks forming economic deposits to be mined. Deposits typically range grades from 0.5 to 3% Ni and 0.2 to 2% Cu. Individual deposits range in size from thousands to millions of metric tons of bulk ore. Two massive Ni-Cu districts dominate the Ni sulfide resource and production. One of them is the Sudbury district located in Ontario, Canada with 19.8 Mt of nickel; and the Noril'sk-Talnakh district in Siberia, Russia with 23.1 Mt (Klaus J. Schulz, 2014).

With estimated land resources of approximately 300 million tons, nickel is broadly dispersed throughout the world. Of these, 60% correspond to laterite deposits and 40% to sulfide deposits. The figure shown below represents the distribution of the element at different world locations.

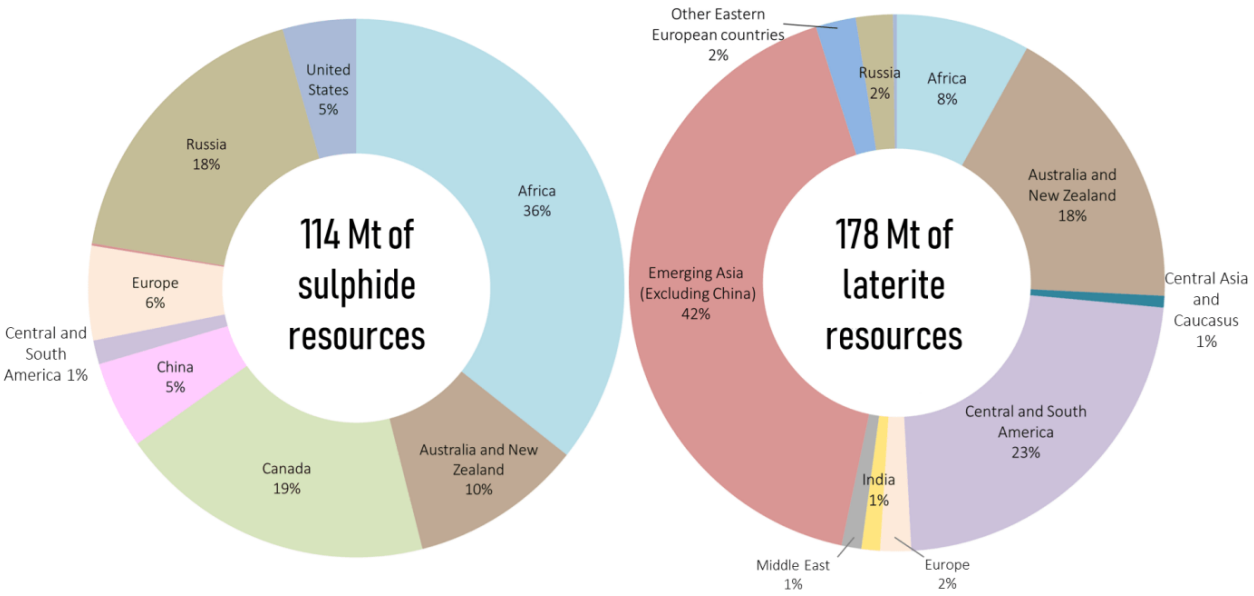

Figure 11. The distribution of world nickel resources by deposit type (Emmanuel, et al., 2021).

2.3.3.1 Alternative Nickel Sources

With the increase in mining costs, the depletion of resources, and the concerns about environmental protection, researchers are on the lookout for secondary sources of nickel to supply the needs demanded by the international markets. Alternative or secondary sources of nickel are driven by spent batteries, spent nickel catalysts, and alloy waste. As the literature reports, it demands 6.2 MJ of energy to generate one kilogram of nickel from secondary sources, which is significantly less than the 150 MJ needed to produce the same kilogram from primary sources. Additionally, the recovery of nickel from secondary sources lessens the need to extract it from natural resources and solves challenges related to the disposal of industrial waste (Junwei Han, 2022).

2.4 Feedstock background

2.4.1 Acid Mine Drainage (AMD)

Mine drainage is defined as water that has been polluted from contact with mining operations and is normally associated with coal and hard rock mining. Acid mine drainage is caused when the water flows through sulfur-bearing materials, generating acid solutions with low pH (2 to 4) and

high metal concentrations. The runoff formed from ore or coal mining has developed their activities, exposing the rocks, which contain sulfur-bearing materials such as pyrite (FeS_2) and iron sulfide (Fe II) that, once in contact with air and water, react chemically precipitating metals such as iron, copper, lead, mercury, zinc, among others. The main reaction in the process is oxidation, which results in the production of sulfuric acid. The equation shown below explains the reaction generated by the contact of these components. These elemental sediments at the bottom of the streams form solids that usually have a dark red, orange, or yellow color. The rate and degree of the formation of acid mine drainage can be increased by the action of acidophiles, in particular Acid thiobacillus ferroxidase, which are bacteria that increase the oxidation of pyrite by ten times (R.W.Gaikwad, 2007).

$$FeS_2 + 7/2O_2 + H_2O \rightarrow Fe^{2+} + 2{SO_4}^{2-} + 2H^+ \quad [1]$$

The reactivity of mineral sulfides varies depending on their physical and chemical characteristics; some metal sulfides tend to form low-solubility minerals, which prevent the dissolution by encapsulating and protecting them from further oxidation. Crystalline structure is an important factor in the reactivity of the sulfides for two main factors: the stability of the crystalline structure provides more resistance to oxidation; the second factor is the availability of the surface area because it increases the reactivity, which means that small particles are more likely to react than the large ones. For this last reason, the mining tailings produce more drainage acids because the material has been subjected to comminution treatments (crushing and grinding), producing smaller particles with more surface area available. Other factors propitious for the generating rate of AMD are the pH and temperature (R.W.Gaikwad, 2007).

As discussed in the previous paragraphs, AMD incorporates heavy metals and sulfuric acid into the environment by the flow of the solution in currents and the land. A certain quantity of AMD can be assimilated naturally by the environment through biological activity, dilution, and neutralization. However, the natural treatment of AMD is limited by specific conditions, such as the drainage pattern, temperature, topography, dilution rate, biological activity, and the presence of acid-consuming minerals such as calcite ($CaCO_3$) and carbonates of iron, magnesium, and aluminum. Related to the consequences generated by AMD, the increase of the acidity in the water with lower pH degrades the quality of the waterway so that the aquatic life cannot tolerate these harsh conditions and gradually create inhabitable ecosystems. The effects of AMD also spread to the surrounding communities, affecting the well-being of fauna, flora, and humans due to the lack of drinking water and poisoning of fields and animals.

Acid mine drainage (AMD) is one of the main causes of polluted water in the United States, generating serious problems for the streams and the land surrounding the operations due to the filtration through the ground. According to OSM in Pennsylvania, there are 4688 miles of waterways polluted by acid drainage; governmental organizations have estimated that the cost of reclaiming these streams is between $3.8 and $5 billion (Joule Bergerson, 2004). Currently, many efforts and controls are being applied to the mines to minimize the impact of AMD, preventing the

spread in surrounding zones and streams; added to these efforts are new strategies developed by mining companies to extract value-added products from AMD

2.5 Acid mine drainage treatment

Although sometimes it can be viewed as a resource of rich metals, the elemental composition of AMD varies on geological and environmental factors, making their handling a challenge in most cases. Researchers have concentrated their efforts on describing the usual metal composition of AMD. The principal metals found in most cases include Al, Fe, Mg, Cu, Ca, Mn, and Zn. Treatment methods can be passive, which include compost wetlands, anaerobic wetlands, aerobic wetlands, and vertical flow rector, or active methods, such as sulphidization, sedimentation, precipitation, nanofiltration, and reverse osmosis. Passive treatment often concentrates on minimizing danger to the environment and human health. Active methods instead enable the commercialization of AMD since they can produce high-quality metals (Venegas, et al., 2023). Active treatment involves the addition of alkaline chemical reagents on a continual basis to neutralize the acidity. The most common reagents used for the neutralization include lime (CaO), sodium hydroxide (NaOH), anhydrous ammonia (NH3), and slaked lime (Ca $(OH)_2$). Active treatment demands continuing operating and maintenance costs, as well as frequent energy supply. Additionally, it entails the possibility of accidental releases of chemicals like NH_3 or NaOH that could endanger human health or the environment (Skousen, et al., 2017).

The use of an aqueous biphasic system made up of ionic liquids and Na_2SO_4 has shown the viability of extracting heavy metals from real AMD. Other approaches have also suggested alternatives such as the combination of NaOH precipitation and ion absorption in the AMD to achieve selective precipitation of different heavy metals present in the solutions. The precipitation of metals in the AMD is given for a series of intricate oxidation, hydrolysis, and precipitation events that lead to the recovery of metals at different levels of pH. Protons and metal cations with the capacity to hydrolyze protons are two factors that enhance acidity. The reaction that represents one of the most common components in AMD (Fe) is represented in the following expression.

$$Fe^{3+} + 3H_2O \leftrightarrow Fe(OH)_3(s) + 3H^+ \quad [2]$$

On the other hand, alkalinity has the capacity to neutralize the acidic conditions in the solutions. Alkalinity can be achieved by the addition of alkaline materials such as limestone ($CaCO_3$) where the reaction can be expressed as follows.

$$CaCO_3 + H^+ \leftrightarrow Ca^{2+} + HCO_3^- \quad [3]$$

The kind and quantity of sulfides and related neutralizing minerals, including dolomite and calcite, regulate the acidity level, metal composition, and compositions of AMD. Carbonate and sulfide minerals are indicators of the potential production of acid in AMD sources. When there is a lack of carbonates, the silica base elements can provide good levels of alkalinity; however, under high values and sufficient amounts of carbonate and silica elements present in the solutions, some metal ions can persist. For instance, Fe^{2+} and Mn^{2+} are more soluble than metals with high oxidation states, such as Fe^{3+} and Mn^{4+} (Skousen, et al., 2017).

Membrane technologies find applications in various active treatments for AMD and wastewater effluents. Since they allow the volume reduction of the streams treated, favoring the selective recovery of metal ions from AMD decreasing the concentration of metals in the acid streams, allowing the reusing of acid, and reducing the production of sludge, membrane technology has become popular in recent years. The most promising membrane technologies include forward osmosis (OF), diffusion dialysis (DD), electrodialysis (ED), nanofiltration (NF), membrane distillation (MD), and reverse osmosis (RO) (López, et al., 2021).

2.6 CM recovery by metallurgical processes

How to recover nickel and cobalt from laterites has been extensively investigated; however, the only two commercial methods used are high-pressure acid leaching and reduction roasting combined with ammonia leaching. These methods are used depending on the type of material to be treated. For instance, serpentines possess a high content of magnesium, which represents a high acid consumption, making the high-pressure leaching no suitable for the recovery of these elements. The reduction roasting has a low cobalt recovery rate of approximately 50% as opposed to about 90% in high-pressure acid leaching. For this reason, both procedures yield a concentration of mixed elements requiring further refinement. The refinement and separation of these elements are given by the application of hydrometallurgical procedures, which generally involve the leaching of the bulk concentrates, commonly compounded by nickel, cobalt, copper, and zinc. Then, cobalt and nickel are precipitated and followed by selective dissolution to separate nickel from cobalt (Hawkins, 1998).

The potential applicability of several technologies in the extraction of manganese from solutions, particularly the ones generated during leaching, involves techniques such as solvent extraction, ion exchange, hydroxide precipitation, sulfide precipitation, and oxidative precipitation. The selectivity, reagent, costs, efficiency, and quality of these procedures depend on the initial chemistry of the solution and the experimental parameters. Oxidative precipitation uses inexpensive oxidants like SO_2/O_2 mixture, which is extremely selective for manganese. On the other hand, in solvent extraction, a crucial factor is the base used to neutralize the solution. Depending on the amount of impurities, such as magnesium, carbonate precipitation, hydroxide precipitation, or ion exchange can have different behaviors in the selectivity of manganese or other metals (Wensheng Zhang, 2007).

Other methodologies implemented for extracting valuable methods via pyro- and hydrometallurgical techniques have been subjected to numerous investigations. Methods documented for the extraction of cobalt from secondary sources include crushing, acid leaching, precipitation, and solvent extraction. However, some of these methods come with their own issues such as slow kinetics, low purity, high processing cost, etc. For the extraction of metals from the leach liquor and effluents, solvent extraction (SX) has been widely used. There have been reports of metals, such as cobalt, nickel, and manganese, by leaching-SX utilizing different methods and extractants, such as PC-88A, Cyanex 272, and D2EHPA (Basudev, et al., 2007).

The extraction of manganese, cobalt, and nickel is mostly dominated by the hydrometallurgical processes, which, with the proper experimental settings, can generate good extraction of these elements for primary and secondary sources. As mentioned above, these processes involve leaching, precipitation, and solvent extraction, which will be described in the sections below.

2.6.1 Leaching

In mining, leaching is a chemical process used to remove valuable elements from the rock ore using acid or water. Leaching also takes place in nature when water comes into contact with the rocks or soil, making the elements of the rock dissolve and migrate to the liquid phase, leaving a lower content of the elements in the material subjected to the leaching process. There are two basic ways of leaching: simple leaching at room temperature and atmospheric pressure, and the other consists of accelerating the process by increasing both factors: pressure and temperature. The technique selected is determined by the quality of the feed material and the elements that can be leached by the process. Also, the effectiveness of the process depends on factors such as the leaching agent, particle size, agitation, and solid-liquid ratio (Faraji, et al., 2020).

Depending on the nature of the ore, different acids or solvents with varied concentrations can be used in the process . Sulfates can be leached using water or sulfuric acid, although oxides must be leached by using sulfuric acid or sodium carbonate solvent. Sodium hydroxide is utilized for oxides, while ammonium hydroxide is suitable for carbonates, sulfides, and native ores. Precious metals are dissolved by cyanide solutions while certain chlorides are dissolved by sodium chloride (Charles, et al., 2023). For instance, the common chemical reaction obtained during the dissolution of metals (M) using hydrochloric acid is shown by the following stoichiometry reaction.

$$M_s + 2HCl_{(aq)} \gg\gg MCl_{2\ (aq)} + H_{2(g)}$$

The following images illustrate the kinetics of the leaching process when the solid particles are in contact with the liquid solvent or acid.

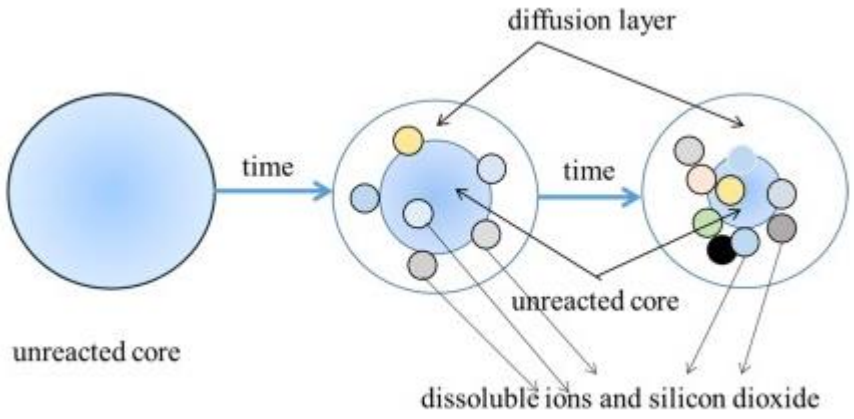

Figure 12. leaching kinetics in solid degradation (Zhou, et al., 2020).

2.6.2 Solvent extraction

Solvent extraction (SX) consists of a solute or solutes distributed between two immiscible liquids or phases, generally, one aqueous phase and one organic phase. The SX method includes moving the target metal from the aqueous phase to the organic phase under specific experimental settings, which creates a liquid-liquid equilibrium between the phases that can be represented by the following expression (Alvial-Hein, et al., 2021)

$$[M]_{aq} \leftrightarrow [M]_{org} \quad [4]$$

The standard conditions of solvent extraction involve temperature, pressure, and composition. In the organic phase, the extractant is typically dissolved in diluent and occasionally includes a modifier and a synergistic agent. The modifier is used to improve the physical features of the system and the synergistic agent aims to enhance and improve the extraction performance of the extractant. The solutes, contaminating substances, and acids make up the aqueous phase, also known as the feed phase (Kislik, 2011). There are two specific parameters that govern the efficiency of the process: the percentage extraction (E%) and the separation factor (β). These factors can be calculated by the following expressions (Alvial-Hein, et al., 2021).

$$\%E = \frac{100D}{D + \frac{V_{aq}}{V_{org}}} \quad [5]$$

$$\beta = \frac{D_A}{D_B} \quad [6]$$

Where D represents the distribution ratio of both phases, and it is represented by the ratio between the distribution of the metals ($D = [M]_{org} / [M]_{aq}$), and V is the volume of aqueous and organic phases. When β is higher than 1000 between two metals, it is assumed that the process had an affective separation; if the value of β is between 100 and 1000, it indicates a potential separation and β values less than 100 suggest insufficient separation between the metals. The figure below represents the interaction among the components in the organic and aqueous phases.

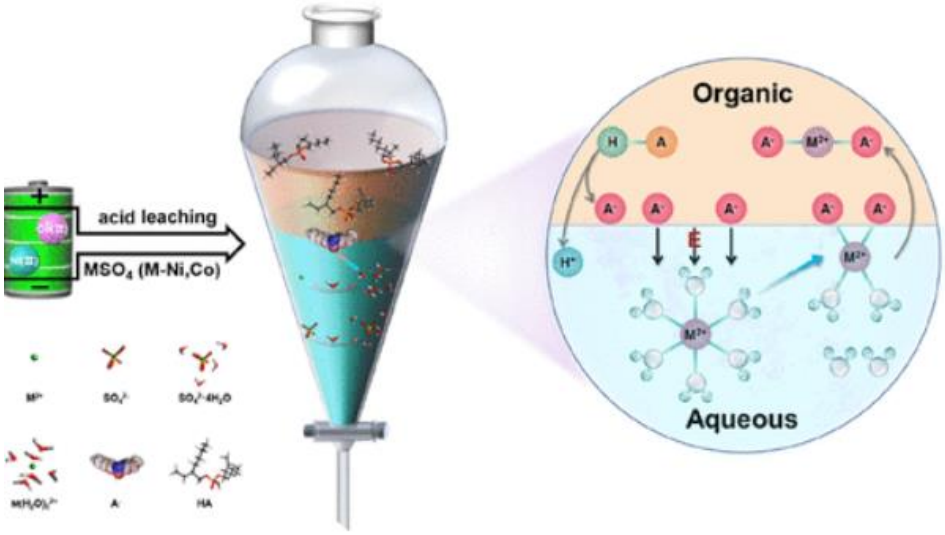

Figure 13. Solvent extraction mechanism in metal extraction (Yuan, et al., 2022).

After the liquid-liquid phases reach equilibrium, stripping and scrubbing processes are carried out to recover the target elements using the acid solution to strip/scrub the organic phase (Kuleshov, 2017).

$$M_s + 2HCl_{(aq)} \gg\gg MCl_{2\ (aq)} + 2H \quad [7]$$

2.6.3 Precipitation

Applying chemical compounds to a solution charged with variable contaminants changes the physical conditions of the dissolved solids, which are then removed from the media by sedimentation, known as chemical precipitation. Depending on the insolubility of the chemical compounds present in the solution, the separation rate of the procedure varies (Hualpa-Cutipa, et al., 2022). The principles that govern the precipitation process are the insolubility of the components, the reactant used to enhance the state change of the dissolved solids, and the amount of each component. The process is controlled by the change of the pH in the solution, which allows for performing bulk or selective precipitation. According to the varied solubilities of the dissolved metals, some researchers have explored the precipitation pH of different elements through simulations or lab-scale experiments. Previous studies demonstrated that iron (Fe) started to precipitate as hematite around pH 2, aluminum (Al) begins the precipitation as diaspora before reaching levels pH of 4.5, copper (Cu) between 5 and 6, and zinc (Zn) and nickel (Ni) at pH values of 8 to 9 (Venegas, et al., 2023)

The sulfide precipitation method provides benefits in terms of metal precipitation, including quick reaction rate, low yield, high stability of the residue, and the capacity to feed the precipitate sulfide into melting systems that researchers have favored in recent years. Lower solubility product values show that dissolving solids becomes more challenging. According to the transformation theory, sulfide products with high solubility can transform into small solubility products. When metal ions interact with hydrogen sulfide to release H^+ ions, insoluble sulfides are precipitated because of the interaction. The metal ion concentration for a given element determines the H^+ concentration at which the precipitation process begins and ends; every metal ion possesses a distinct pH range that leads to minimal solubility of sulfides and optimal sulfide deposition (Xingfei Zhang, 2023).

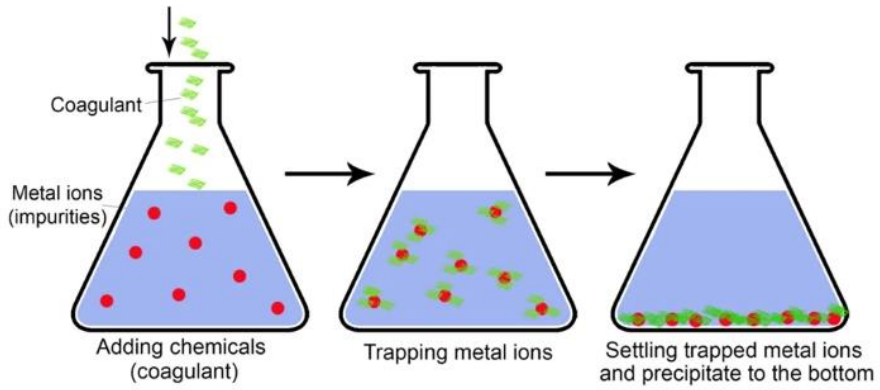

Figure 14. Scheme of the metal precipitation process (Qasem, et al., 2021).

3. FEEDSTOCK CHARACTERIZATION AND PROCESS OVERVIEW

3.1 Initial feedstock

The original feedstock used for the extraction of critical minerals is a coal-based acid mine treatment sludge, which was selected by performing a characterization analysis in 20 different AMD-related samples generated by coal mines located in the Central and North Appalachian regions. Of all the samples procured, 13 were raw water, and the other seven corresponded to sludge materials. The samples collected from each location were analyzed by Inductively Coupled Plasma Mass Spectrometry (ICP-MS) analysis in the WVU's National Research Center for Coal and Energy (NRCCE) Laboratory. After an extensive characterization study of all samples for Rare Earth Elements (REEs) and Critical Minerals, the promising sample chosen as the feedstock for the research was the sample identified with the code CA-M01, which is due to confidential and identity protection agreements between the research team and the mining company. The elemental composition of the feedstock provided by the ICP-MS analysis is shown in the following table.

Table 5. ICP-MS characterization (in ppm on a dry-mass basis) of the feedstock samples identified as CA-M01

Sample	CA-M01
Al	26,335.70
Co	226.01
Mg	11,125.15
Mn	5,540.67
U	1.85
Ca	3,840.73
Fe	10,001.41
Ni	298.24
Si	18,167.45
Zn	628.36
Th	1.03
TREE	356.78

Once the feedstock was selected, the material was subjected to a series of experiments to separate the impurity elements, such as aluminum, iron, magnesium, etc., from the REE and critical minerals. The process carried out for the extraction of the REE involves an initial leaching using sulphuric acid (H_2SO_4) to dissolve the REE and generate a pregnant solution (PLS) rich in these elements. Then, the PLS was subjected to hydrogen peroxide oxidization followed by NaOH precipitation to precipitate most of the impurities, such as iron and aluminum. The solution remaining after the precipitation was used as the feedstock to perform solvent extraction at an O: A ratio of 1 with Di(2-ethylhexyl) phosphoric acid (DEHPA) diluted in kerosene. The loaded

organic solution with REEs and other elements was subjected to two stripping phases using hydrochloric acid (HCl). Finally, oxalic acid precipitation was carried out to generate REE oxalates, followed by roasting to eventually produce REE oxides. The washing procedure with distilled water was then performed on the final oxide product to obtain a mixed REO product with a purity of 80 wt.%. The flowsheet of the developed hydrometallurgical process is given below.

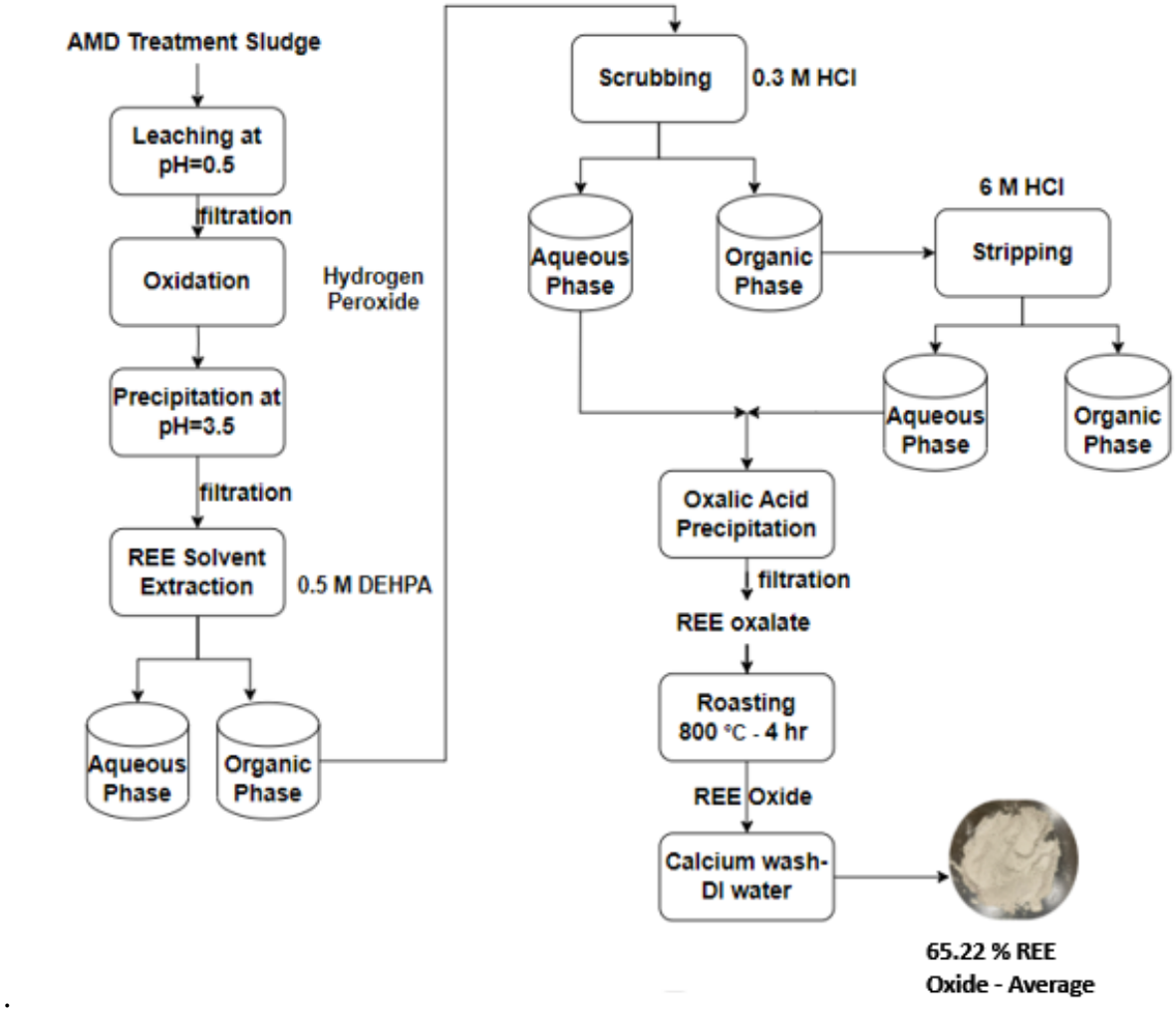

Figure 15. Experimental flowchart developed for REO production from the AMD treatment sludge (Cicek, et al., 2023).

3.2 CM extraction from SX raffinate solution

As mentioned in previous sections, a hydrometallurgical process was developed to extract REEs from acid mine drainage (AMD) treatment sludge. In addition to the extraction of rare earths, the partitioning of other critical minerals (CMs), including cobalt (Co), manganese (Mn), nickel (Ni), and zinc (Zn) throughout the REE recovery process was also monitored. Nickel and zinc were not considered critical minerals following the 2018 Federal Register List of Critical Minerals. However, they are deemed critical based on the 2022 Final List of Critical Minerals (USGS, 2022). Therefore, they are added to the list of CMs for a recovery potential. The distribution of these select CMs at each unit process was systematically evaluated following the post-oxidization & solvent extraction process developed by Cicek et al. (Cicek, et al., 2023).

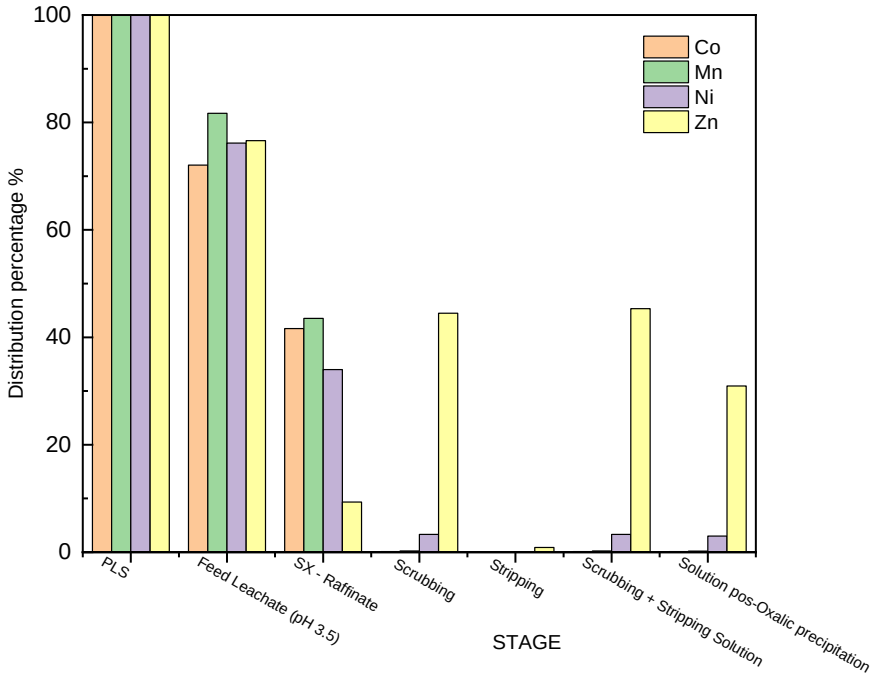

Figure 16. Distribution of Co, Mn, Ni, and Zn throughout the REE extraction process following the previously developed post-oxidation SX methodology.

It can be seen from Figure 16 that most of the Mn, Co, and Ni stayed in the raffinate after REE SX. In contrast, most Zn was co-extracted with REEs and eventually reported to the solution post oxalate precipitation. Data presented in Table 6 further show that the concentration of Mn, Co, and Ni in the raffinate solution was around 370.69, 38.34, and 69.41 mg/L, respectively. The contents of these select CMs are noticeably higher than the rest of the aqueous solution streams. Therefore, the rare earth solvent extraction raffinate (Figure 17) was selected as a feedstock for the continuous extraction of Mn, Co, and Ni for added value.

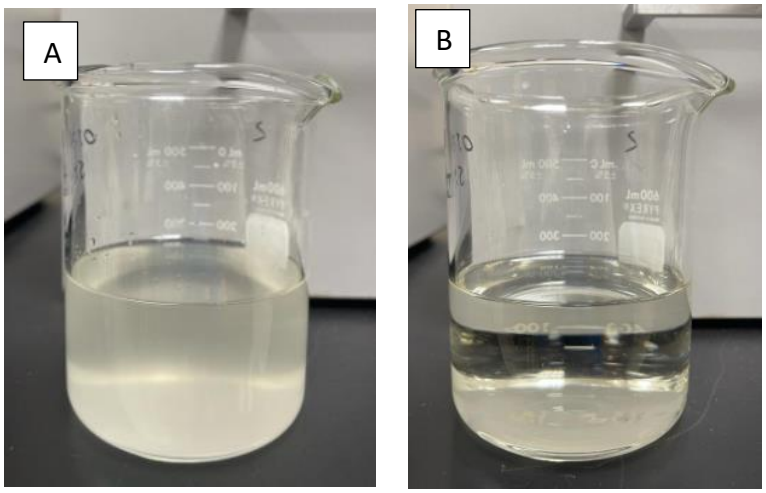

Figure 17. Rare earth SX raffinate solution before filtration (A) and after filtration (B).

Table 6. Distribution of REEs, CMs, and impurities at each stage of the post-oxidation REE extraction process.

Element Concentration, mg/L							
Element	**PLS**	**Feed Leachate (pH 3.5)**	**SX - Raffinate**	**Scrubbing**	**Stripping**	**Scrubbing + Stripping Solution**	**Solution post-Oxalic precipitation**
TREEs	108.14	86.09	2.27	15.60	32.64	21.85	1.26
Al	7,723.88	5,586.75	3,463.10	12.77	60.92	28.30	23.58
Ca	781.83	660.59	224.14	193.74	3.28	123.15	70.89
Co	66.35	47.80	38.34	0.14	0.00	0.05	0.24
Fe	2,974.40	715.96	159.17	0.18	254.29	238.62	276.19
Li	13.96	4.73	3.89	0.17	2.04	0.87	8.51
Mg	4,055.68	3,313.28	2,161.38	15.92	0.16	9.83	7.79
Mn	830.50	632.44	370.69	36.90	0.18	42.22	31.25
Ni	120.17	95.58	69.41	0.20	0.01	0.09	5.12
Si	2,562.65	302.28	151.78	1.50	0.53	0.46	3.38
Zn	281.71	215.85	34.36	115.08	8.24	57.56	52.48
Sc	1.00	0.79	0.00			0.00	0.00
Y	33.23	26.80	0.01			6.85	0.55
La	8.99	6.78	0.78			1.81	0.13
Ce	23.74	17.92	0.96			4.75	0.28
Pr	3.03	2.33	0.10			0.66	0.01
Nd	13.39	10.44	0.37			3.07	0.02
Sm	3.56	2.85	0.02			0.77	0.00
Eu	0.96	0.75	0.00			0.21	0.00
Gd	5.51	4.26	0.02			1.20	0.01
Tb	0.86	0.72	0.00			0.20	0.00
Dy	5.56	4.29	0.00			1.18	0.02
Ho	1.07	0.90	0.00			0.24	0.01
Er	2.85	2.52	0.00			0.61	0.02
Tm	0.37	0.31	0.00			0.06	0.01
Yb	2.21	1.83	0.00			0.23	0.03
Lu	0.31	0.27	0.00			0.02	0.00
Th	0.09	0.09	0.00			0.00	0.00

U	0.45	0.44	0.00	0.01	0.01

4. EXPERIMENTAL METHODOLOGY

In order to perform a selective extraction of manganese, cobalt, and nickel from the aqueous solution produced during the REE solvent extraction process, a series of experiments were developed under controlled conditions to obtain the highest purity of the elements aimed by this research. The experimental procedures involved in the study include hydrometallurgical processes covering stagewise precipitation with sodium hydroxide (NaOH) and sodium sulfide (Na_2S), solid dissolution with nitric acid (HNO_3) and hydrochloric acid (HCl), oxidative precipitation with ozone (O_3), and solvent extraction with Cyanex 272 diluted in Kerosene. Additionally, to the main processes mentioned above, supplemental experimental procedures such as filtration and centrifugation were performed to separate the different streams generated to enrich the solutions or solids and obtain high-grade critical minerals. Characterization analyses were also carried out to study the products, including ICP-MS, XRD, and SEM-EDS analyses.

4.1 Feedstock

As mentioned in previous sections, the feedstock selected for this research was the raffinate solution generated in the oxidative solvent extraction process developed by Cicek et al. (2023) to extract REEs from the AMD treatment sludge. The feedstock was chosen after characterizing all the unit process streams generated during REE extraction to identify the one with a high amount of critical minerals such as cobalt, nickel, and manganese. The concentration values determined for these elements correspond to 38.34 ppm of Co, 370 ppm of Mn, and 69.41 ppm of Ni. The detailed elemental composition of the feed solution is shown in the table below.

Table 7. Elemental composition of the REE SX raffinate following the post-oxidization and solvent extraction methodology.

Element	TREEs	Al	Ca	Co	Fe	Li	Mg	Mn	Ni	Si	Zn
Concentration mg/L	0.7	3,463.1	224.1	38.3	159.2	3.9	2,161.4	370.7	69.4	151.8	34.4

4.2 Materials

Each process developed in this research involved different equipment and chemicals needed to fulfill the goal of each stage. The equipment used during the performance of the experiments was taken from the particle-size laboratory located in Room 169 of the Mineral Research Building (MRB). Chemicals and materials were purchased from authorized sellers through the website platform, i.e., the WVU marketplace. Fisher Scientific, LabChem, and Sigma Aldrich were some of the vendors supplying analytical reagents to perform different tests, including 98 wt.% sulfuric acid (H_2SO_4), sodium hydroxide pellets (NaOH), hydrolyzed sodium sulfide (Na_2S), kerosene, and

nitric acid (HNO_3). Moreover, free lab scale testing amounts of Cyanex 272 were provided by Solvay U.S.A. The NaOH pellets were used in different concentrations to perform various precipitation tests to separate CMs from the impurities and adjust the pH of the solutions. Similarly, hydrolyzed Na_2S was also used in the precipitation of CMs and other elements. Nitric acid was applied in solid dissolution to remove Co, Ni, and other elements from Mn and obtain a high-purity Mn product. Finally, Cyanex 272 and kerosene were employed in the solvent extraction process to separate Co and Ni as separated products.

The pH of the solutions was measured using the Mettler Toledo Seven Compact pH meter with two types of probes: to measure pH in organic solutions, the pH sensor InLab Science Pro-ISM was used, while to measure aqueous solutions, the probe used was the pH sensor InLab Expert DIN. Various types of mixers were used to agitate the solutions, a four-paddle jar tester from Phipps & Bird's INC was used in NaOH precipitation to perform several tests at the same time. A magnetic stirrer plate was utilized to mix and heat solutions during nitric acid dissolution, and the Caframo light-torque overhead mixer was employed to mix the organic solutions used in the general SX process. During the solid precipitation processes, the variable-speed horizontal centrifuge with four tube spots was used to centrifugate the samples and sediment the solid; in addition, the solids were removed from the liquid by utilizing laboratory vacuum filtration with a funnel and filter paper with 0.45-µm pore size made of mixed cellulose ester membranes. The oxidative precipitation was carried out using the CAMECO Ozone Machine Dual Mode to charge the solution with O_3 during oxidation, and water circulation pump BYT-7A014A DC 12V was utilized to recirculate the solution into the beaker.

To avoid contamination, all laboratory glassware, including cylinders, beakers, funnels, stirrers, flasks, and tubes, among others, were carefully washed with soap detergent and rinsed with DI water to ensure no contaminants in the samples. Additionally, before the experiment, all the supplies were cleaned with acetone. The furnace located at MRB 157 was used to dry samples, and the samples were properly covered to avoid any external contamination.

4.3 CM production test methodology

4.3.1 Stagewise precipitation

In order to remove the main impurity from the raffinate solution, i.e., aluminum (Al), stagewise precipitation was run utilizing sodium hydroxide. Furthermore, aluminum, and other elements such as iron (Fe) and phosphorus (P) were also removed during this stage. On the other hand, this procedure targeted the precipitation of manganese, cobalt, and nickel from the raffinate solution. The stagewise precipitation procedure was divided into two pH regions to achieve the goals mentioned above. The first pH value reached was 5, where most of the impurities were precipitated, and the second value was 10, where most of the critical minerals' precipitation could be achieved. During the first stage of the process, the main reaction that occurred by adding NaOH to the solution was aluminum precipitation. Based on the research work conducted by Zhang et al. (2020), aluminum hydroxide precipitates at pH values around 4.5 (Zhang & Honaker, 2020).

Moreover, a secondary main reaction of iron also takes place in this pH range. According to Sun et al. (2019), at the pH range from 2 to 3, the predominant Fe^{+2} species turned into Fe^{3+} ions and ferric hydroxide sediments (Sun, et al., 2019). The stoichiometric reactions of aluminum and iron occurred by the addition of NaOH are provided below:

$$Al^{3+}{}_{(aq)} + 3OH^{-}{}_{(aq)} \rightarrow Al\,(OH)_{3(s)} \quad [7]$$

$$Fe^{3+}{}_{aq} + 3NaOH_{aq} \rightarrow Fe(OH)_{3_s} + 3Na^{+}{}_{aq} \quad [8]$$

Similarly, after reaching pH 5, the addition of sodium hydroxide continued until the pH value of 10 was reached. In this pH range, the alkaline environment allowed the precipitation of manganese, cobalt, and nickel. The main stoichiometry reactions involved in this stage of the process are guided by these three elements and they are represented as follows.

$$Co^{2+}{}_{aq} + 2NaOH_{aq} \rightarrow Co(OH)_{2_s} + 2Na^{+}{}_{aq} \quad [9]$$

$$Ni^{2+}{}_{aq} + 2NaOH_{aq} \rightarrow Ni(OH)_{2_s} + 2Na^{+}{}_{aq} \quad [10]$$

$$Mn^{2+}{}_{aq} + 2NaOH_{aq} \rightarrow Mn(OH)_{2_s} + 2Na^{+}{}_{aq} \quad [11]$$

To perform the experiment, a sample from the SX raffinate solution of approximately 500 ml with an initial pH of 2 was filtrated using 0.45 um filter paper to remove the remaining solids in the raffinate. The pH of the solution was increased with 2M NaOH until it reached a value of 5; at this point, to separate the solids generated in the process, the samples were centrifuged for 12 minutes at 4000 RPM and filtrated with 0.45 um filter paper. Solids were collected and dried while the aqueous solution was used to continue to perform the second precipitation stage until it reached a pH of 10. The solids were then separated from the liquid in the same way as in pH 5. The pictures shown below represent the raffinate solution at pH values of 2, 5, and 10.

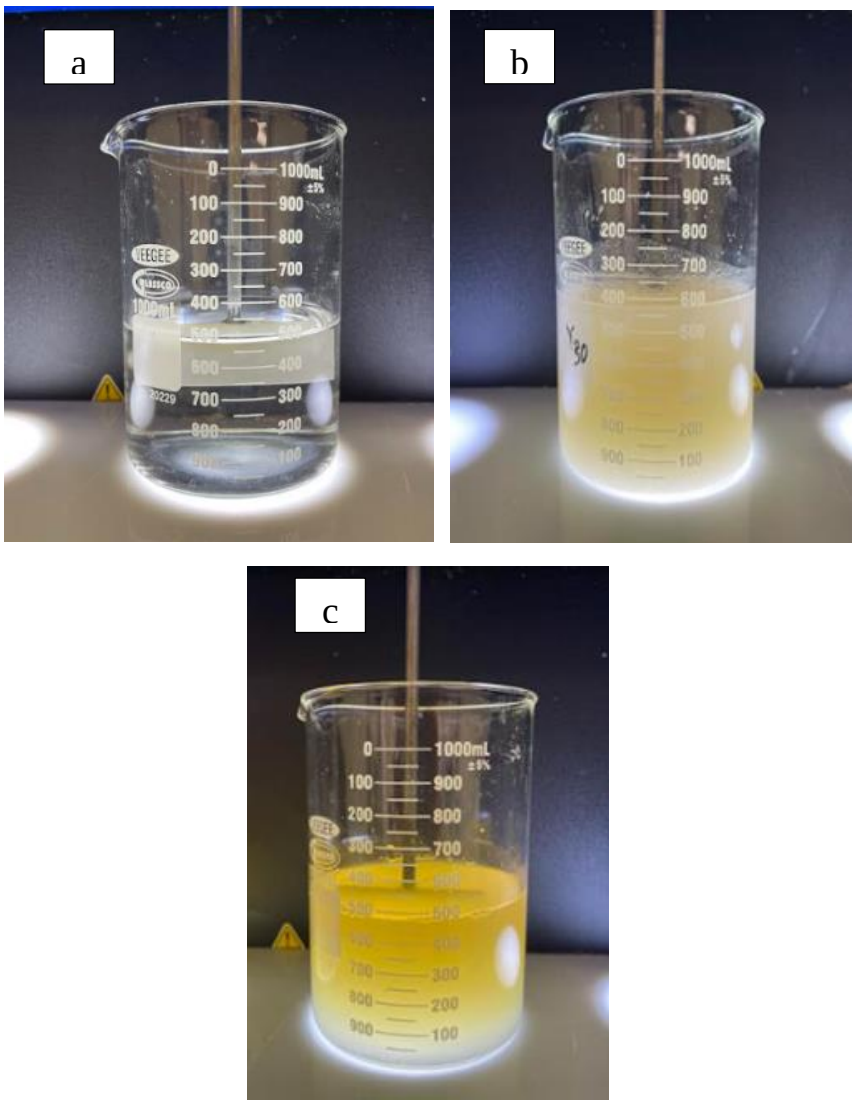

Figure 18. NaOH stagewise precipitation process. a) pH 2, b) pH 5, c) pH 10.

4.3.2 Nitric acid dissolution

Aiming for the continuous extraction of CMs, the solids collected at the high pH range (i.e., pH 5-10) by NaOH precipitation were subjected to a dissolution process to separate the critical minerals from the remaining impurities. Based on the data research published by Boukerche et al. (2010), under acidic conditions and depending on the type of acid media used, exposure time, acid concentration, and temperature, critical minerals such as manganese, cobalt, and nickel can have dissolution rates between 80% and 99%. However, the modification of these factors can generate low dissolution rates of these elements, while impurities such as iron and aluminum are mostly dissolved (Boukerche, et al., 2010).

After the separation from the liquid phase in the previous stage, the solid product rich in cobalt, manganese, and nickel was initially dried for 24 hours, and after that, they were placed in partial dissolution in 0.5 M nitric acid to separate the remaining impurities and critical minerals including cobalt and nickel to obtain a high purity of manganese. The test was carried out by mixing the solids with the nitric acid in a solid-liquid ratio equivalent to 1:100 and stirring them for 1 hour at 75º C. Once the experiment was completed, the remaining solids were centrifugated at 4000 RPM for 12 minutes and separated from the liquid phase by utilizing void pressure in the funnel with filter paper of 0.45 µm pore size. The experimental conditions set for the experiment are shown in Table 8.

Table 8. HNO_3 dissolution parameters.

Time	1 h
RPM	100
Acid	HNO_3
Acid concentration	0.5 M
Temperature	75 ºC
S:L ratio	1:100

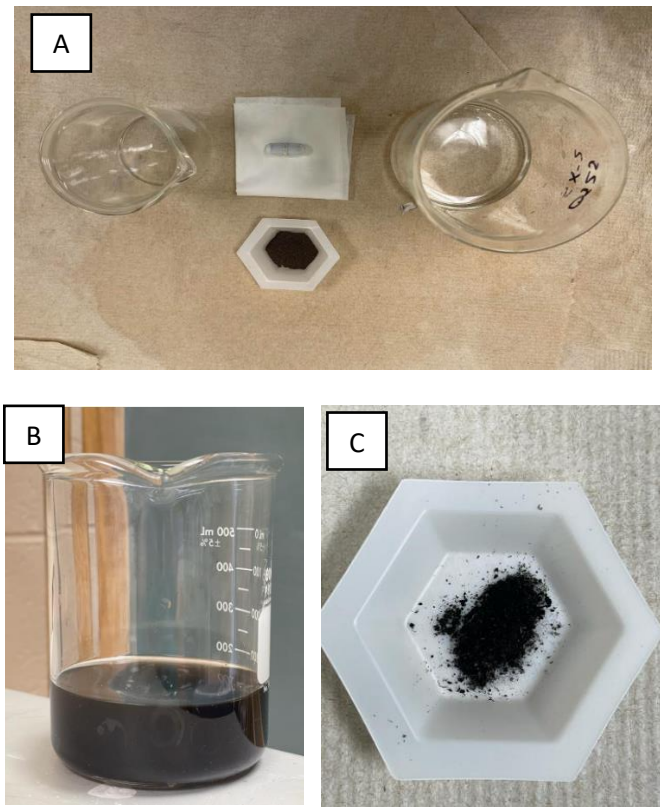

Figure 19. Experiment preparation (A). Nitric acid dissolution (B). Dried solids after dissolution (C).

4.3.3 Sodium sulfide stagewise precipitation

A new solution with extractable amounts of cobalt and nickel was also generated during the dissolution of solids utilizing 0.5 M HNO_3. The solution generated during the dissolution was mainly rich in cobalt and nickel, but low amounts of manganese and other impurities were still present in the remaining e.HNO_3 solution. Sodium sulfide precipitation was conducted based on experimental data obtained from previous testing, and it was also supported by literature review studies. One example is the procedure developed by Li et al. (20220 where the addition of Na_2S to a solution with Co, Mn, and Ni allowed the total precipitation of Co and Ni at pH values around 4, while the precipitation of manganese was approximately 15% (Li & Zhang, 2022).

The test was conducted by preparing a 1M Na2S solution to be added progressively to the remaining HNO_3 solution and mixed at 150 RPM. Throughout the test, three precipitation stages were established for selectively removing solids, which corresponded to pH 5, 10, and 12. Starting from an initial pH of approximately 1, the pH of the solution was increased until it reached the value of 5; at this point, the solution was centrifugated at 4000 RPM, and further separation of the solid-liquid phases was performed by vacuum filtration. The separated solids were dried for 24 hours so a subsequent ICP-MS analysis could be performed. The same procedure was repeated in each pH stage of the process.

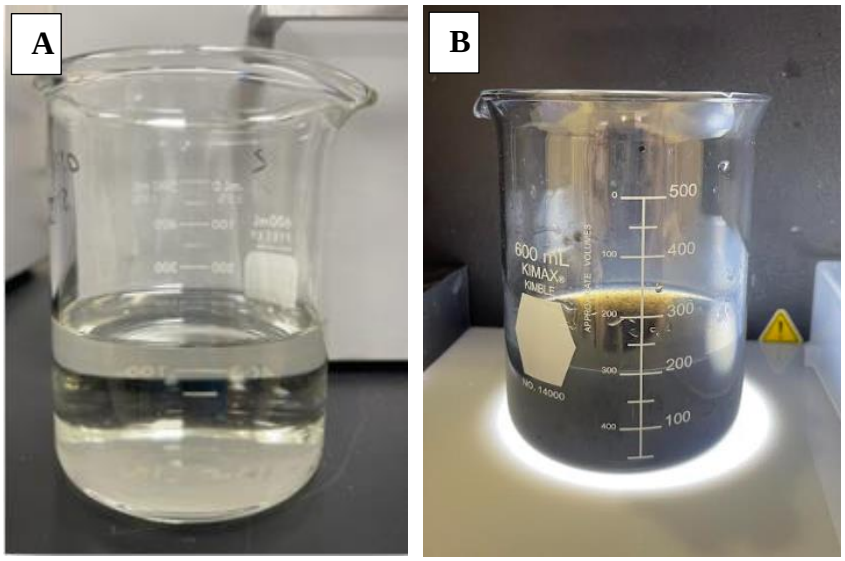

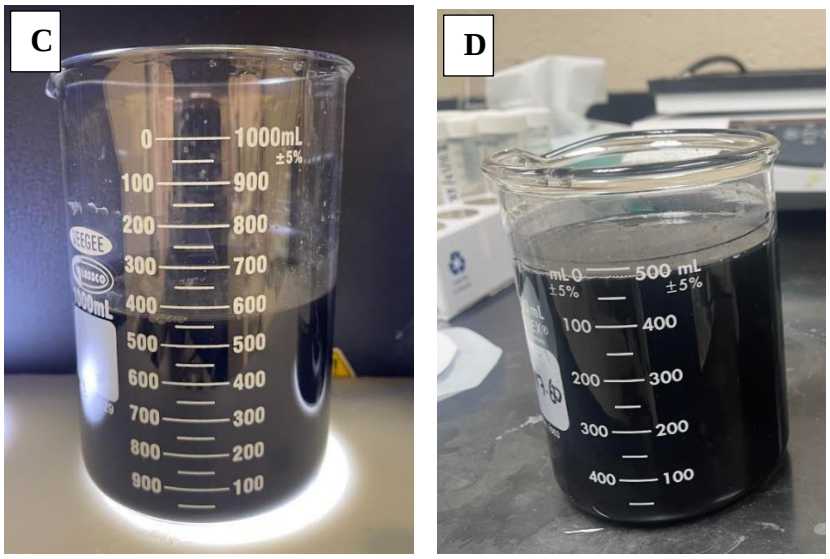

Figure 20. Na_2S stagewise precipitation process. a) solution at pH 1, b) solution at pH 5, c) solution pH at 10 d) solution at pH 12.

4.3.4 Hydrochloric acid dissolution

During the previous CM recovery stage (HNO_3 dissolution), a solid precipitate with extractable amounts of cobalt and nickel and trace levels of manganese and other impurities was produced. For further purification and selective extraction of cobalt and nickel, the solid product was subjected to a redissolution stage with hydrochloric acid (HCl) to generate a pure solution rich in these elements. Due to the reactivity of these metals, the dissolution of the elements is achieved by the formation of soluble chloride salts because of the release of chloride ions (Cl^-) in the reaction. The possible stoichiometric reactions during this process according to the simulation with Visual MINTEQ correspond to the following:

$$CoS_{(s)} + 2HCl_{(aq)} \rightarrow CoCl_{2_{aq}} + H_2S_{(g)} \quad [12]$$

$$NiS_{(s)} + 2HCl_{(aq)} \rightarrow NiCl_{2_{aq}} + H_2S_{(g)} \quad [13]$$

The experiment was accomplished by mixing the solids with 2M hydrochloric acid in a solid-liquid ratio of 1:100; the process was carried out for two hours by heating the solution at 85ºC and mixing it at 100 RPM. Once the experiment was completed, the solids were separated from the liquid by

centrifugation and filtration. The following table shows the experimental parameters defined for the procedure.

Table 9. Operating parameters for HCl dissolution.

Acid type	HCl
Acid concentration	2M
Time	2 Hours
S:L ratio	1:100
Temperature	85º C
Stirrer speed	100 RPM

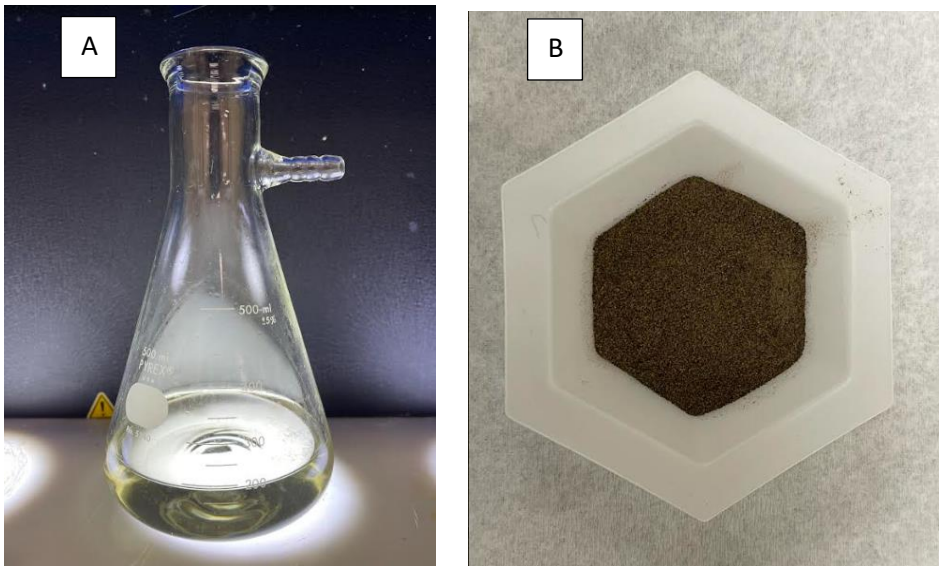

Figure 21. Dissolved solution enriched in cobalt and nickel (A). Remaining solids post HCl dissolution (B).

4.3.5 Oxidative precipitation

Oxidative precipitation targets the selective extraction of nickel by oxidating cobalt and manganese to increase their precipitation rates while maintaining nickel in the solution. Three oxygen atoms make up the triatomic molecule known as ozone (O_3), which has a standard redox potential of 1.24 V in alkaline solutions. Ozone is considered an effective oxidizing agent, surpassing oxygen (O_2). It is widely used in several industries, including environmental protection, the pharmaceutical sector, and the chemical industry. When ozone is introduced to a solution with nickel and cobalt, ozone oxidizes the cobalt preferentially, raising it to a higher oxidation state and leaving the nickel in the solution due to its relative stability with this agent. The oxidizing

mechanism of this process can be described by the following stoichiometric reaction (Qing-hua, et al., 2010).

$$2Co^{2+} + O_3 + 3H_2O \rightarrow 2CoO(OH)_s + 4H^+ + O_2 \quad [14]$$

The experimental procedure developed consists of an oxidation pretreatment in the reactor (Figure 22) for two hours under the conditions shown in Table 10. Afterward, the pretreated solution was subjected to precipitation using sodium hydroxide to adjust the pH to a value of 5. Once the desired pH was reached, the solid and liquid were separated by centrifugation and filtration.

Table 10.Oxidative precipitation parameters in the heated reactor for the pretreatment of the HCl dissolved solution.

O_3 rate	1 L/min
Stirrer speed	300 RPM
Temperature	75º C
Oxidation time	2 Hr.
Oxidizing agent	Ozone (O_3)

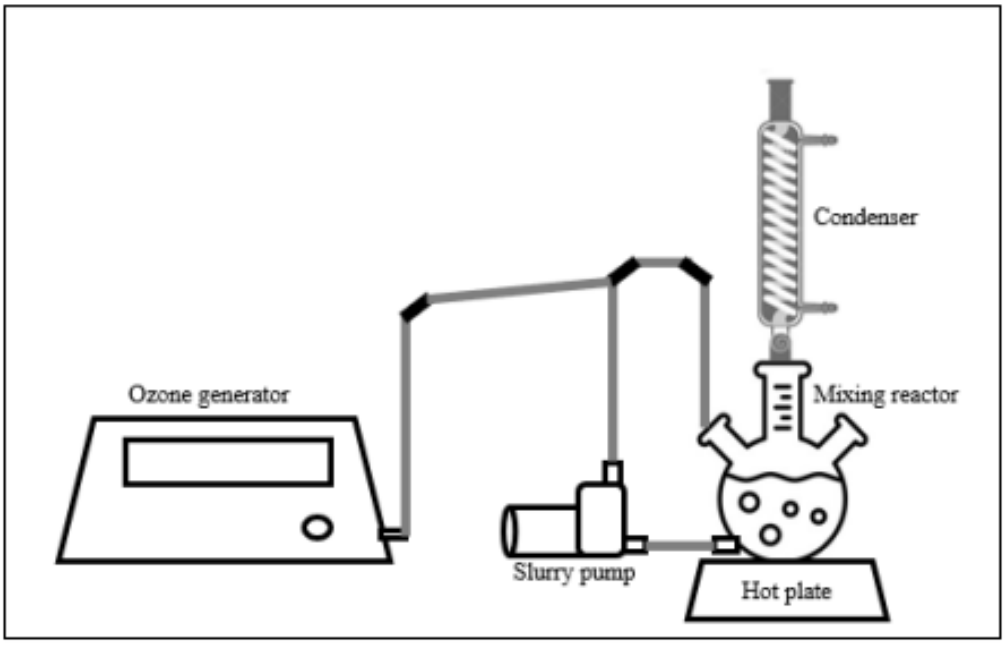

Figure 22. Experimental setup for oxidative precipitation.

4.3.6 Solvent extraction

Aiming for the selective recovery of cobalt and nickel dissolved during the hydrochloric acid dissolution, solvent extraction with Cyanex 272 was implemented as a second alternative in the CM recovery process. Cyanex 272, with an active component of bis(2,4,4-trimethylpentyl) phosphonic acid, is a commercial reagent proven to be an alternative to separate cobalt from nickel in sulfate as well as chloride solution (SOLVAY, 2017). The chemical composition of Cyanex corresponds to $C_{16}H_{34}PO_2H$, and it is represented by the structure shown below:

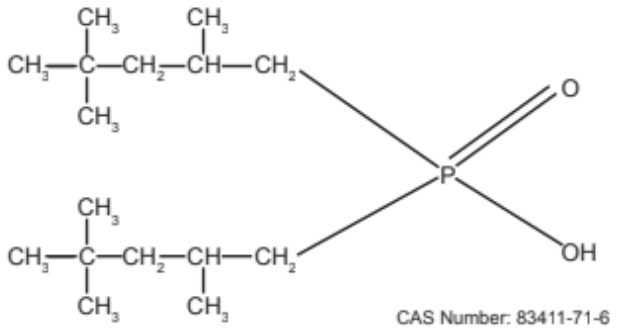

Figure 23. Chemical structure of Cyanex 272.

Many investigations have been conducted in the metallurgy field to develop alternatives that are selective for either of these two metals. Although many efforts have been made to extract nickel (II) over cobalt (II), the most common approach is the extraction of cobalt through the organic solution while leaving nickel in the aqueous solution. The selection of cobalt is carried out by a cationic exchange mechanism, which is represented by the following expression in sulfuric media, where A represents the conjugate base of the extractant (Rodrigues, et al., 2022).

$$2H_2A_2 + CoSO_4 \rightarrow CoA_2.H_2A_2 + H_2SO_4 \quad [15]$$

Strict pH control throughout the process is necessary because this mechanism is pH dependent. Saponification, or neutralization of the extractant, is a typical technique for controlling the pH during the extraction of the elements aimed for the process. During saponification, the extractant undergoes a partial conversion into its sodium salts (Na-Cyanex 272), which, as well as Cyanex 272, is miscible with the majority of aromatic and aliphatic diluents. While extractant saponification is a straightforward pH control technique, it also increases the solubility of the extractant in the aqueous phase (Rodrigues, et al., 2022).

During the previous stage, a solution rich in cobalt and nickel was produced from the HCl dissolution of the concentrate produced by the Na_2S precipitation. The new solution had a pH value

of -0.5, and it was then subjected to a downstream procedure of solvent extraction to separate cobalt from nickel. The extractant employed in this process corresponds to Cyanex 272, which was diluted with kerosene to obtain a concentration of 0.5 M. Additionally, the organic solution was saponified at 50% using 0.25M NaOH and washed with distilled water to enhance the recovery of cobalt. The pH of the feed solution was increased to 6 in order to stabilize the metal ions and remove some impurities, such as aluminum, through precipitation activity. The procedure was then carried out by using an organic-aqueous (O: A) ratio of 1:1, mixing the organic and aqueous phases for 20 minutes at 800 RPM, and keeping an equilibrium pH between 4.5 and 5, which, according to the data provided by Solvay Inc. in chloride solutions, is suitable for the separation of cobalt and nickel (Figure 24).

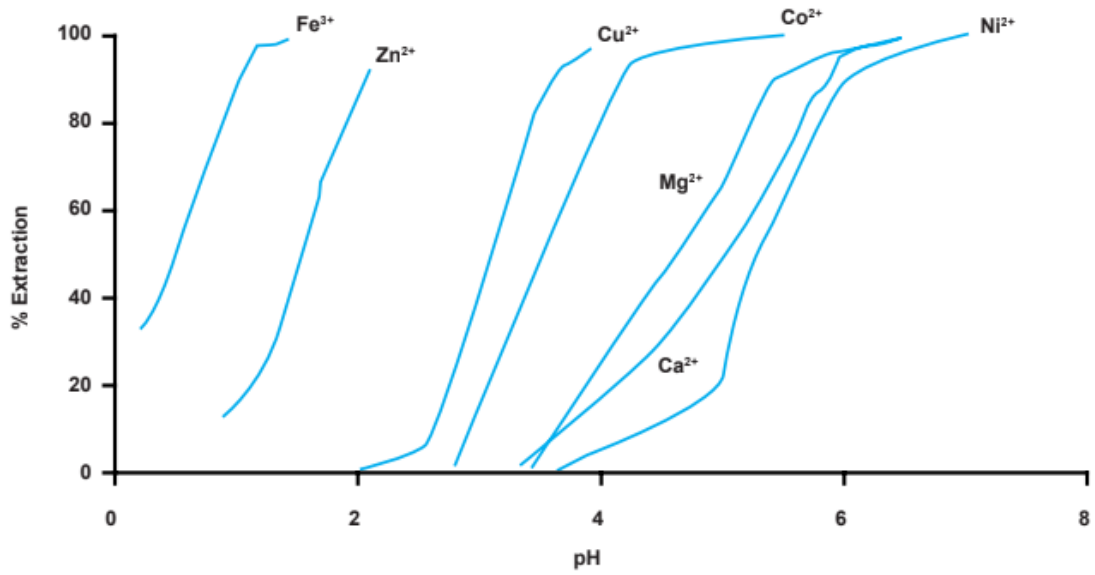

Figure 24. Extraction percentage of metal ions from chloride solutions using CYANEX 272 (SOLVAY, 2017).

The organic: aqueous phase was left in the separation funnel for around 10 hours to guarantee a proper separation between the phases and remove the organic solution loaded with cobalt, followed by stripping the solution and transferring the cobalt into an aqueous media. The stripping procedure was accomplished by using 2M sulfuric acid as a reagent at an A: O ratio equal to 1:1; the organic solution was mixed with the reagent for 5 minutes at 600 RPM and placed in the funnel for 20 minutes to subsequently separate both phases and obtained an aqueous solution rich in cobalt. The experimental parameters for solvent extraction and stripping processes are summarized in Table 11.

Table 11. Solvent extraction and stripping experimental parameters in CM extraction.

Parameter	Solvent extraction	Stripping
Equilibrium pH	4.5 - 5	-
Extractant	Cyanex 272	-
Extractant Con. (mol/L)	0.5	-
Reagent	-	H2SO4
Reagent Con (mol/L)	-	2
O: A ratio	1:1	1:1
Mixing time (min)	20	5
Mixing speed (RPM)	800	600

4.3.6.1 pH adjustment

As mentioned above, the solution used as the feed in solvent extraction had a pH value of -0.5, which was adjusted to 5 using 2M sodium hydroxide (NaOH). During the pH modification, some solids began to appear in the solution as a result of the precipitation of some elemental components. The solids were removed by centrifuging the solid-liquid phase at 4000 RPM for 12 minutes. Then, both phases were separated by vacuum filtration. The following figure shows the solids generated during the pH adjustment.

Figure 25. Solids precipitated during the pH adjustment of the SX feed solution.

4.3.6.2 Saponification procedure

The organic solution used during solvent extraction was 0.5 M Cyanex 272 dissolved in kerosene, and 50% of Cyanex 272 was saponified with 0.25 M of sodium hydroxide in order to mitigate the release of hydrogen ions, which can hinder the effectiveness of the extraction. During the saponification process, NaOH is added to the organic phase to react with Cyanex 272, generating sodium-Cyanex compounds. The procedure was carried out by mixing 0.5M Cyanex 272 and 0.25M sodium hydroxide at an O: A ratio of 1:1 for 2 hours at 800 RPM. After 2 hours, the aqueous-organic solution was placed into a separation funnel to remove NaOH. A washing procedure was subsequently performed on the organic solution to eliminate the remaining impurities in the organic phase and sodium salts formed during the saponification.

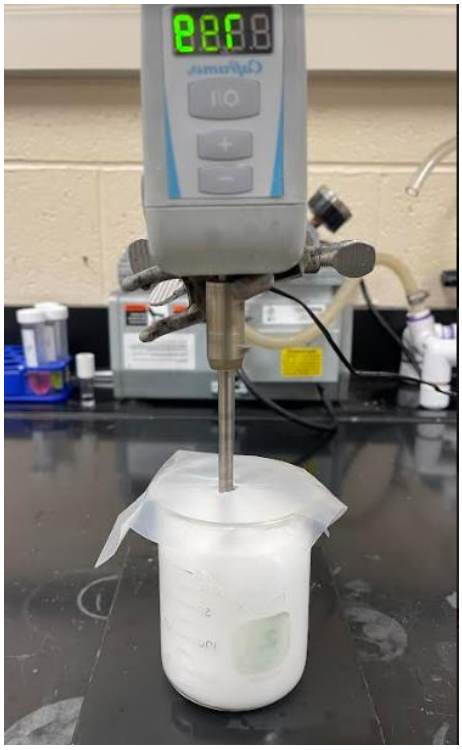

Figure 26. Cyanex 272 saponification process at a ratio of 50% by weight.

Once the NaOH aqueous phase was separated from the organic phase, the organic solution was subjected to a washing stage with distilled water. The washing process consisted of six stages run at an O: A ratio of 1:1 at 800 RPM for 1 minute. After mixing, the solution was placed into the funnel for approximately 20 minutes. During the procedure, the first washing stages generated milky solutions that became clearer over each stage.

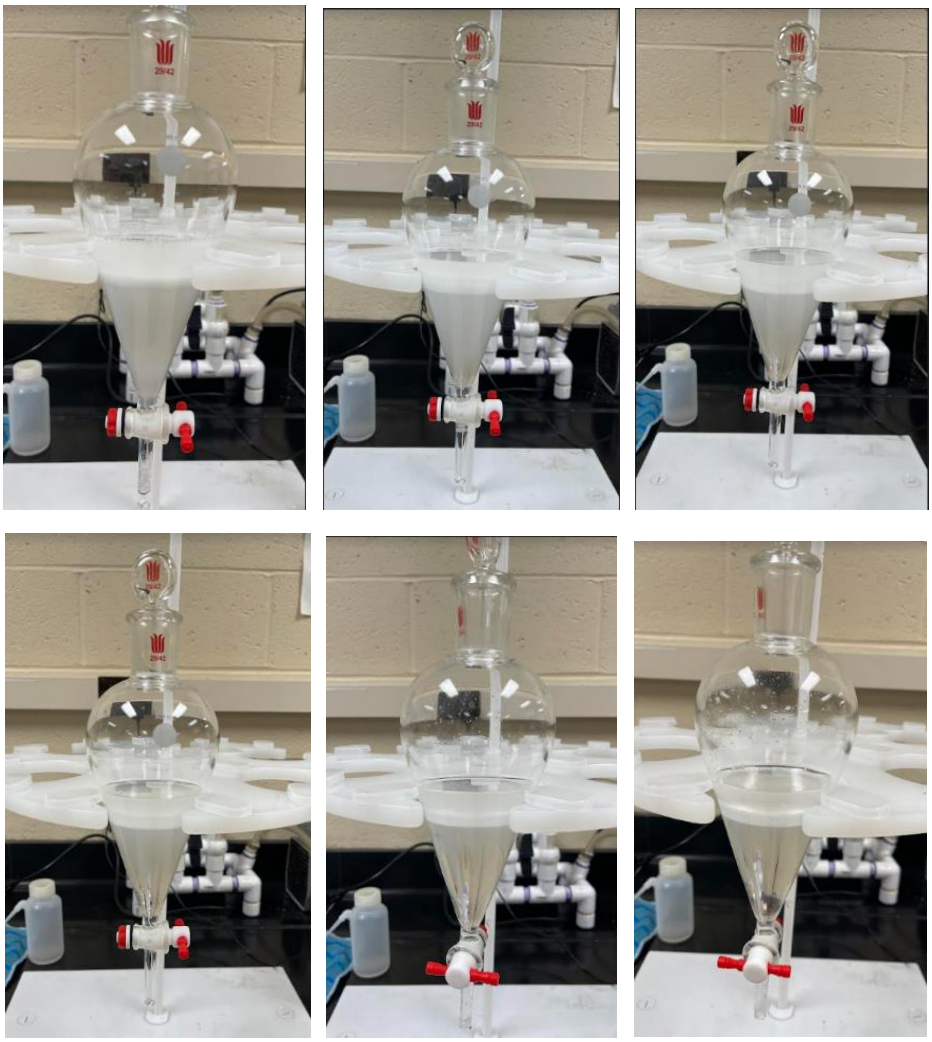

Figure 27. Six washing stages of Cyanex 272 with distilled water.

4.3.7 MINTEQ Software

In order to simulate the reaction behavior of the elements present in the solutions generated through the process, the software Visual MINTEQ Version 3.1 was used to model the NaOH and Na_2S precipitation stages. Visual MINTEQ is a freeware software used to determine chemical parameters in natural waters, including sorption, metal speciation, and solubility equilibrium. By using the software, the possible chemical reactions during both NaOH and Na_2S precipitation were generated with their respective equilibrium solubility constants (log K), which is an important factor in understanding the formation and control of the insoluble compounds, enabling the selective removal of specific ions from the solution, thus enhancing the effectiveness of the precipitation process (Deniz Talan, 2022).

The simulation performed by the software consisted of an initial setup of the concentrations and chemical environment of the solutions. For NaOH precipitation, the simulation was run from an initial pH equal to zero until a final pH value of thirteen. The concentrations used corresponded to the elemental compositions of the raffinate solution, and for the solution media, which was sulfuric acid and sodium hydroxide, the concentrations were equivalent to 2 M for both. The simulation of Na_2S precipitation was conducted in the same pH range, but the concentration and media were replaced by the values obtained after the nitric acid dissolution and 0.5M nitric acid was used instead of sulfuric acid. Both simulations were carried out at room temperature of 25º C. The saturation index (SI), which indicates whether a species will remain dissolved or precipitate, was also used to study the precipitation mechanisms of the elements (Deniz Talan, 2022). The Saturation Index is represented by the equation shown below:

$$SI = Log\ (IAP) - Log(K) \quad [16]$$

where IAP is the ion activity product, which is a measure of the degree to which an ionic compound is saturated in a solution and allows to predict if the compound will remain or not in the solution; K is described as the equilibrium constant for a chemical reaction where an ionic molecule that is sparingly soluble dissolves in water and partitions into its individual ions. The K values of all the chemical reactions for both processes are represented in Tables 12 and 13. The interpretation of the values obtained for the solubility index is described as follows.

$$SI < 0 \quad Undersaturation$$

$$SI = 0 \quad Apparent\ equilibrium$$

$$SI > 0\ Oversaturation$$

Table 12. Sodium hydroxide precipitation chemical reactions and solubility constant at 25º C.

Chemical reaction	Solubility constant (log K)
$Co^{2+} + 2OH^- \rightleftharpoons Co\ (OH)_{2\ (aq)}$	-18.794
$4Co^{2+} + 4OH^- \rightleftharpoons Co_4(OH)_4{}^{+4}$	-30.488
$Co^{2+} + OH^- \rightleftharpoons CoOH^+$	-9.697
$Co^{2+} + SO_4{}^{-2} \rightleftharpoons CoSO_{4\ (aq)}$	2.3
$Ni^{2+} + 2(OH)^- \rightleftharpoons Ni\ (OH)_{2\ (aq)}$	-18.994
$Ni^{2+} + 2SO_4{}^{2-} \rightleftharpoons Ni\ (SO_4)_2{}^{-2}$	0.82
$Ni^{2+} + OH^- \rightleftharpoons NiOH^+$	-9.897
$Ni^{2+} + SO_4{}^{2-} \rightleftharpoons NiSO_4$ (aq)	2.3
$Mn^{2+} + 4(OH)^- \rightleftharpoons Mn\ (OH)_4{}^{-2}$	-48.288
$2Mn^{2+} + (OH)^- \rightleftharpoons Mn_2(OH)^{3+}$	-23.891

$Mn^{2+} + (OH)^{-} \rightleftharpoons MnOH^{+}$	-10.597
$Mn^{2+} + SO_4^{2-} \rightleftharpoons MnSO_{4\,(aq)}$	2.25
$Al^{3+} + OH^{-} \rightleftharpoons Al\,(OH)^{2+}$	-10.294
$Al^{3+} + 3OH^{-} \rightleftharpoons Al\,(OH)_3\,(aq)$	-16.691
$2Al^{3+} + 2OH^{-} \rightleftharpoons Al_2(OH)_2{}^{+4}$	-7.694
$3Al^{3+} + 4OH^{-} \rightleftharpoons Al_3(OH)4^{+5}$	-13.888
$Al^{3+} + OH^{-} \rightleftharpoons AlOH^{+2}$	-4.997
$Mg^{2+} + (OH)^{-} \rightleftharpoons MgOH^{+}$	-11.417
$Mg^{2+} + SO_4^{2-} \rightleftharpoons MgSO_4\,(aq)$	2.26
$Fe^{2+} + 2(OH)^{-} \rightleftharpoons Fe\,(OH)_2\,(aq)$	-20.494
$Fe^{2+} + (OH)^{-} \rightleftharpoons FeOH^{+}$	-9.397

Table 13. Sodium sulfide precipitation chemical reactions and solubility constant at 25º C.

Chemical reaction	Solubility constant (log k)
$Co^{2+} + NH_3 \rightleftharpoons Co(NH_3)^{+2}$	-7.21
$Co^{2+} + 2\,NH_3 \rightleftharpoons Co(NH_3)_2^{+2}$	-14.99
$Co^{2+} + 3NH_3 \rightleftharpoons Co(NH_3)_3^{+2}$	-23.3
$Co^{2+} + 4NH_3 \rightleftharpoons Co(NH_3)_4^{+2}$	-31.91
$Co^{2+} + 5NH_3 \rightleftharpoons Co(NH_3)_5^{+2}$	-41.09
$Co^{2+} + 2OH^- \rightleftharpoons Co(OH)_{2\,(aq)}$	-18.794
$4Co^{2+} + 4OH^- \rightleftharpoons Co_4(OH)_4^{+4}$	-30.488
$Co^{2+} + HS^- \rightleftharpoons CoHS^+$	5.2
$Co^{2+} + OH^- \rightleftharpoons CoOH^+$	-9.697
$Ni^{2+} + 2(NH_3) \rightleftharpoons Ni(NH_3)_2^{+2}$	-13.61
$Ni^{2+} + 3(NH_3) \rightleftharpoons Ni(NH_3)_3^{+2}$	-21.19
$Ni^{2+} + 4(NH_3) \rightleftharpoons Ni(NH_3)_4^{+2}$	-29.31
$Ni^{2+} + 5(NH_3) \rightleftharpoons Ni(NH_3)_5^{+2}$	-37.89
$Ni^{2+} + 6(NH_3) \rightleftharpoons Ni(NH_3)_6^{+2}$	-47.17
$Ni^{2+} + 2(OH)^- \rightleftharpoons Ni(OH)_{2\,(aq)}$	-18.994
$Ni^{2+} + HS^- \rightleftharpoons NiHS^+$	5.49
$Ni^{2+} + OH^- \rightleftharpoons NiOH^+$	-9.897
$Mn^{2+} + 2(NH_3) \rightleftharpoons Mn(NH_3)_2^{+2}$	-17.24
$Mn^{2+} + 3(NH_3) \rightleftharpoons Mn(NH_3)_3^{+2}$	-26.35
$Mn^{2+} + 4(NH_3) \rightleftharpoons Mn(NH_3)_4^{+2}$	-35.74
$2Mn^{2+} + (OH)^- \rightleftharpoons Mn_2(OH)^{3+}$	-23.891
$Mn^{2+} + HS^- \rightleftharpoons MnHS^+$	5.14
$Mn^{2+} + (NH_3) \rightleftharpoons MnNH_3^{+2}$	-8.4
$Mn^{2+} + OH^- \rightleftharpoons MnOH^+$	-10.597
$Al^{3+} + 2OH^- \rightleftharpoons Al(OH)_2^+$	-10.294
$2Al^{3+} + 2OH^- \rightleftharpoons Al_2(OH)_2^{+4}$	-7.694
$3Al^{3+} + 4OH^- \rightleftharpoons Al_3(OH)_4^{+5}$	-13.888
$Al^{3+} + OH^- \rightleftharpoons AlOH^{+2}$	-4.997
$Mg^{2+} + 2(NH3) \rightleftharpoons Mg(NH_3)_2^{+2}$	-18.29
$Mg^{2+} + OH^- \rightleftharpoons MgOH^+$	-11.417

4.3.8 Experimental flowsheet design for CM extraction

To summarize the experimental procedure developed to extract manganese, cobalt, and nickel from the SX-raffinate solution produced during the extraction of REEs from acid mine drainage (AMD) sludge, a flowsheet diagram was developed and is shown in Figure 28. The flowsheet comprises an initial stagewise precipitation with NaOH to separate the impurities, such as aluminum and iron at pH 5, from cobalt, manganese, and nickel, which are later precipitated at a pH value of ten. The NaOH precipitation is followed by the dissolution of the CM concentrate produced to obtain a high-purity solid product of manganese and dissolve the cobalt and nickel into a nitric acid solution. Then, the nitric acid (HNO_3) media solution was subjected to a new stagewise precipitation using sodium sulfide (Na_2S) to separate cobalt and nickel from the remaining manganese and magnesium; the Na_2S precipitation was carried out in a 3-stage separation, where Co-Ni solids were removed at pH 5, Mn at pH 10, and Mg solids at pH 12. The Co-Ni product collected at pH 5 was then subjected to a hydrochloric acid (HCl) redissolution stage to dissolve the elements, and the Co-Ni-rich solution was subsequently used in solvent extraction.

The solvent extraction process was carried out using 0.5M Cyanex 272 diluted in kerosene, where the goal was the separation of cobalt from nickel and residual impurities in the solution. After loading the organic solution with cobalt, the raffinate solution was subjected to a precipitation process with Na_2S to obtain a solid product of nickel. On the other side, the organic solution was stripped with 2M H_2SO_4 to remove the cobalt from the organic solution, followed by a second stage of Na_2S precipitation to finally obtain a cobalt solid product.

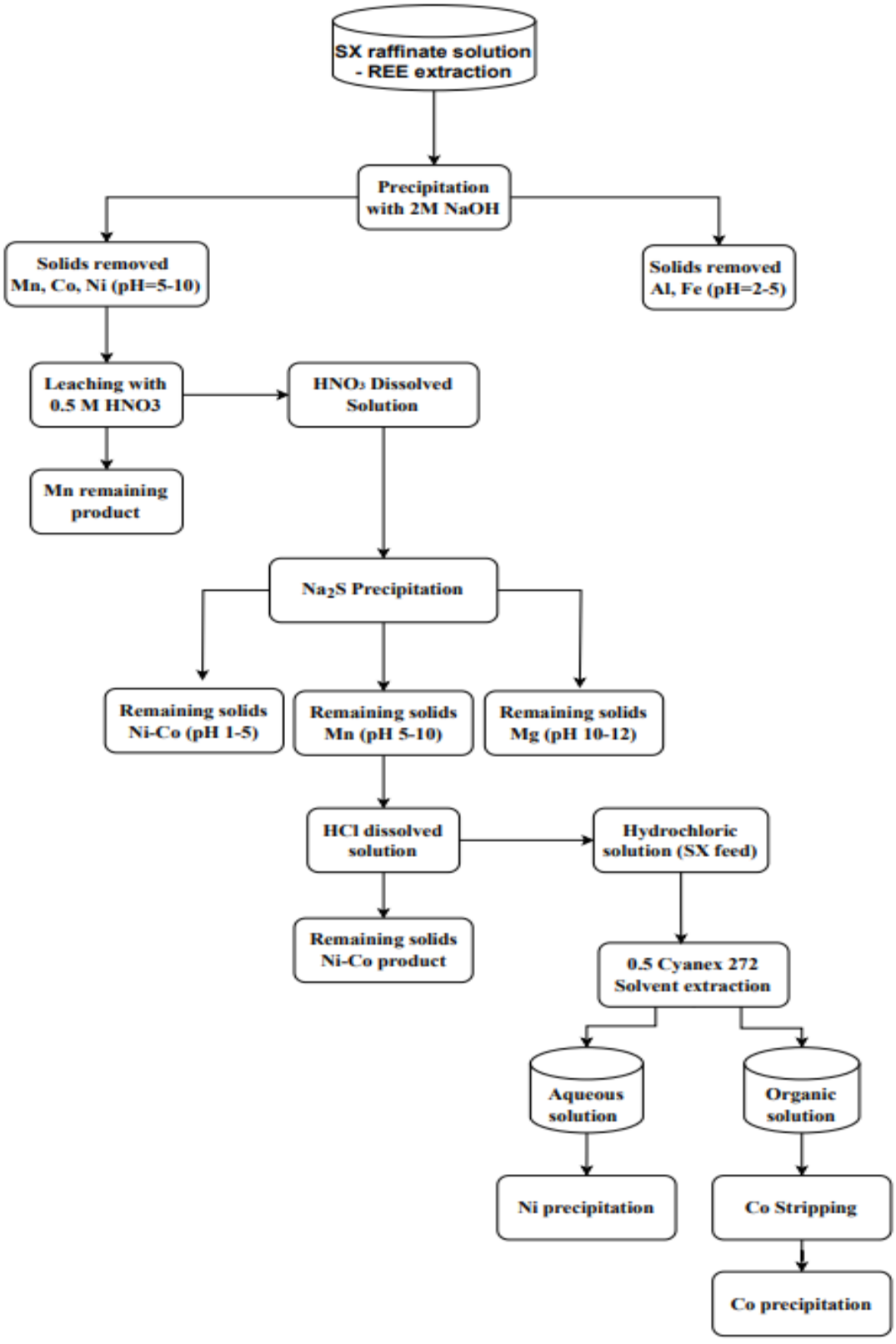

Figure 28. Experimental flowsheet designed for the selective recovery of CMs.

5. EXPERIMENTAL RESULTS AND DISCUSSION

5.1 NaOH stagewise precipitation

The solution generated during the solvent extraction process developed for the extraction of REEs was subjected to stagewise precipitation in order to evaluate the precipitation behavior of the critical minerals targeted for this research at different pH values and the associated impurities. As mentioned above in previous sections, the procedure was carried out by using 2 mol/L of sodium hydroxide (NaOH) to control the pH of the solution and reach the pH value desired for evaluation. The pH values analyzed were 2, 3, 4, 5, 6, 7, 8, 9, 10, and 11; after centrifugation and filtration, representative samples of each pH setpoint were taken to perform ICP-MS characterization and determine the elemental composition of the solution. Figure 29 shows the solid and liquid products obtained during the experiment.

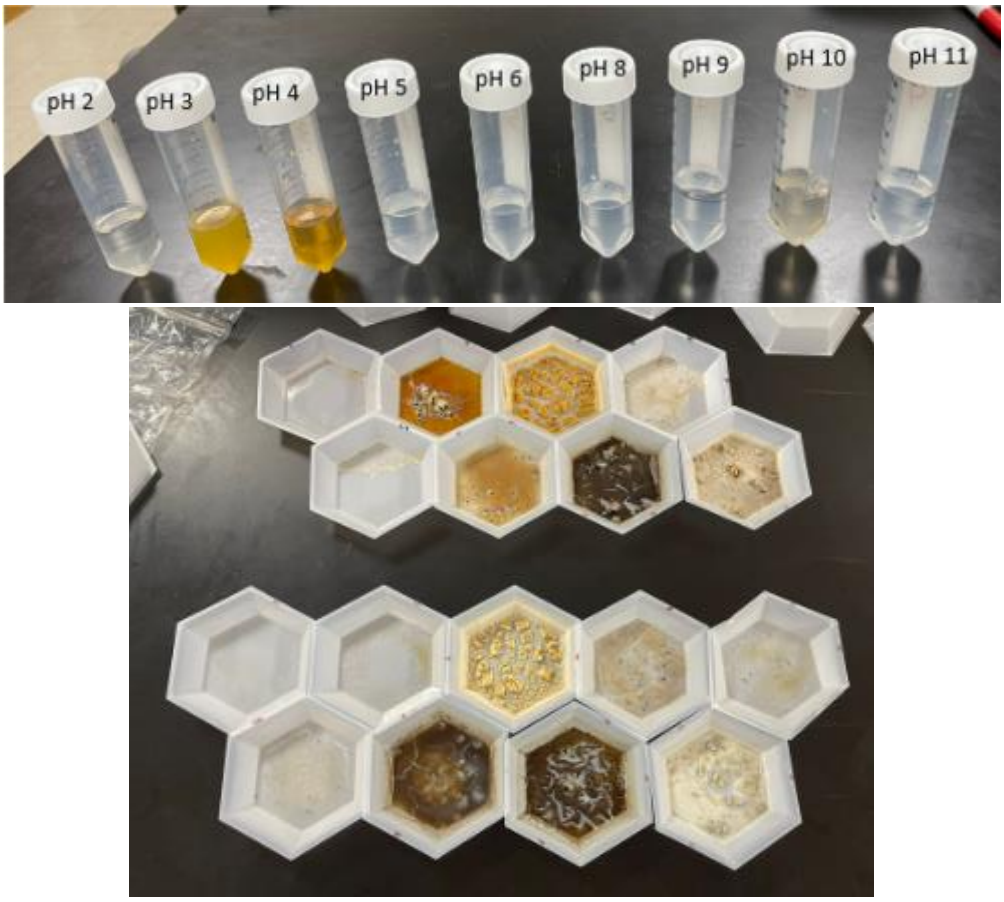

Figure 29. Precipitated solids generated from pH 2 to 11.

According to the data obtained from ICP-MS analysis shown in Table 14, main impurities such as aluminum and iron were precipitated during the pH range from 2 to 5. The concentration of these elements decreased slowly from pH 2 to 4. However, aluminum concentration was drastically reduced at pH 5, decreasing from 3089 mg/L at pH 4 to 19.61 mg/L at pH 5. Iron had a similar behavior at the same pH range, with a concentration of 257.25 mg/L at pH 4 and reaching a concentration of 1.41 mg/L at pH 5. Other elements, such as silicon and phosphorus, the concentrations of which were also significantly reduced at this pH. On the other side, according to the values shown in Table 15, at pH 5, the cumulative precipitation of manganese is 28.91 wt.%, cobalt of 40.41 wt.%, and nickel of 44.87 wt. %, representing a reduction of 11.99 mg/L, 64.35 mg/L, and 23.85 mg/L, respectively, from the initial concentration. Therefore, pH 5 is a promising value for removing impurities while keeping suitable concentrations of Co, Mn, and Ni even though high concentrations of magnesium and calcium remain in the solution. Table 15 and Figure 30 present the cumulative precipitation of the elements.

Table 14. ICP-MS characterization of the filtrate samples generated with 2M NaOH stagewise precipitation from pH 2 to 11.

Elemental composition of the filtrate samples at different pH values (mg/l) - Average										
Element	**Initial pH (2)**	**pH 3**	**pH 4**	**pH 5**	**pH 6**	**pH 7**	**pH 8**	**pH 9**	**pH 10**	**pH 11**
Li	0.55	0.43	0.34	0.08	0.17	0.00	0.08	0.06	0.08	0.00
Be	0.69	0.68	0.59	0.00	0.00	0.00	0.00	0.00	0.00	0.00
Na	15,264.73	15,573.52	16,243.60	20,038.16	20,142.63	18,831.95	19,914.29	19,455.84	19,079.63	22,508.47
Mg	2,008.57	1,940.87	1,811.54	1,650.19	1,654.54	1,710.24	1,630.95	1,547.59	1,463.65	225.74
Al	3,599.77	3,449.24	3,089.62	19.61	6.76	6.35	7.33	5.86	5.62	5.57
Si	124.59	128.34	102.51	28.72	26.86	20.02	18.69	8.26	5.23	6.89
P	53.82	43.53	36.11	0.56	0.77	0.30	0.45	0.58	0.51	0.45
K	8.56	10.93	13.07	8.51	8.57	8.36	9.13	10.61	11.60	10.09
Ca	27.45	29.16	24.63	22.86	23.35	25.98	23.07	22.43	22.12	5.43
Ti	0.11	0.05	0.06	0.00	0.00	0.00	0.05	0.00	0.00	0.00
Cr	0.27	0.27	0.26	0.00	0.00	0.00	0.00	0.00	0.00	0.00
Fe	446.83	304.16	257.25	1.41	1.46	1.28	1.31	1.31	1.31	1.38
Mn	323.63	311.93	289.77	259.28	254.69	243.97	229.66	103.79	37.05	1.40
Co	36.35	35.33	32.95	24.36	22.26	19.67	12.04	1.09	0.58	0.57
Ni	62.53	60.55	56.44	38.68	35.32	30.93	19.09	0.90	0.21	0.19
Cu	2.35	2.33	2.20	0.12	0.00	0.00	0.00	0.00	0.00	0.00
Zn	23.31	23.13	21.38	10.62	8.60	4.89	1.45	0.19	0.18	0.15
TREE	2.73	2.75	2.60	1.79	1.70	1.41	0.98	0.78	0.78	0.06

Table 15. Cumulative percentages of different elements precipitated during the 2M NaOH stage-wise precipitation.

Element	Cumulative Precipitation %									
	pH									
	2.2	**3.2**	**3.94**	**5.04**	**6.19**	**7.4**	**7.91**	**9**	**9.96**	**10.94**
Mg	0.00	2.37	10.47	**26.97**	29.49	32.05	38.00	45.40	71.38	92.31
Al	0.00	3.20	15.11	**99.52**	99.84	99.86	99.87	99.90	99.91	99.93
Si	0.00	0.00	22.60	**80.27**	82.24	83.43	89.04	95.46	97.18	96.84
P	0.00	18.51	34.41	**99.09**	98.98	99.60	99.62	99.66	99.76	99.72
K	0.00	0.00	0.00	**41.90**	43.32	45.07	47.47	47.47	51.64	64.15
Ca	0.00	3.96	21.73	**34.44**	35.47	39.88	43.46	48.35	65.60	88.14
Fe	0.00	27.46	36.32	**99.67**	99.68	99.73	99.75	99.76	99.77	99.86
Mn	0.00	2.62	11.06	**28.91**	32.75	35.61	46.08	76.75	94.35	99.72
Co	0.00	1.83	10.01	**40.41**	47.49	51.96	75.78	97.87	98.92	98.95
Ni	0.00	2.17	10.41	**44.87**	51.44	55.74	77.82	99.00	99.78	99.79
Zn	0.00	0.84	9.96	**59.97**	68.75	77.99	95.54	99.42	99.53	99.58
TREE	0.00	0.00	7.35	**43.00**	48.06	59.19	73.67	80.20	89.73	98.54

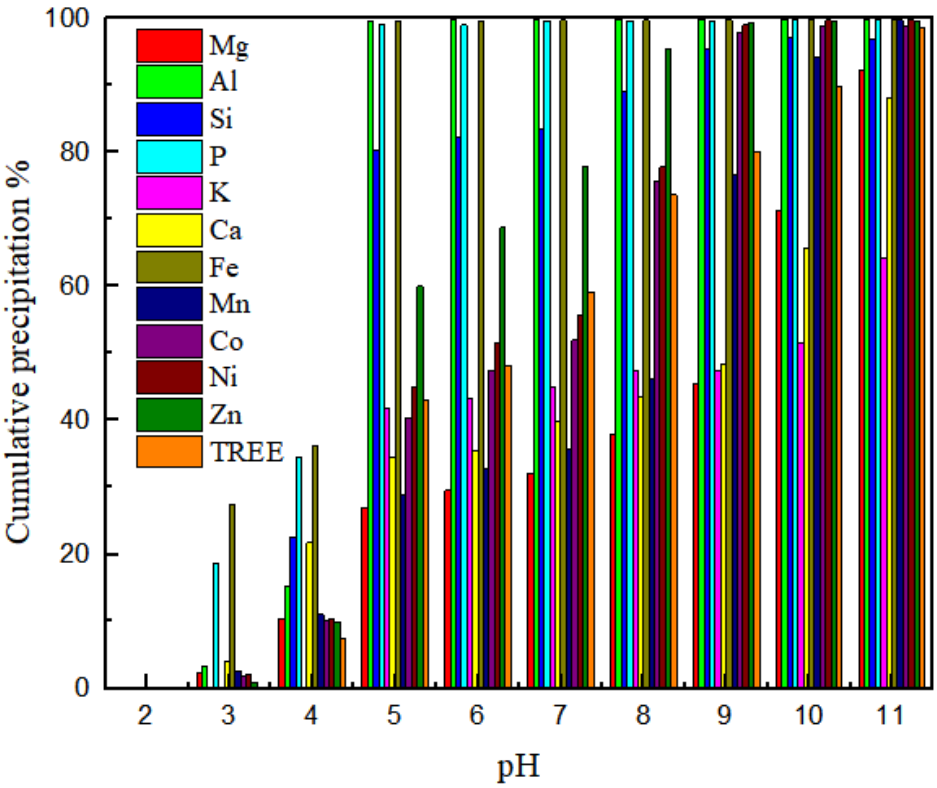

Figure 30. Cumulative precipitation percentages of different elements obtained from stagewise precipitation with 2M NaOH.

Based on the information previously obtained, the decision to collect the solids in two different pH ranges (i2 to 5 and 5 to 10) was made to produce a pre-concentrate of cobalt, manganese, and nickel, which was obtained from the pH 5 to 10 range. At pH 5, around 99 wt.% of Ni and Co were precipitated while Mn only reached a cumulative precipitation of 74 wt.%; about 99 wt.% of Mn precipitation was achieved at pH 11; however, at this pH, other impurities, such as Mg, precipitated. Due to this reason, the solid collection stopped at pH 10 where the precipitation of Mn was 94 wt.%, and the precipitation of additional impurities could be avoided. The solids collected in both ranges were analyzed to determine the elemental compositions and the grade of critical minerals and impurities. As expected, most of the impurities were precipitated in the low range, with a corresponding grade of 8.3 wt.% for Al and 1.2 wt.% for Fe; the solids generated in the high pH range had a content percentage by weight of 2.7 wt.%, 0.35 wt.%, and 0.67 wt.% for Mn, Co, and Ni, respectively. The elemental composition obtained from both solids is shown in Table 16.

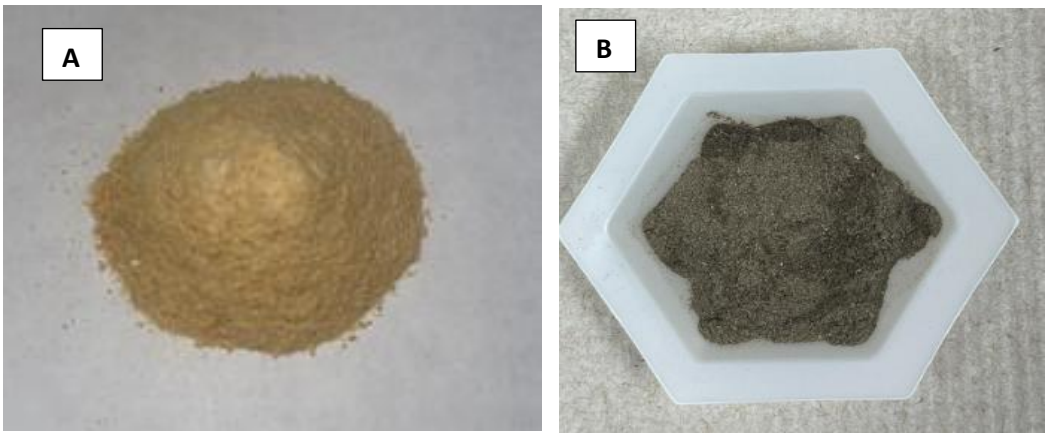

Figure 31. Solid precipitated at pH 2-5 (a). Solids precipitated at pH 5-10 (b).

Table 16. ICP-MS characterization of the solids generated at different pH ranges.

Solids precipitated - ICP-MS Characterization.					
Solids at pH 2-5			**Solids at pH 5-10**		
Element	**ppm**	**wt.%**	**Element**	**ppm**	**wt.%**
Mg	2,967.17	0.30	**Mg**	17,193.83	1.72
Al	83,427.86	8.34	**Al**	3,501.33	0.35
Si	2,099.86	0.21	**Si**	1,823.17	0.18
P	911.92	0.09	**P**	ND	ND
S	126,692.61	12.67	**S**	160,415.50	16.04
K	ND	ND	**K**	ND	ND
Ca	446.92	0.04	**Ca**	1,440.50	0.14
Ti	ND	ND	**Ti**	ND	ND
V	ND	ND	**V**	ND	ND
Cr	ND	ND	**Cr**	ND	ND
Mn	1,645.06	0.16	**Mn**	27,724.00	2.77
Fe	12,380.44	1.24	**Fe**	477.17	0.05
Co	347.28	0.03	**Co**	3,559.33	0.36
Ni	756.31	0.08	**Ni**	6,772.17	0.68
Cu	60.67	0.01	**Cu**	24.67	0.00
Zn	443.25	0.04	**Zn**	1,991.33	0.20
As	ND	ND	**As**	ND	ND
Se	ND	ND	**Se**	ND	ND
Rb	1.00	0.00	**Rb**	1.17	0.00
Sr	2.42	0.00	**Sr**	4.50	0.00
Y	ND	ND	**Y**	1.67	0.02
Zr	5.50	0.00	**Zr**	5.00	0.00
Nb	ND	ND	**Nb**	ND	ND
Mo	3.00	0.00	**Mo**	3.33	0.00
Ba	42.53	0.00	**Ba**	49.67	0.00

Th	7.58	0.00	**Th**	ND	ND

5.1.1 Comparing experimental data to simulation outcomes in NaOH precipitation.

To validate the results obtained by the experimental procedure, Visual MINTEQ 3.1 was used to simulate the stagewise precipitation, which began at an initial pH value of zero and was completed at pH 14. The simulation allows it to predict the chemical species precipitated at different pH values based on the elemental composition and water chemistry of the feedstock solution used in laboratory testing. Tables 17 and 18 present the predicted species with their respective saturation index values for pH 5 and pH 10, respectively. As previously mentioned, a positive value indicates precipitation, and negative values suggest that the mineral remains dissolved in the solution. According to the information provided by the software, the results obtained in the experimental section are well correlated to the predicted results. The chemical species are predicted to precipitate are aluminum and iron compounds, including Boehmite ($Al_2O_3.H_2O$), Diaspore ($AlO(OH)_3$), Gibbsite ($Al(OH)_3$), Hercynite ($FeAl_2O_4$), Mirabilite ($Na_2SO_4.10H_2O$), and other compounds such as $Al_4(OH)10SO_4(s)$ and $AlOHSO_{4(s)}$. On the other hand, at pH 10, compounds of Mn, Co, and Ni are precipitated according to the simulation, including $Co(OH)_2$, CoO(s), $Ni(OH)_2$, $Ni_4(OH)_6SO_4(s)$, and Pyrochroite ($Mn(OH)_2$).

Table 17. Predicted species formed during 2M NaOH stagewise precipitation with Visual MINTEQ 3.1 at pH 5.

Mineral	Saturation index
$Al(OH)_3$ (am)	-1.574
$Al(OH)_3$ (Soil)	0.936
$Al_2O_3(s)$	-1.116
$Al_4(OH)10SO_4(s)$	3.81
$AlOHSO_4(s)$	2.062
Boehmite	0.676
Brucite	-9.96
$Co(OH)_2$ (am)	-8.119
$Co(OH)_2$ (c)	-7.315
CoO(s)	-8.584
$CoSO_4(s)$	-8.221
$CoSO_4:6H_2O(s)$	-3.115
Diaspore	2.381
Epsomite	-1.324
$Fe(OH)_2$ (am)	-7.779
$Fe(OH)_2$ (c)	-7.179
Gibbsite (C)	1.486
Hercynite	1.383

Melanterite	-2.67
$Mg(OH)_2$ (active)	-11.654
Mirabilite	0.022
$MnSO_4$(s)	-6.884
Morenosite	-3.256
$Ni(OH)_2$ (am)	-7.7
$Ni(OH)_2$ (c)	-5.6
Ni_4(OH)6SO_4(s)	-21.635
Periclase	-14.416
Pyrochroite	-9.101
Retgersite	-3.333
Spinel	-11.143
Thenardite	-1.132

Table 18. Predicted species formed during 2M NaOH stagewise precipitation with Visual MINTEQ 3.1 at pH 10.

Mineral	**Saturation index**
$Al(OH)_3$ (am)	1.26
$Al(OH)_3$ (Soil)	3.77
Al2O_3(s)	4.559
Al_4(OH)10SO_4(s)	5.293
AlOHSO_4(s)	-4.957
Boehmite	3.512
Brucite	-0.088
$Co(OH)_2$ (am)	1.684
$Co(OH)_2$ (c)	2.488
CoO(s)	1.222
$CoSO_4$(s)	-8.271
$CoSO_4$:6H_2O(s)	-3.179
Diaspore	5.217
Epsomite	-1.321
$Fe(OH)_2$ (am)	2.071
$Fe(OH)_2$ (c)	2.671
Gibbsite (C)	4.32
Hercynite	16.909
Melanterite	-2.69
$Mg(OH)_2$ (active)	-1.782
Mirabilite	-0.022
$MnSO_4$(s)	-7.269

Morenosite	-3.304
$Ni(OH)_2$ (am)	2.121
$Ni(OH)_2$ (c)	4.221
$Ni_4(OH)6SO_4$(s)	7.798
Periclase	-4.542
Pyrochroite	0.367
Retgersite	-3.378
Spinel	4.406
Thenardite	-1.153

5.1.2 Chemical species distribution during NaOH precipitation

The precipitation CMs and main impurities were also modeled with Visual MINTEQ 3.1 to generate the chemical species distribution diagrams, as shown in Figure 32. According to the data provided by the diagrams, the divalent Mn, Co, and Ni ions show a decreasing trend as the pH in the solution rises, with these species being predominant at a low pH value. It is consistent with the observed behavior of metal ions, which became less prevalent in alkaline solutions. Moreover, the chemical compounds such as $Mn_2(OH)_3^+$, $Co(OH)_2$, $Co(OH)_3^-$, and $Ni(OH)_3^-$ increase significantly at high pH, suggesting that these species can be formed in highly alkaline conditions. This phenomenon can be explained through the metal ion hydrolysis process, where hydronium ions (H_3O^+) decrease due to the increase of the pH and the hydroxyl ions (OH^-), allowing for the formation of basic salts made up of metal hydroxides. Sulfate species also appears in the predicted species, showing a constant presence up to pH 10, and its concentration drastically decreases after this value. On the other hand, the behavior of the impurities in the solution provides valuable information, especially on aluminum, for which, in the pH range of 1 to 5, the prevalent species are $Al(SO_4)^-$, but the concentration decreased substantially after this range. Magnesium and iron species present a steady trend until pH 10, at which sulfate compounds tend to decrease while hydroxide species begin to appear in the solution. In terms of critical minerals, the data obtained from the diagrams are well correlated with the experimental results since manganese, cobalt, and nickel tend to precipitate in alkaline conditions based on the experimental results as well as the simulation. The behavior of aluminum also matches the experimental results because aluminum sulfate demonstrates a similar behavior in the simulation, suggesting that this compound can appear in the precipitated product.

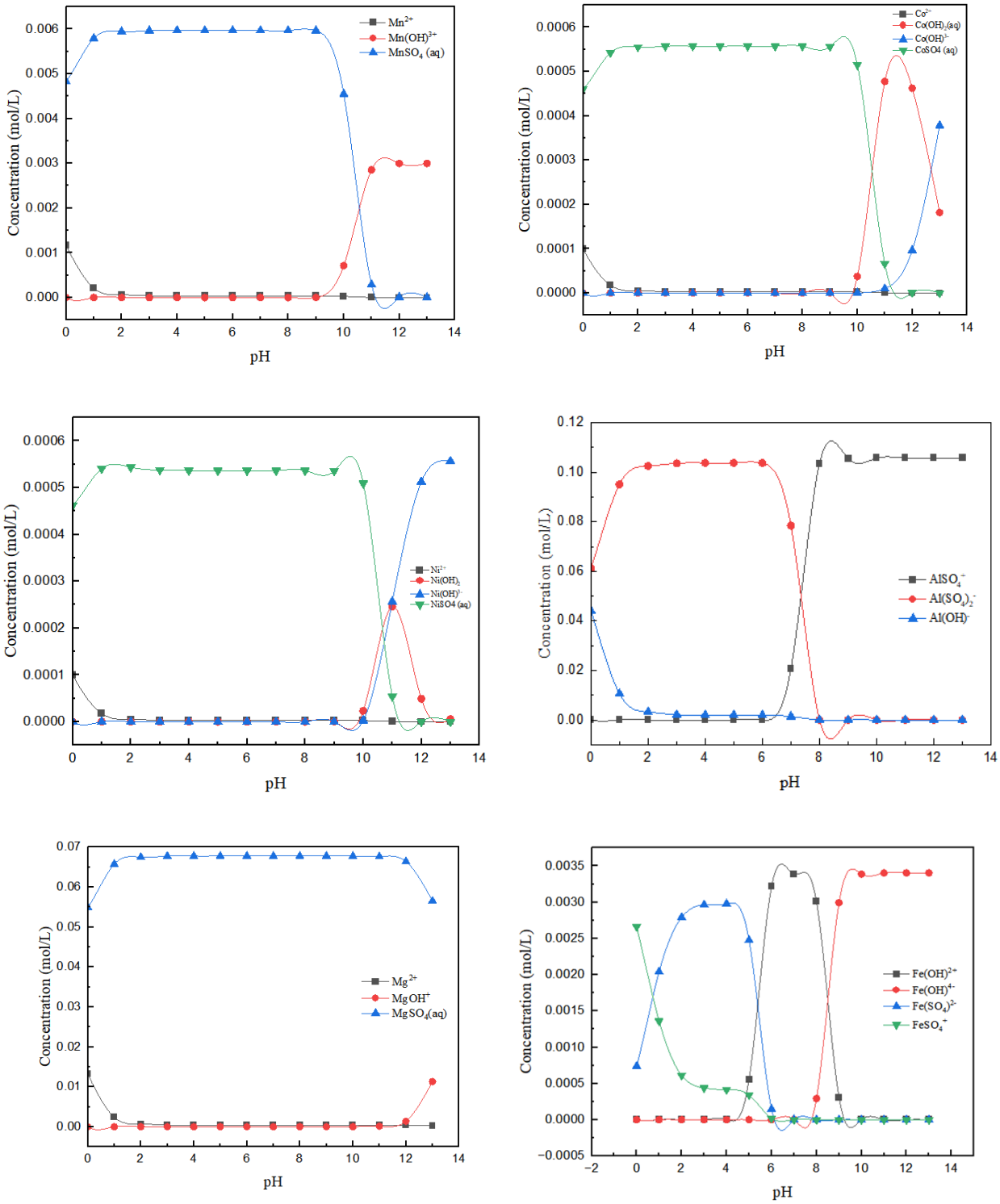

Figure 32. Chemical species distribution diagram of Mn, Co, Ni, Al, Fe, and Mg in NaOH precipitation.

5.1.3 Evaluation of precipitation with sodium hydroxide in the separation of impurities from CMs

To assess the selectivity generated by different precipitants, sodium sulfide (Na_2S) was also tested under the same conditions as the tests performed with sodium hydroxide, but the concentration of Na_2S was changed to 1M due to the sensitivity in pH changes with this chemical (Zhang & Honaker, 2020). During the test, the most remarkable change in the appearance of the solids was the color; at low pH, the color of the solids was dark, and at high values, they became clearer. The removal of impurities was similar to the values obtained with NaOH. However, almost all cobalt and nickel were precipitated with aluminum, iron, phosphorus, and other impurities. Around 40% of the manganese was also precipitated. The following Figure shows the solids obtained at different pH values.

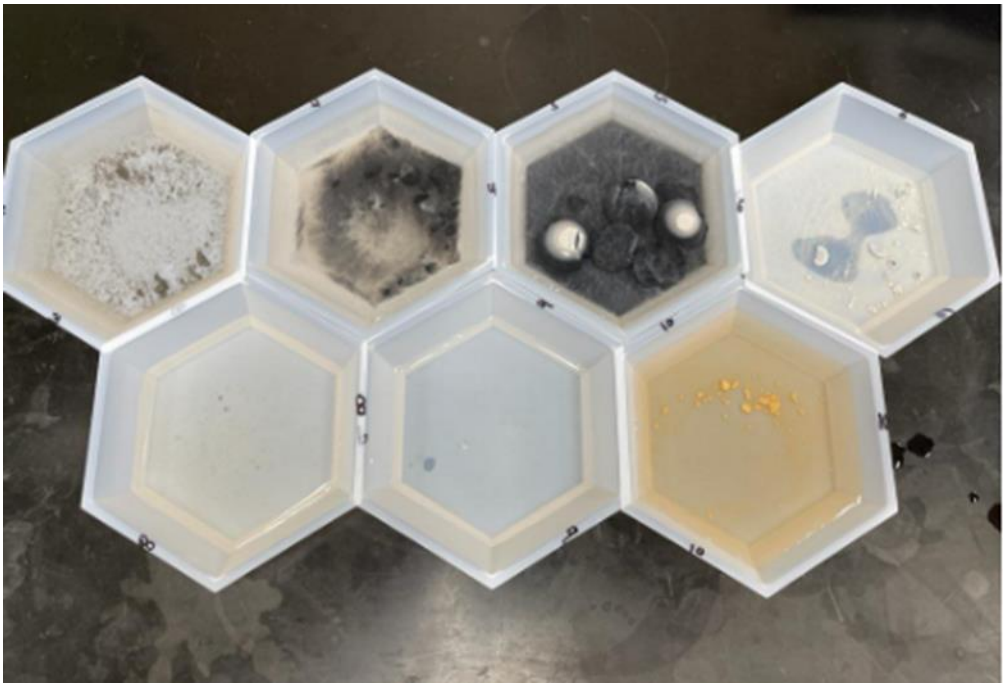

Figure 33. Solids generated throughout Na2S stage precipitation at pH 2-11.

The data obtained from the ICP-MS analyses are shown in Tables 18 and 19. According to the elemental composition of the liquid samples obtained, at a pH value of 5, the elements, with the highest precipitation were aluminum with a percentage value of 98.23%, along with 97.94% of phosphorus, 93.08% of iron, 96.35% of cobalt, and 98.27% of nickel; other elements such as manganese and zinc were precipitated with values of 37.82% and 62.43%, respectively. The concentration and cumulative precipitation data at each pH set-point evaluated are shown below.

Table 19. ICP-MS characterization of the filtrate samples generated with 1M Na2S stagewise precipitation from pH 2 to 11.

Filtrate composition from stagewise precipitation at different pH values (mg/l).									
Element	**pH**								
	2	**3**	**4**	**5**	**6**	**8**	**9**	**10**	**11**
Mg	2,475.16	2,350.07	1,848.00	1,459.00	1,409.53	1,449.25	1,434.24	1,405.65	246.62
Al	4,601.84	4,323.18	3,421.45	70.53	94.51	80.52	96.75	83.10	7.00
Si	171.28	167.36	140.61	37.85	38.60	36.01	39.20	20.04	17.57
P	65.21	59.82	45.38	1.16	1.76	0.68	1.78	4.67	4.01
K	26.00	34.91	36.71	17.04	16.95	18.08	20.48	10.34	10.44
Ca	42.63	37.57	32.80	24.97	26.42	25.38	24.97	21.82	23.88
Fe	315.20	338.00	561.70	34.26	68.60	29.11	29.44	123.72	3.21
Mn	364.73	344.47	269.64	196.06	188.62	190.73	186.26	57.86	0.22
Co	41.35	37.23	9.40	1.31	1.36	1.22	1.23	0.81	0.82
Ni	73.16	66.19	17.92	1.09	0.72	0.53	0.57	0.00	0.00
Zn	23.69	1.77	0.89	0.56	0.84	0.57	19.72	0.00	0.00
TREE	3.63	3.60	3.02	2.63	2.21	1.53	1.53	5.86	5.78

Table 20. Cumulative percentage of different elements precipitated during 1 M Na2S stage-wise precipitation.

	Cumulative Precipitation %								
pH	2.2	3.1	3.94	5	6.12	7.7	8.97	9.96	10.94
Mg	0.00	7.62	14.59	**31.82**	32.95	32.95	37.16	43.45	90.19
Al	0.00	8.59	14.95	**98.23**	97.58	98.05	98.05	98.46	99.87
Si	0.00	0.00	1.22	**73.11**	72.09	75.30	75.30	88.41	88.41
P	0.00	10.75	20.39	**97.94**	97.94	99.24	99.24	99.24	99.36
K	0.00	0.00	0.00	**53.06**	52.49	52.49	52.49	52.49	52.58
Ca	0.00	0.00	0.00	**23.03**	23.03	29.87	34.67	47.58	47.58
Fe	0.00	0.00	0.00	**93.83**	93.83	97.52	97.62	97.62	99.94
Mn	0.00	8.11	15.43	**37.82**	39.11	41.60	46.00	84.60	99.94
Co	0.00	12.39	74.00	**96.35**	96.13	96.71	96.86	98.10	98.09
Ni	0.00	11.97	71.98	**98.27**	98.84	99.20	99.17	100.00	100.00
Zn	0.00	0.00	40.96	**62.43**	62.43	75.88	100.00	100.00	100.00
TREE	0.00	0.00	0.00	**11.90**	24.81	50.49	53.06	53.06	54.21

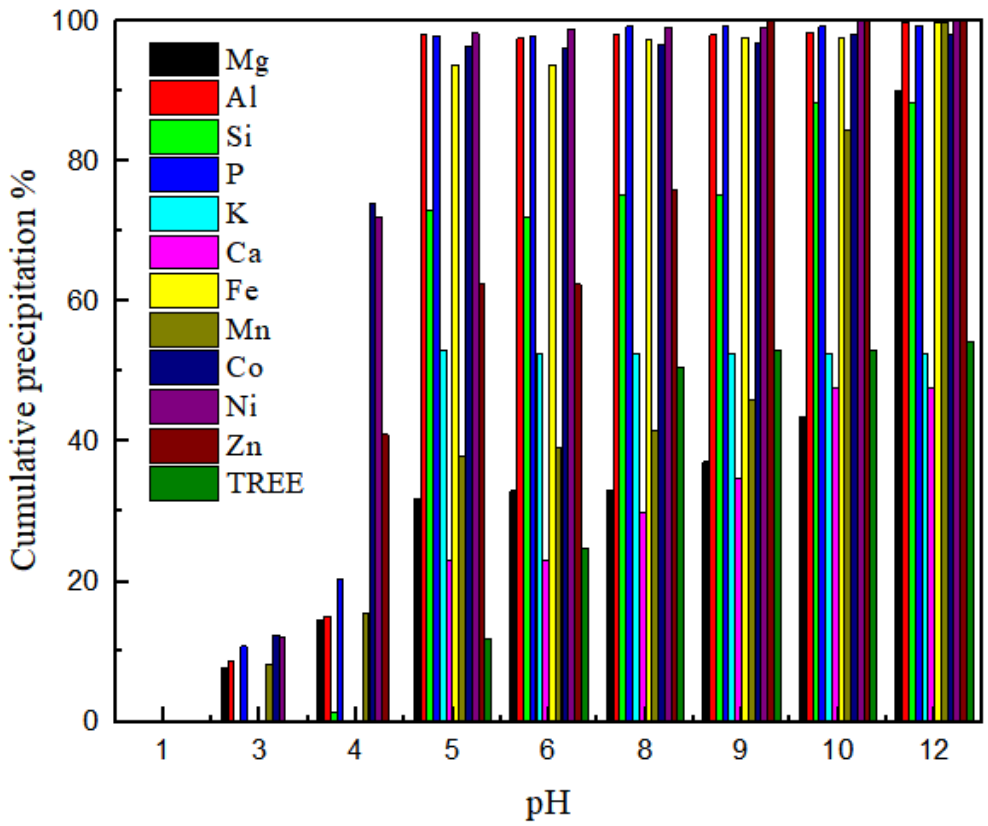

Figure 34. Cumulative precipitation of various elements for stagewise precipitation with 1M Na2S.

Both sodium hydroxide and sodium sulfide generated promising results in removing aluminum, iron, and other impurities, with removal percentages over 95%. In the case of NaOH, critical minerals were separated from impurities. The remaining filtrate solution generated a concentration of 25 mg/l, 266 mg/l, and 39 mg/l was generated for cobalt, manganese, and nickel, respectively. Cobalt, manganese, and nickel concentrations were 1.31 mg/l, 196 mg/l, and 1.09 mg/l, separately, in the filtrate generated at pH 5 with Na_2S. Sodium sulfide could separate manganese from the impurities, with cobalt and nickel co-precipitated. For the primary objective of this stage, this chemical does not qualify to be used in the process. Still, it could selectively extract manganese in future steps or optimize the process to remove impurities simultaneously.

5.2 Nitric acid dissolution

The solids obtained during NaOH precipitation in the pH range of 5 to 10 with valuable amounts of Co, Ni, and Mn were subjected to a nitric acid dissolution process to enhance manganese purity. In general, the experiment successfully removed impurities and increased the purity of the

elements, as is the case of manganese, where the element purity was increased from 2.77 wt.% to 46.99 wt.%. Cobalt and nickel slightly decreased in their percentage by weight values, corresponding to a grade of 0.6 wt.% and 0.24 wt.%, respectively. During the process, around 94% of the initial mass was dissolved into the nitric acid, generating low quantities of solids and the need to perform the tests repeatedly to generate enough solids for analysis. Based on the elemental composition of the dissolved solution, this procedure was reliable for the selective manganese extraction.

Figure 35. Manganese solid product with a purity of 46.99 wt.% generated during HNO3 dissolution.

The procedure described above generated two products: one was the solution with the elemental concentration shown below (Table 21), which was later used to perform a Na_2S precipitation to separate different CMs present in the solution. The other product was a solid concentrate containing 46.9 wt.% of manganese. The elemental compositions provided by ICP-MS analysis of the remaining solids and dissolved solution are shown below.

Table 21. ICP-MS characterization of the dissolved solution with HNO3.

Element	Concentration (mg/L)
Na	12,738.36
Mg	2,437.21
Al	477.72
Si	410.77
P	5.40
K	31.88

Ca	55.39
Sc	0.01
Ti	0.42
Fe	19.68
Mn	2,053.40
Co	393.02
Ni	619.87
Cu	5.21
Zn	225.18
TREE	15.5

Table 22. ICP-MS characterization of the solid concentrate post HNO3 washing.

Element	Concentration (mg/Kg)	wt. %
Na	8,580.0554	0.86
Mg	2,396.6066	0.24
Al	419.87535	0.04
Si	6,820.741	0.68
P	200.20776	0.02
K	193.3518	0.02
Ti	13.054017	0.00
Cr	5.2285319	0.00
Fe	210.04155	0.02
Mn	469,913.43	46.99
Co	5,989.4737	0.60
Ni	2,373.9612	0.24
Cu	28.878116	0.00
Zn	4,313.0194	0.43
TREE	691.6	0.07

5.3 Na_2S stagewise precipitation

Once most of the manganese was separated from the solids produced in NaOH precipitation through the nitric acid dissolution process, the solution remaining with Co and Ni as the main elements to be separated was subjected to a 3-stage precipitation process using 1M sodium sulfide (Na_2S). The solids obtained from the 3-stage precipitation showed promising results regarding the

potential separation of Ni, Co, Mn, and Mg. In the pH range of 1 to 5, the concentration of Ni and Co in the precipitated solids were 8.35 wt.% and 5.25 wt.%, respectively; However, aluminum also existed with a concentration of 4.27 wt.% in the precipitates. When the pH was increased to a high range of 5-10, a solid with a Mn grade of 20.15 wt.% was generated, indicating a new stream in the process for Mn extraction. Finally, an Mg concentrate was obtained at pH 10-12, with a purity of 27.49% wt.%. The ICP-MS characterization of the solids is shown in Table 23.

Table 23. ICP-MS characterization of solids generated from the three-stage Na2S precipitation.

Elemental composition of solids at different pH values (mg/kg)						
Element	pH 1-5	Wt. %	pH 5-10	Wt. %	pH 10-12	Wt. %
Na	86,679.39	8.67	112,989.17	11.30	96,340.96	9.63
Mg	2,746.48	0.27	23,343.90	2.33	274,850.24	27.49
Al	44,148.99	4.41	1,879.66	0.19	268.59	0.03
Si	3,923.31	0.39	7,439.58	0.74	5,821.73	0.58
P	167.61	0.02	49.42	0.00	129.73	0.01
Sc	0.08	0.00	0.00	0.00	0.00	0.00
Cr	2,957.74	0.30	49.99	0.00	0.00	0.00
Fe	12,202.95	1.22	215.20	0.02	0.00	0.00
Mn	15,605.02	1.56	201,452.24	20.15	915.17	0.09
Co	50,758.91	5.08	13.36	0.00	0.00	0.00
Ni	80,183.40	8.02	42.87	0.00	93.78	0.01
Cu	722.52	0.07	0.00	0.00	0.00	0.00
Zn	50,458.63	5.05	0.00	0.00	0.00	0.00
TREE	0.00	0.00	2,271.43	0.23	13.53	0.00

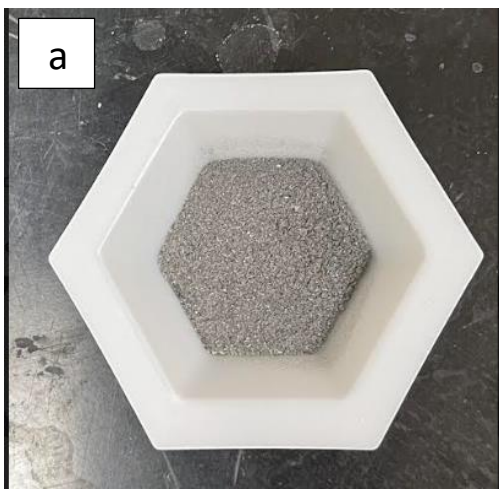

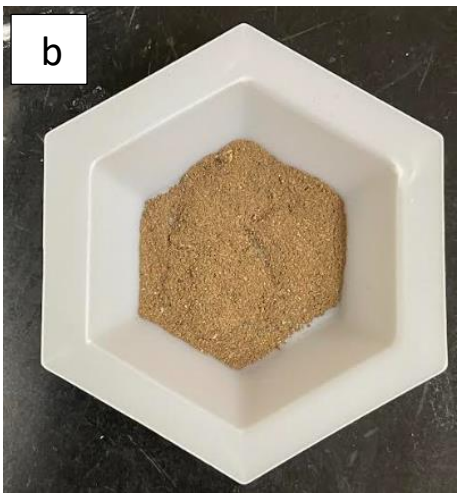

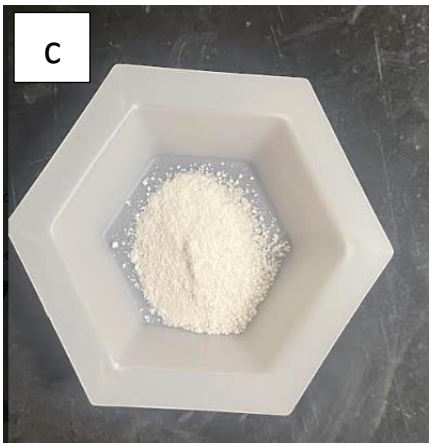

Figure 36. Ni and Co concentrate with a purity of 8.35 wt.% and 5.25 wt.%, respectively (a). Mn concentrates with a purity of 20.15 wt.% (b) Mg concentrates with a purity of 27.49% wt.% (c).

5.3.1 Comparing experimental data to simulation outcomes in Na_2S precipitation.

Validation of the results obtained by the experimental section was made by using Visual MINTEQ 3.1 to generate the species distribution diagrams and calculate the saturation indexes of the chemical species, as shown in Table 24 and Figure 37. According to the experimental section from pH 1 to 5, most of the cobalt and nickel compounds were precipitated; this fact can be validated by the software where, based on the simulation, cobalt and nickel compounds are precipitated at pH 5, including CoS (alpha), CoS (beta), NiS (alpha), and NiS (beta). Moreover, at a pH range of 5 to 10, manganese sulfide (MnS) is likely precipitated. The third stage, which was performed between pH values of 10 and 12, produced a solid product of magnesium with a purity of 27.49 wt. %. According to the software simulation, the solid species likely to appear at this pH region are pyrochroite ($Mn(OH)_2$) and spinel ($MgAl_2O_4$). Spinel appears at both pH 10 and 12, indicating that this element starts to format a pH value close to 10. The saturation indexes at each pH value are shown below.

Table 24. Simulation of the 1M Na2S stagewise precipitation with Visual MINTEQ 3.

Mineral	Saturation Index at pH 5	Saturation Index at pH 10	Saturation Index at pH 12
Al(OH)3 (am)	0.915	-0.322	-2.322
Al(OH)3 (Soil)	3.425	2.188	0.188
Al2O3(s)	3.777	1.303	-2.697
Boehmite	3.137	1.9	-0.1
Brucite	-8.868	1.019	4.45
Co(OH)2 (am)	-9.148	-1.179	2.473
Co(OH)2 (c)	-8.344	-0.375	3.277

CoO(s)	-9.64	-1.671	1.98
CoS (alpha)	4.337	9.315	10.969
CoS (beta)	8.637	13.615	15.269
Diaspore	4.842	3.605	1.605
Gibbsite (C)	3.975	2.738	0.738
Mg(OH)2 (active)	-10.562	-0.675	2.756
MgS(s)	-16.477	-9.581	-8.148
MnS (grn)	-2.182	2.818	4.579
MnS (pnk)	-5.182	-0.182	1.579
Ni(OH)2 (am)	-9.048	-2.345	1.26
Ni(OH)2 (c)	-6.948	-0.245	3.36
NiS (alpha)	2.332	6.045	7.652
NiS (beta)	7.832	11.545	13.152
NiS (gamma)	9.532	13.245	14.852
Periclase	-13.352	-3.465	-0.034
Pyrochroite	-10.366	-2.375	1.383
Spinel	-5.186	2.227	1.658

5.3.2 Evaluation of precipitation with sodium sulfide in the separation of impurities from CMs

Like NaOH precipitation, the chemical species distribution diagrams were built using Visual MINTEQ 3.1 to identify the species formed during the reactions. However, iron was not considered for this process due to the concentration in the initial solution was as low as 1 ppm. According to the simulation, manganese, cobalt, and nickel predominantly exist as divalent ions at low pH values. Through pH 2 to 4, hydrogen sulfide components start to appear in the solution, which indicates that divalent species disappear to favor the formation of hydrogen sulfides such as $MnHS^+$, $CoHS^+$, and $NiHS^+$. cobalt-nickel hydrogen sulfide compounds begin to decrease their concentration in the aqueous solution at pH 8. On the other hand, the content of $MnHS^+$ starts to decrease around pH 11. After pH 8, cobalt turns into a cobalt hydroxide ($Co(OH)_2$, nickel had the same behavior but multiples species being formed at this pH as shown in Figure 37. Mn also transforms into a hydroxide product after pH 11, suggesting that hydroxide species of the three elements appear under high alkaline conditions. Under the conditions established in the simulation, aluminum presented multiple hydroxide species across the entire pH range, where the highest reaction activity was seen between pH 4 and 6. After pH 6, the predominant species was $Al(OH)_4^-$, which had a constant concentration after reaching pH 7.5. Nitrate magnesium species are dominant in acidic conditions, which start turning into magnesium hydroxides at pH 8 and become the predominant species under alkaline conditions. The corresponding chemical species diagrams are shown in the following figure.

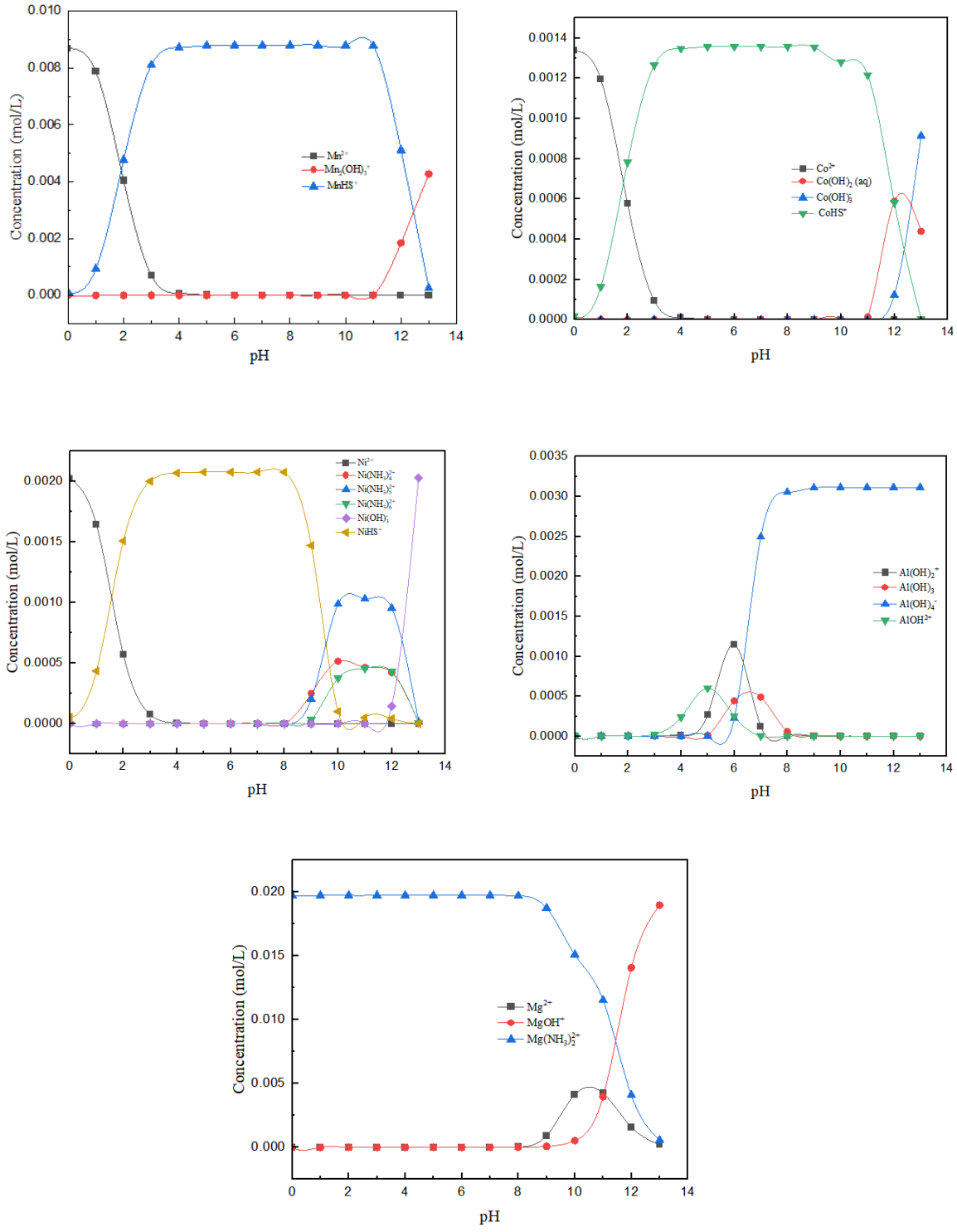

Figure 37. Chemical species distribution diagrams of Mn, Co, Ni, Al, and Mg in Na2S precipitation.

5.4 HCl dissolution

The dissolution of the Co-Ni concentrate generated in the previous stage was further subjected to a redissolution test with hydrochloric acid to transfer the elements into dissolved ions. Solid redissolution was tested at different acid concentrations to determine which provided a better dissolution rate and favorable elemental composition for subsequent oxidative precipitation. Two different tests were conducted in this stage: one used an acid concentration of 2M, and the other one used a concentration of 4M. The test with 2M HCl resulted in a total mass dissolution of 97.59%. However, the experiment with 4M HCl had a total dissolution of 85%, which was not expected. The experiment was repeated to validate the results, and the dissolution rate was similar. Even though this is an unexpected result, the phenomenon can be attributed to the reaction of the products where new species may be formed at the given acid concentration. The elemental composition of the dissolved solutions from the two tests is shown below.

Table 25. ICP-MS characterization of the dissolved solution at different HCl concentrations.

Element	Concentration (mg/l)	
	4 M (84%)	**2M (98%)**
Na	1,536.40	4,995.20
Mg	51.60	1020.60
Al	385.60	172.00
Si	69.00	121.60
P	2.40	1.00
K	2.00	2.20
Ca	11.80	19.00
Sc	0.00	0.00
V	0.02	0.00
Cr	4.80	0.00
Fe	25.40	0.80
Mn	102.40	973.40
Co	243.40	206.00
Ni	490.20	338.80
Cu	0.40	5.00
Zn	351.80	149.60
Y	0.02	0.04
Nb	0.04	0.00
La	0.74	5.34
Ce	0.75	4.84
Pr	0.09	0.53
Nd	0.32	1.80
Sm	0.02	0.10

Eu	0.00	0.01
Gd	0.01	0.06
Dy	0.00	0.11
Yb	0.00	0.00

According to the result shown in Table 25, the test with 4M HCl produced a better redissolution of the main elements since Mn remained in the solid residue, providing a purer solution in terms of Co and Ni concentrations. The corresponding Co and Ni contents were 243 mg/l and 490 mg/l, respectively. In contrast, 2M HCl produced 206 mg/l of Co and 338 mg/l of Ni in the solution. The most significant difference was seen in the concentration of Mn. A content value of 102.4 mg/l was generated by 4 M HCl, considerably lower than 973.4 mg/l of Mn obtained from 2 M HCl. Therefore, 4M HCl was selected as the acid to redissolve the solid preconcentrate for Co and Ni extraction. During this procedure, two products were generated: a dissolved solution containing Co and Ni as the main elements and others with a lower amount, such as Mn and Al, and a precipitated solid with approximately 9.92 wt. % Co, 10.93 wt.% Ni, and 0.28 wt.% Mn. The elemental composition of the solid is shown in the following table.

Table 26. ICP-MS characterization of the solid generated from 4 M HCl redissolution.

Element	Concentration (mg/kg)	wt. %
Na	6,389	0.64
Mg	294	0.03
Al	1,625	0.16
Si	2,635	0.26
P	406	0.04
Ti	17	0.002
Cr	254	0.03
Fe	6,592	0.66
Mn	2,773	0.28
Co	99,196	9.92
Ni	109,353	10.94
Cu	2,037	0.20
Zn	2,943	0.29
Y	1	0.0001
La	7	0.0007
Ce	8	0.0008
Pr	1	0.0001
Nd	4	0.0004

5.5 Oxidative precipitation

Targeting the selective recovery of cobalt and nickel, the solution obtained from HCl dissolution was subjected to oxidative precipitation with ozone, which was carried out in an ozone reactor where the solution was heated at 85 Celsius degrees, stirred at 350 RPM, and injected with ozone in a rate of 1 L/h for 2 hours. Replicate experiments with an initial volume of 500 ml using the raffinate solution were conducted to generate approximately 170 ml feedstock solution to carry out ozone precipitation. The following table shows the solution produced during the hydrochloric acid dissolution test.

Due to the large amount of volume needed to generate enough feedstock for oxidative precipitation and the limited amount of raffinate solution generated in the REE extraction process, the decision was made to use the remaining solution from nitric acid washing, which had an elemental composition (Table 27) close to the solution generated after hydrochloric acid dissolution. This procedure was targeted to evaluate the behavior of the elements of interest in the solution under the conditions established for ozone oxidative precipitation. The solutions were similar in terms of Co, Ni, Al, and Fe concentrations. For example, approximately 393.02 mg/l of Co, 629.87 mg/l of Ni, 477.72 mg/l of Al, and 19.68 mg/L Fe were seen in the nitric acid washing solution. At the same time, the content was 243.2 mg/l, 490.4 mg/l, 386.6 mg/l, and 25.4 mg/l, respectively, for hydrochloric acid redissolved solution. The biggest difference between the solutions is the concentration of Mn and Mg, which was 2053.4 mg/l of Mn and 2437. 21 mg/l of Mg in nitric acid washing solution. In contrast, the dissolved solution with hydrochloric acid had lower concentrations, equivalent to 102.4 mg/l of Mn and 385.6 mg/l of Mg.

Table 27. ICP-MS characterization of the remaining solution from nitric acid washing.

Element	Concentration (mg/l)
Na	12,738.36
Mg	2,437.21
Al	477.72
Si	410.77
P	5.40
K	31.88
Ca	55.39
Sc	0.01
Ti	0.42
Fe	19.68
Mn	2,053.40
Co	393.02
Ni	619.87
Cu	5.21
Zn	225.18
Y	0.26

Ba	2.01
La	5.92
Ce	4.62
Pr	0.55
Nd	1.85
Sm	0.12
Eu	0.02
Gd	0.09
Dy	0.04
Er	0.02
Yb	0.01
Th	0.02
U	0.01

5.5.1 Parametric evaluation of oxidative precipitation

Therefore, nitric acid washing solution from the previously established step was used as the feedstock for the subsequent ozone oxidization tests. Three different pretreatment periods corresponding to 30 minutes, 60 minutes, and 120 minutes were applied following the other parameters shown in Table 10 to investigate the effect of pretreatment/oxidization time. In addition to the pretreatment time, the precipitation kinetics were also studied in the experiments to identify the optimum time to remove the solid from the solution and enhance the process selectivity. The evaluation was carried out by taking samples at different times throughout two hours once pH 5 was reached, including the 15^{th} min, 30^{th} min, 45^{th} min, 60^{th} min, and 120^{th} min.

The results obtained from the three different experiments are summarized in Tables 28 and 29. Figure 39 shows the recovery of the main elements in the solution at different pretreatment times. According to these data, the selective extraction of Ni from Mn and Co was not successful. Most nickel was precipitated with cobalt and manganese with various recovery values at different pretreatment times. At 30 minutes of pretreatment, the Mn, Co, and Ni recovery values were 31.09%, 29.60%, and 33.33%, respectively. The recovery values were 25.68% for Mn, 24.43% for Co, and 25.46% for Ni following the 60-min pretreatment. Finally, at 120 minutes of ozone pretreatment, the recovery values of these elements were equal to 67.33%, 98.61%, and 98.48% for Mn, Co, and Ni, respectively. Ozone oxidative precipitation tends to increase the precipitation rate of the elements when the solution has long exposure to ozone. However, this method could not achieve selectivity between Mn, Co, and Ni. One possible parameter that could affect the experiment's performance is the acid media used. The experiment was performed using nitric acid, contrary to the experiment developed by Z.T. Ichlas (2020), which was carried out using sulphuric acid. However, in the same study, the researchers reported that similar studies performed by other researchers had significant variations in the separation of these target elements.

Table 28. ICP-MS characterization of the remaining solution in oxidative precipitation at different pretreatment times.

Element	Concentration (mg/L)		
	30 min	60 min	120 min
Na	11,485.60	13,190.91	11,759.80
Mg	341.68	387.70	295.21
Al	23.74	25.01	2.14
Si	34.16	48.18	23.23
P	0.72	1.57	1.18
K	6.49	37.56	11.64
Ca	16.30	23.66	19.83
Ti	0.28	0.31	0.00
Fe	1.90	2.00	0.00
Mn	258.66	351.92	113.12
Co	43.37	82.71	0.79
Ni	64.13	125.13	1.38
Cu	0.91	1.17	0.00
Zn	54.58	227.00	0.71
Sr	0.29	1.78	0.64
Y	0.02	0.02	0.00
Ba	0.00	0.22	0.00
La	1.00	3.57	0.01
Ce	0.65	3.33	0.01
Pr	0.08	0.42	0.00
Nd	0.26	1.45	0.00
Sm	0.01	0.06	0.00
Eu	0.00	0.01	0.00
Gd	0.01	0.03	0.00

Table 29. ICP-MS characterization of the solids generated from oxidative precipitation at different pretreatment times.

Element	Concentration (mg/L)			Wt. %		
	30 min	60 min	120 min	30 min	60 min	120 min
Na	150,549.39	132,334.12	117,707.07	15.055	13.233	11.771
Mg	5,667.70	4,581.59	32,591.55	0.567	0.458	3.259
Al	55,424.43	77,124.10	25,864.53	5.542	7.712	2.586
Si	7,551.28	9,113.50	10,261.59	0.755	0.911	1.026
P	258.88	386.82	204.36	0.026	0.039	0.020
K	0.00	401.50	0.00	0.000	0.040	0.000

Ca	0.00	97.34	0.00	0.000	0.010	0.000
Sc	0.76	2.05	0.00	0.000	0.000	0.000
Ti	62.24	144.29	0.00	0.006	0.014	0.000
Cr	279.18	69.79	0.00	0.028	0.007	0.000
Fe	1,685.63	3,532.87	1,592.15	0.169	0.353	0.159
Mn	36,859.78	25,393.69	74,896.90	3.686	2.539	7.490
Co	4,892.39	3,319.39	20,664.58	0.489	0.332	2.066
Ni	15,189.60	7,735.12	33,131.40	1.519	0.774	3.313
Cu	18,282.51	6,725.70	4,808.04	1.828	0.673	0.481
Zn	19,719.66	26,468.39	65,796.56	1.972	2.647	6.580
Sr	0.00	24.55	0.00	0.000	0.002	0.000
Y	18.76	29.71	7.36	0.002	0.003	0.001
Nb	0.00	25.35	0.00	0.000	0.003	0.000
Ba	0.00	17.96	0.00	0.000	0.002	0.000
La	406.85	588.28	636.82	0.041	0.059	0.064
Ce	1,131.81	2,425.30	795.20	0.113	0.243	0.080
Pr	120.42	190.08	91.52	0.012	0.019	0.009
Nd	461.11	777.09	338.91	0.046	0.078	0.034
Sm	51.10	76.99	27.99	0.005	0.008	0.003
Eu	8.62	11.65	4.22	0.001	0.001	0.000
Gd	33.05	40.58	16.44	0.003	0.004	0.002
Tb	1.89	2.91	0.82	0.000	0.000	0.000
Dy	5.83	12.12	2.45	0.001	0.001	0.000
Ho	0.76	1.60	0.00	0.000	0.000	0.000
Er	1.32	3.16	0.44	0.000	0.000	0.000
Tm	0.00	0.30	0.00	0.000	0.000	0.000
Yb	0.54	1.39	0.00	0.000	0.000	0.000
Lu	0.00	0.15	0.00	0.000	0.000	0.000
Th	1.04	230.56	1.70	0.000	0.023	0.000
U	1.56	0.65	0.58	0.000	0.000	0.000

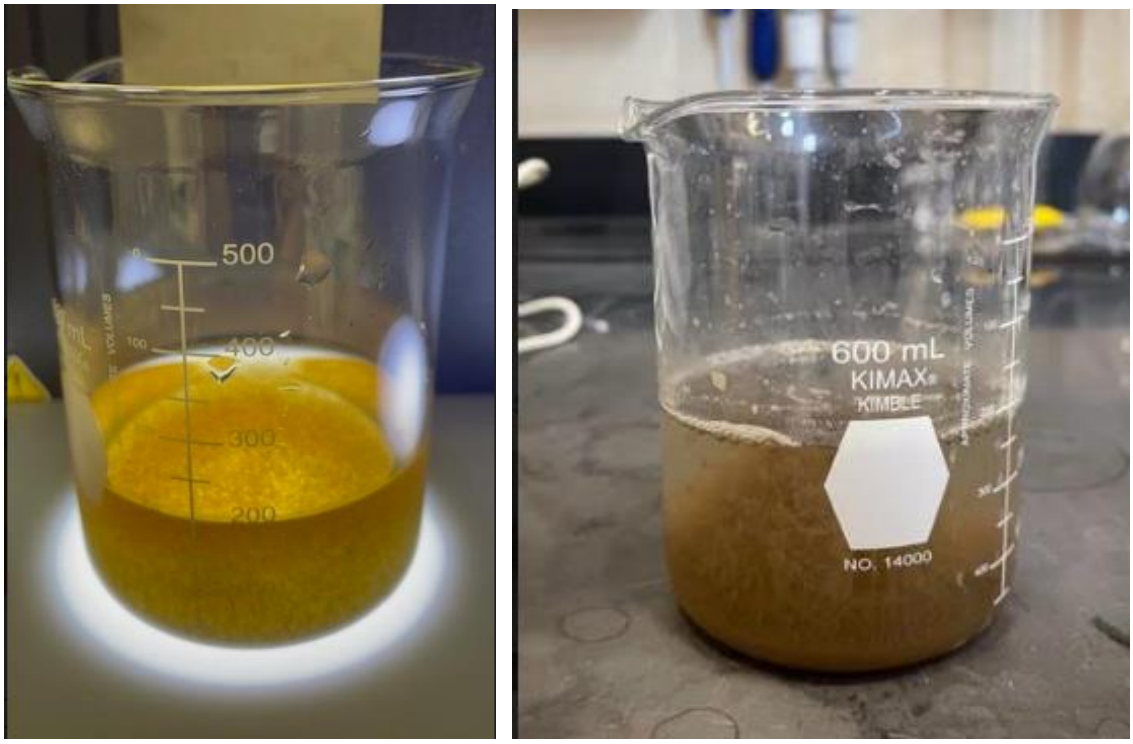

Figure 38. Solids produced at pH 5 in the oxidative precipitation process using NaOH (two hours pretreatment).

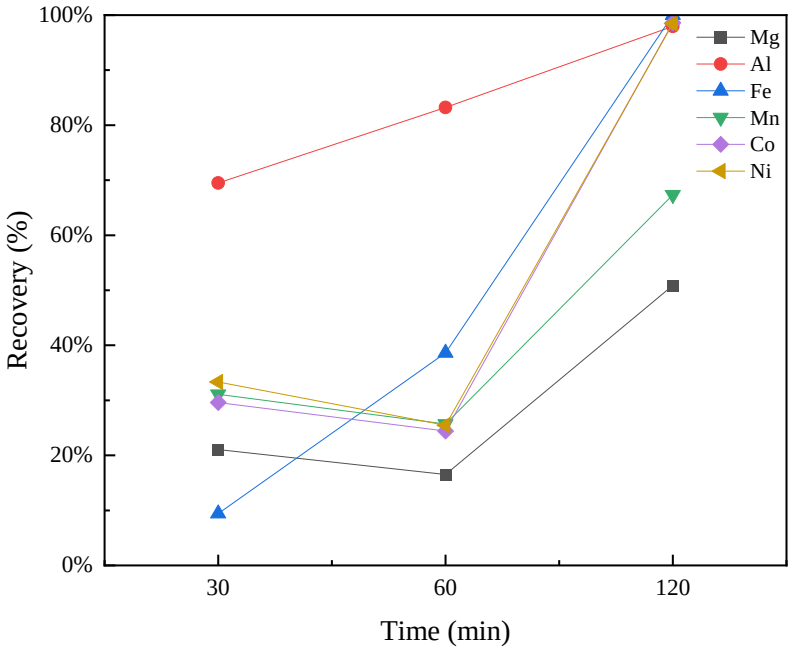

Figure 39. Recovery of the main elements in the precipitation of the pretreated solution with ozone at different pretreatment times.

As mentioned above, the precipitation kinetics were also evaluated in two of the three experiments by taking samples at different times for the two-hour precipitation time. Figures 36 and 37 show the concentration of the main elements in the solution as a function of time after reaching pH 5. During the period evaluated (i.e., two hours), the concentration values were relatively constant, which suggests that solid precipitation occurred during the first 15 minutes, and the extension of precipitation time beyond 15 minutes did not increase the solid recovery values. In addition, a higher concentration of Mg and Mn was also seen compared to other elements such as Ni, Co, and Al.

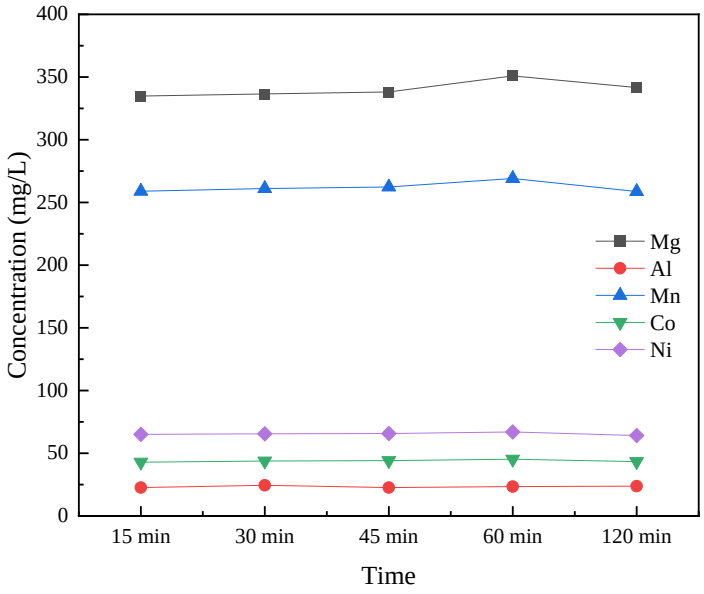

Figure 40. Kinetic behavior of CMs in the NaOH precipitation after 30 min ozone pretreatment.

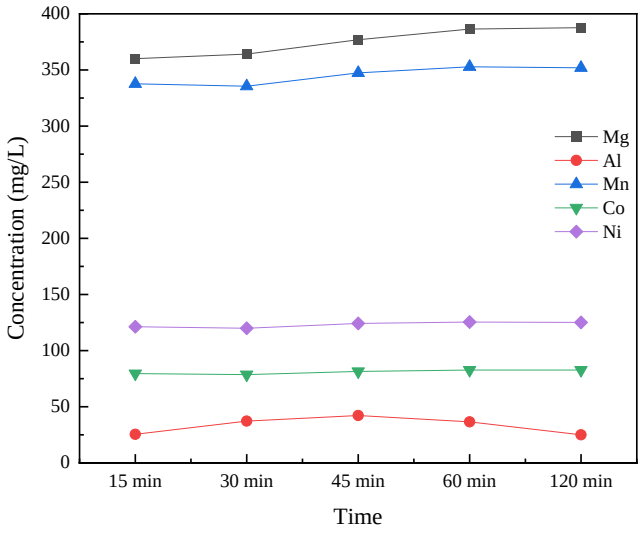

Figure 41. Kinetic behavior of CMs in the NaOH precipitation after 60 min ozone pretreatment.

New tests were performed using sulfuric acid (H_2SO_4) and hydrochloric acid (HCl) that aimed to improve the process selectivity. The experiments were run under similar conditions to the experiment performed with the nitric acid media to evaluate the influence of the acid environment

on the experiment. After performing the tests, the results obtained were not satisfactory because the recovery of nickel in the sulfuric acid test was 27.3%, while cobalt and manganese were 27.4% and 37%, respectively. This indicates that the elements remained in the solution after the initial precipitation. On the other side, the recovery of CMs in the hydrochloric acid tests was 9%, 8.45, and 16.6% for Mn, Co, and Ni, respectively. The values obtained in both experiments can be seen in the appendix section.

Many factors were involved in the oxidation process, including temperature, stirring speed, ozone rate, acid media, elemental concentration, reaction time, and precipitation pH, which could affect the process and did not provide a satisfactory separation result. One of the main factors contributing to the failure of the experiment could be the original feedstock regarding the concentration of nickel. The experiment carried out by Ichlas et al. 2020 used an industrial mixed hydroxide precipitate (MHP) as the feedstock, which originated from a laterite sample with a corresponding Ni concentration of 45 wt.%. During the study, the researchers were able to separate nickel from manganese and cobalt by oxidative precipitation, obtaining a solution with 43.8 g/l of Ni, 0.001 mg/l of cobalt, and 0.0001 g/l of manganese. The solution used in this research had a concentration of 619 mg/l, which was a significantly lower concentration that may affect the result. Even though the composition of both solutions was similar in terms of Co, Mn, Fe, Ni, and Al elements, the higher content values of nickel in the MHP could allow a high interaction between Ni ions and ozone. This fact is also related to the exposure time to oxidation and the ozone rate applied to the elements. Due to the low nickel concentration in the solution, these factors must be modified in order to achieve complete nickel oxidation.

5.6 Solvent extraction

5.6.1 Effect of the feed pH

The separation of cobalt from nickel present in the HCl dissolved solution was carried out by solvent extraction by adjusting experimental parameters such as O: A ratio, extraction time, extractant concentration, feed pH, and equilibrium pH. To evaluate the effect of the pH on the extraction of cobalt, the experiment was initially run by varying the feed pH from 4 to 5 while keeping O: A ratio equal to 1:1, extractant concentration of 0.5 M, extraction time equivalent to 20 min, and a measured equilibrium pH of 7.5. Based on the results shown in Figure 42 and Table 31, the process was able to extract the elements from the feed solution but could not separate cobalt from nickel, which indicates that the feed pH does not have a significant influence on the separation of the elements. The recovery percentage presented in Table 31 indicates that around 99 % of cobalt, manganese, and nickel were extracted to the organic solution along with other impurities, including magnesium and aluminum, while iron remained in the feed solution in the three test run. In order to evaluate the behavior of the CMs and impurities, the feed used in the first run of the experiment corresponded to a solution created from the solids generated in the pH 5-10 NaOH precipitation, which were diluted in a chloride solution to obtain similar conditions to the original SX-feed solution shown in Table 26; this solution contained less amount of critical

minerals and impurities including magnesium. Table 30 shows the elemental characterization of feed and raffinate solutions used in these experiments.

Table 30. ICP-MS characterization of the feed and raffinate solutions at different feed pH values.

Element	Concentration (mg/L)					
	Feed 4	Raffinate (F. pH 4)	Feed 4.5	Raffinate (F. pH 4.5)	Feed 5	Raffinate (F. pH 5)
Na	9886.8	6446	10255.4	6215.2	12274.8	6601
Mg	295.6	5	301.8	5.2	283.8	6
Al	37.2	9.6	23.4	8	12.6	9.6
Si	153	141.2	153.4	139	151.2	119.8
P	3.2	385.8	3	417.2	1.4	378
K	9.4	8.4	11.2	8.8	9.6	13.4
Ca	21.2	25.8	20	29.2	17.8	30.2
Ti	1.4	1.4	1.4	1.4	0	1.4
Cr	0.12	0.12	0.12	0.1	0	0.12
Fe	2	2	2	2	1	2.2
Mn	305.6	1	310.4	1	158.4	1.2
Co	50.6	0	51.4	0	32.8	0
Ni	82.8	0.4	83.4	0.4	47.6	0.4
Cu	0.6	0.2	0.6	0.2	1	0.2
Zn	53.4	1.4	54.4	1.4	38.2	1.6
Ga	0.2	0.2	0.2	0.2	0	0

Table 31. Metal recovery percentages of the SX test runs at different feed pH values.

Element	Recovery %		
	Feed 4	Feed 4.5	Feed 5
Al	74.71%	66.50%	25.33%
Mg	98.34%	98.31%	97.93%
Fe	2.00%	2.00%	0.00%
Mn	99.68%	99.68%	99.26%
Co	100.00%	100.00%	100.00%
Ni	99.53%	99.53%	99.18%

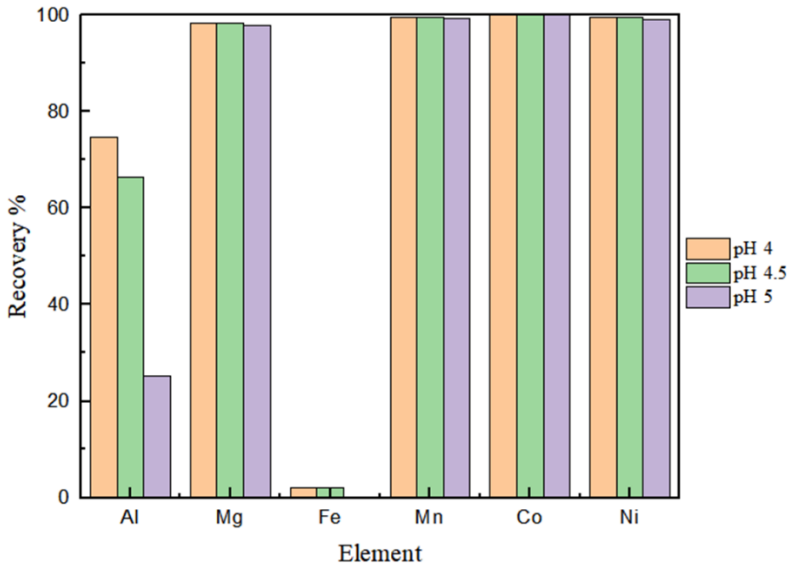

Figure 42. Metal recovery percentages of the SX test runs at different feed pH values.

Even the feed pH within the tested range did not contribute directly to the separation of cobalt and nickel; this factor plays a vital role in the extraction of elements. Swain et al. 2007 investigated the distribution coefficient (D_{SX}) of cobalt, which is related to the stability of the metal species and determines the feasibility of efficient extraction of metals in a solvent extraction process. At the feed pH range of 4 to 6, cobalt extraction varies from 84% to 88%; the study found that the suitable feed pH value for cobalt extraction corresponds to 6. In order to prevent the loss of important minerals, the feed pH value for the experiments designed for this study was set at 5. This choice was based on previous results from NaOH and Na_2S precipitation tests carried out throughout the research.

Table 32. ICP-MS characterization of the SX feed solution after pH adjustment to a value of 5.

Element	Concentration (mg/L)
Na	31,707.72
Mg	34.33
Al	12.19
Si	254.75
P	3.52
K	21.18
Ca	15.79
Sc	0.01

Ti	1.58
Cr	0.78
Fe	4.72
Mn	113.66
Co	62.72
Ni	131.89
Cu	0.33
Zn	135.70
Ga	0.25
Rb	0.08
TREE	0.00

5.6.2 Effect of the equilibrium pH

The separation of cobalt from nickel in the HCl solution was also studied by modifying the equilibrium pH after mixing the 0.5 M Cyanex extractant with the feed solutions. As mentioned above, the feed pH of the solution was set at 5, and the other parameters, such as O: A ratio, and separation time, were kept constant with values of 1:1 and 20 minutes, respectively. After mixing the organic and aqueous solution, the equilibrium pH was raised to approximately 7.5. Based on the information provided by Solvay (2023) and the previous experiment run, Ni and Co are co-extracted after pH reaches 6.5 in chloride solutions, and before pH 3 the extraction percentage is negligible (Table 33). Therefore, the equilibrium pH selected to develop the experiment was 4.7, where most of the cobalt can be extracted along with a low amount of nickel. During extraction, 2M HCl acid was gradually added to the organic-aqueous solution, bringing the pH value down from 7.5 to 4.7 to reach the desired equilibrium pH. Under this controlled condition, the process was able to extract 96 % of cobalt and 10% of nickel into the organic solution. In addition to cobalt, manganese and magnesium were also extracted with an extraction percentage of 92% and 43%, respectively. After the extraction, the organic solution loaded with cobalt, manganese, and other elements was subjected to stripping and the raffinate solution remaining was enriched with nickel and low amounts of other impurities. Figure 43 and Table 34 show the elemental recovery of the solvent extraction process with 0.5 M Cyanex 272.

Table 33. Single extraction of cobalt and nickel with Cyanex 272 in chloride solutions.

Metal	Equilibrium pH	% Extraction
Co	2.8	2%
	3.5	48%

	4.1	87%
	4.4	96%
	5.5	100%
Ni	3.6	0%
	4.9	19%
	5.2	45%
	5.9	85%
	6.3	95%
	7	100%

Table 34. Average recovery percentage of individual metals in SX with 0.5 M Cyanex 272 at an equilibrium pH value of 4.7.

Element	**Mg**	**Al**	**Fe**	**Mn**	**Co**	**Ni**
Recovery percentage	43.0%	12.2%	13.3%	96.3%	92.4%	10.8%

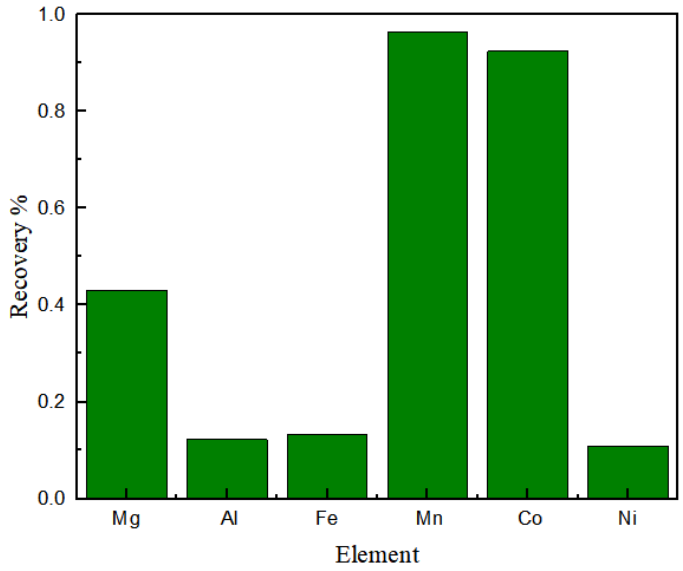

Figure 43. Recovery of metals in SX with Cyanex 272 at an equilibrium pH of 4.7.

5.6.3 Solvent extraction with an equilibrium pH at 4.7

To validate the test results' reproducibility, replicate tests were carried out under the conditions mentioned above with an equilibrium pH of 4.7. For all three tests performed, a raffinate solution was obtained with nickel contents varying between 120 and 133 mg/L, cobalt from 3.8 to 7.3 mg/L, and Mn from 2.1 to 7.1 mg/L. Additionally, some impurities, including Mg, Al, and Fe, remained in the raffinate solution with average concentrations of 20.8 mg/L, 11.4 mg/L, and 5.0 mg/L, respectively (Table 35 and Figure 44). The three experiments were compared by calculating the standard deviation of the concentration of main elements, where Ni had a standard deviation percentage equal to 5%, indicating a good repeatability of the replicate tests. Other elements, such as Co, Mn, and Mg, had higher standard deviations, corresponding to 32%, 46%, and 39%, respectively, but the concentration in the solution remained low, as shown in Table 6. Overall, the experiment successfully separated cobalt from nickel, generating an organic solution loaded with cobalt and a raffinate solution with nickel. The average elemental concentration of the raffinate solution is shown in Table 36.

Table 35. ICP-MS characterization (in mg/L) of the replicate SX tests developed at an equilibrium pH of 4.7 for the separation of cobalt from nickel.

Test	Mg	Al	Fe	Mn	Co	Ni
Test 1	32.3	12.7	4.8	7.1	4.0	120.1
Test 2	14.4	10.9	4.2	2.1	3.8	133.1
Test 3	15.7	10.6	4.1	4.1	7.3	122.3

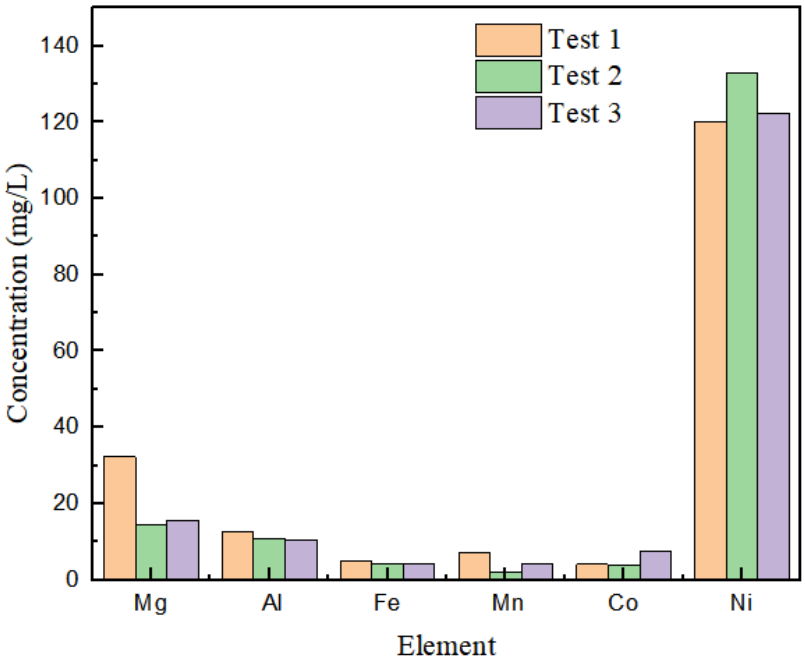

Figure 44. Concentration of the main elements in the three SX tests developed for the separation of Co from Ni.

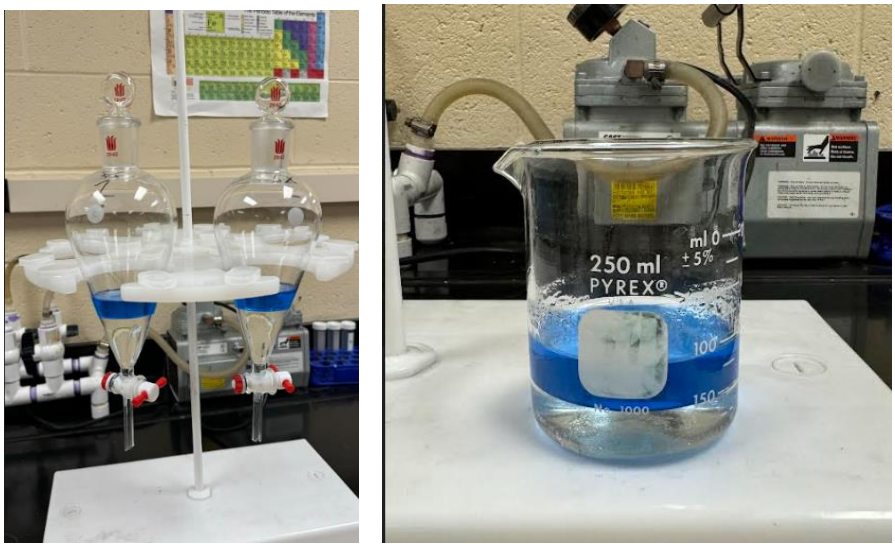

Figure 45. Cobalt extraction process with 0.5 M 50% saponified Cyanex 272.

Table 36. Average ICP-MS characterization of the Cyanex 272 SX-raffinate solution.

Element	Concentration (mg/l)
Na	32046.4
Mg	20.8
Al	11.4
Si	198.2
P	2.3
K	22.7
Ca	15.9
Ti	0.7
Cr	0.6
Fe	4.4
Mn	4.4
Co	5.0
Ni	125.2
Cu	0.2
Zn	1.1
Ga	0.1
Rb	0.1

5.6.4 Stripping of the loaded organic solution

The organic solution was subjected to a stripping process with 2M sulfuric acid (H_2SO_4) after solvent extraction. The experiment was carried out by mixing the organic solution with 2M sulfuric acid at an O: A ratio of 1:1 for 5 minutes at 600 RPM. During this stage, it was noticed the blue color of the organic solution changed to milky white, indicating the transfer of metals, especially cobalt, into the acid solution (Figure 46). The organic and aqueous solutions were then separated, and the new aqueous solution was analyzed by ICP-MS to determine its elemental composition. The new solution had a cobalt recovery of 82% from the organic solution, corresponding to a concentration of 52 mg/L. Manganese and zinc were also extracted into the sulfuric solution with a content of 95.5 mg/L and 106 mg/L, respectively. The data obtained allow it to determine whether solvent extraction was efficient in the separation of nickel from cobalt. However, the organic solution also carried other elements, which reduced the purity of the strip solution in terms of cobalt.

Figure 46. Stripping process developed for the extraction of cobalt from the loaded organic solution.

Table 37. Average ICP-MS characterization data of the stripping solution after SX.

Element	Concentration (mg/L)
Na	695.5
Mg	22.2
Al	12.7
Si	138.4
P	4.0
K	6.8
Ca	16.6
Sc	0.0
Ti	1.5
Cr	0.1
Fe	6.6
Mn	97.8
Co	52.2
Ni	3.0
Cu	0.3
Zn	122.3
Ga	0.4

Rb	0.1
W	0.2
Pb	0.1
TREE	4.8

5.6.5 Na_2S precipitation in the raffinate and stripping solution

During the solvent extraction process developed with Cyanex 272, two aqueous solutions with different critical mineral contents were generated, which were then subjected to precipitation with sodium sulfide (Na_2S) to obtain solid products of nickel and cobalt. As mentioned above, the raffinate solution had a main composition of nickel; the initial pH of the solution (i.e., 5) was raised until pH 10 where the solution became brown, and solids began to form. Solids were later removed by centrifugation and filtration, followed by ICP-MS and SEM-EDS characterization analyses (Figure 47). The other solution subjected to precipitation was the strip solution with Co and Mn. The solution pH was raised from an initial value of 0 to pH 5. During this process, solids started appearing in the solution, which were subsequently removed similarly to those generated in the raffinate solution.

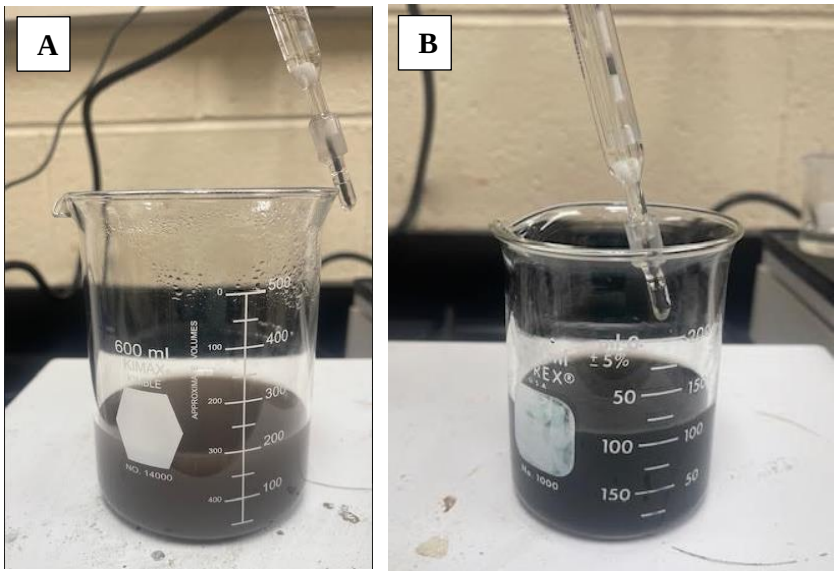

Figure 47. Na2S precipitation procedure applied in the raffinate solution at the pH range of 5 to 10 (A). Na2S precipitation procedure applied in the stripping solution at the pH range of 0 to 5 (B).

Table 38 and Figure 48 show the elemental compositions of the solids generated during each Na_2S precipitation process. According to Table 39, most of the critical minerals targeted by the process were precipitated. In the precipitation of the raffinate solution, 99.5% of the nickel was recovered with a nickel purity of 13.94 wt.%. The purity of other detected elements was all less than 1 wt.% except for silicon, which had a weight percentage of 2.56 wt.%. On the other hand, the precipitation of the stripping solution was unable to generate a cobalt product with a high purity even though 80% of the cobalt was recovered. The low-purity of cobalt, i.e., 0.4 wt. , could be attributed to factors such as the low amount of cobalt in the stripping solution and the presence of other elements such as silicon and zinc, which had a weight percentage of 0.83 wt. % and 1.47 wt.% in the precipitated solid, respectively.

Table 38. Elemental composition of the solids generated during Na2S precipitation of the raffinate and stripping solutions.

Sample	Concentration (mg/kg)			
	Solid raff	Wt. %	Solid strip	Wt. %
Li	56	0.01	0	0.00
Na	191,388	19.14	157,290	15.73
Mg	3,387	0.34	0	0.00
Al	140	0.01	105	0.01
Si	25,572	2.56	8,283	0.83
P	1,141	0.11	209	0.02
K	99	0.01	0	0.00
Cr	586	0.06	0	0.00
Fe	37	0.00	310	0.03
Mn	3,024	0.30	248	0.02
Co	5,875	0.59	3,920	0.39
Ni	139,438	13.94	158	0.02
Zn	0	0.00	14,655	1.47

Table 39. ICP-MS characterization of raffinate and stripping solutions after Na2S precipitation.

Element	Concentration (mg/L)	
	Raff after pre.	Stripping after pre.
Na	8,115.0	13,002.0
Mg	68.7	37.4
Al	11.0	12.3
Si	149.9	167.3
P	143.3	3.7
K	10.2	8.8

Ca	17.2	17.3
Sc	0.0	0.0
Ti	1.5	1.5
Cr	0.1	0.1
Fe	4.5	4.7
Mn	4.6	47.6
Co	0.1	0.7
Ni	2.6	0.7
Cu	0.3	0.2
Zn	1.9	1.9
Ga	0.3	0.3
Rb	0.1	0.1
W	0.2	0.2
Pb	0.1	0.2
TREE	3.3	3.7

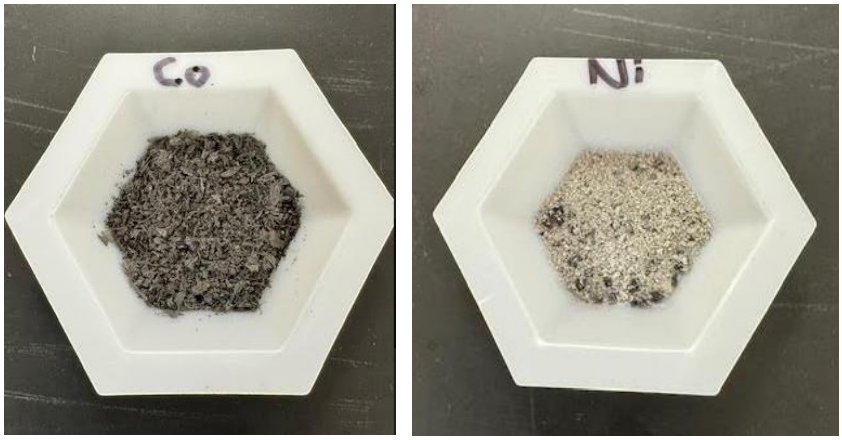

Figure 48. Co and Ni solid products obtained after Na2S precipitation procedures.

5.7 Solid product characterization

5.7.1 Manganese characterization

To obtain the in-depth characterization information on the products generated from the process, the manganese concentrate was subjected to XRD analyses to determine its mineralogy. Using JADE software, the diffraction pattern was compared with different Mn-containing minerals, and it was determined that the produced manganese product predominately exists as manganese oxides, i.e., MnO_2. The surface morphology of the Mn product is shown in Figure 50 through SEM analyses. The rough, layered surface can be seen from the micrographs. In addition, the fused edges between nucleated particles may result from the high temperature used during nitric acid washing, i.e., 75ºC.

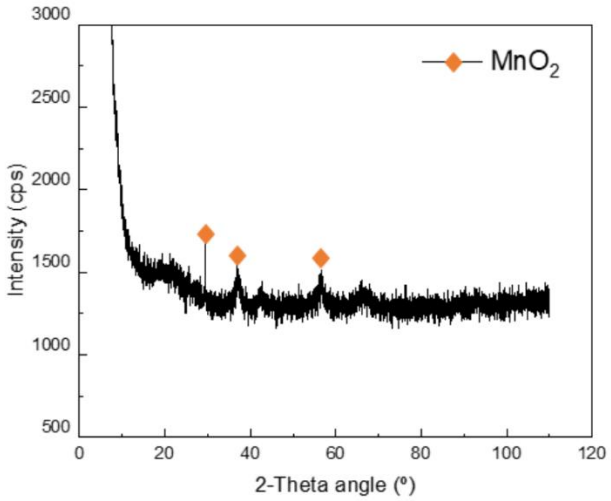

Figure 49. X-ray diffraction pattern of the Mn concentrate – XRD analyses.

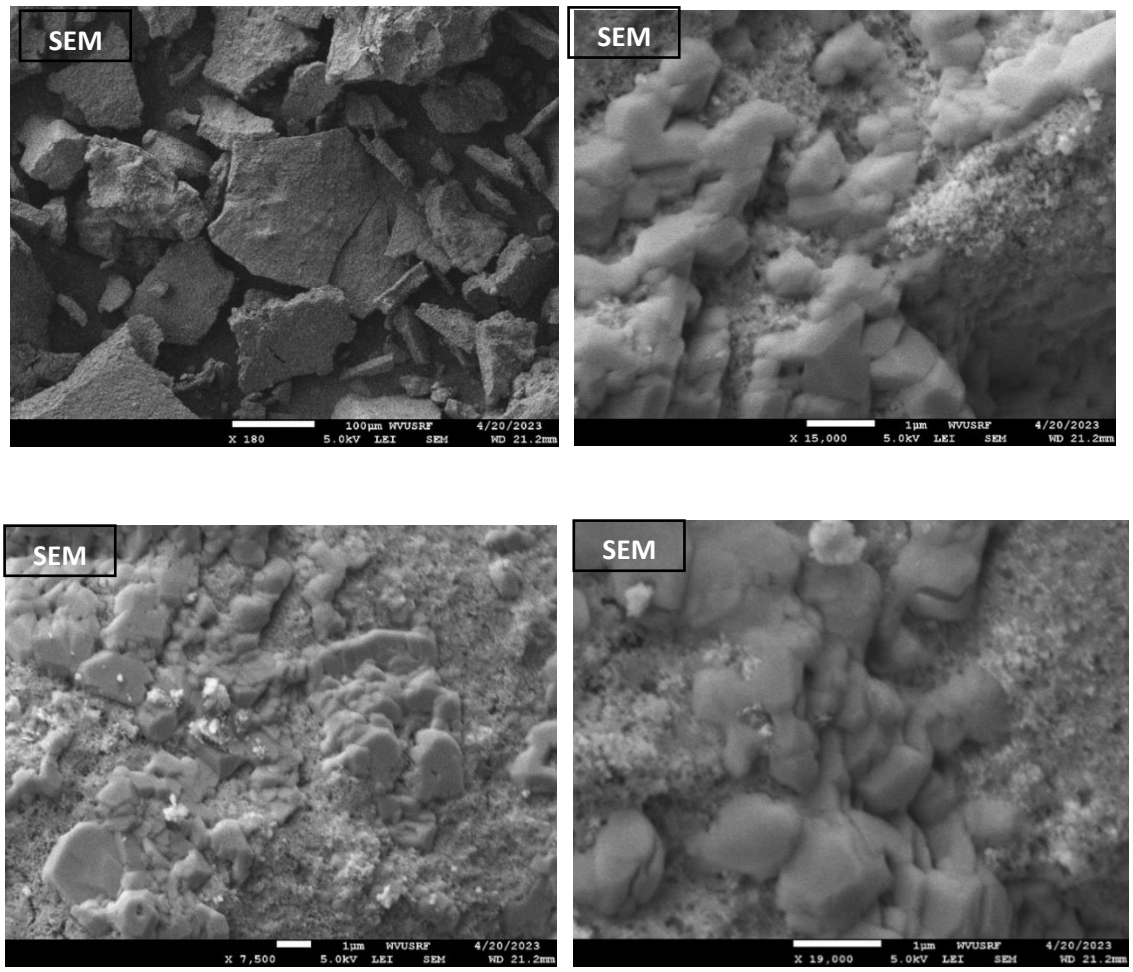

Figure 50. SEM characterization of Mn concentrates (47 wt.% purity) generated in nitric acid washing.

SEM-EDS analyses performed on the manganese sample produced during nitric acid washing reveals a mineral composition characterized by a significant oxygen content (28.18% by weight, 51.36% by atoms), suggesting the presence of oxygen-rich minerals, possibly oxides or silicates. Accounting for 52.68% by weight and 27.97% by atoms, manganese predominates in the composition, indicating the presence of minerals like rhodochrosite ($MnCO_3$) and pyrolusite (MnO_2) that contain manganese. Sodium and sulfur were also detected by the analysis, indicating the presence of sodium-bearing and sulfate minerals. Based on the results obtained from XRD and SEM analyses, it is likely that the predominant mineralogy of the manganese product generated in the process corresponds to MnO_2.

Table 40. Semi-Quantitative EDS analysis results of the Mn product with a purity of 47 wt.%.

Element	Weight %	Atomic %
O	28.18	51.36
Na	9.10	11.54
S	10.04	9.13
Mn	52.68	27.97

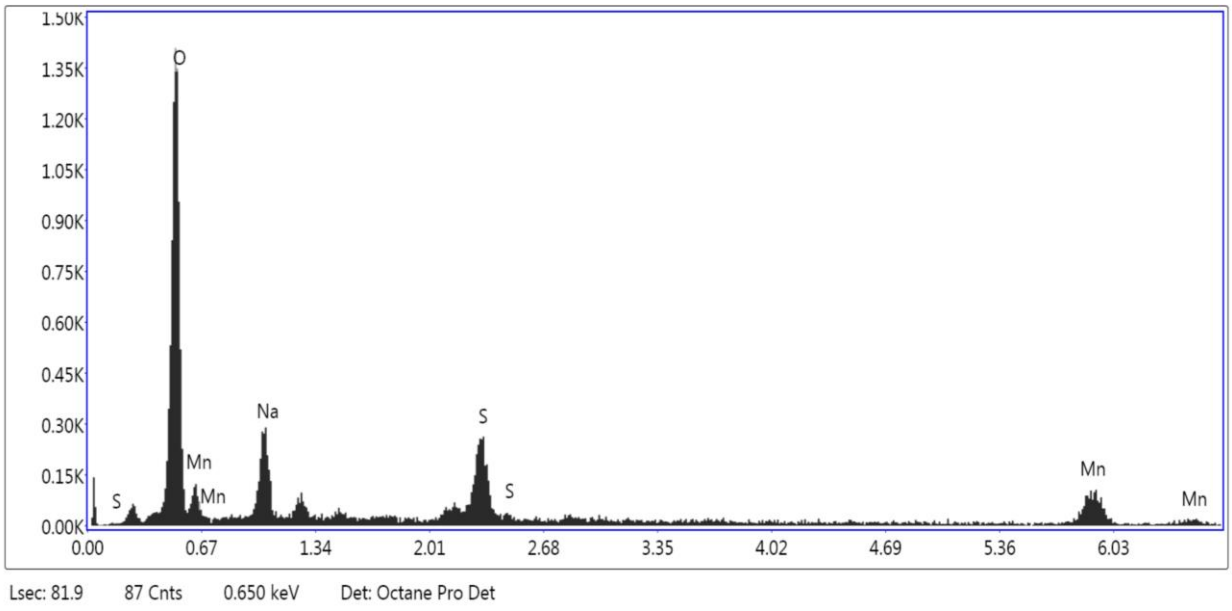

Figure 51. EDS spectrum of the manganese product with a purity of 47 wt.% generated during the nitric acid washing procedure.

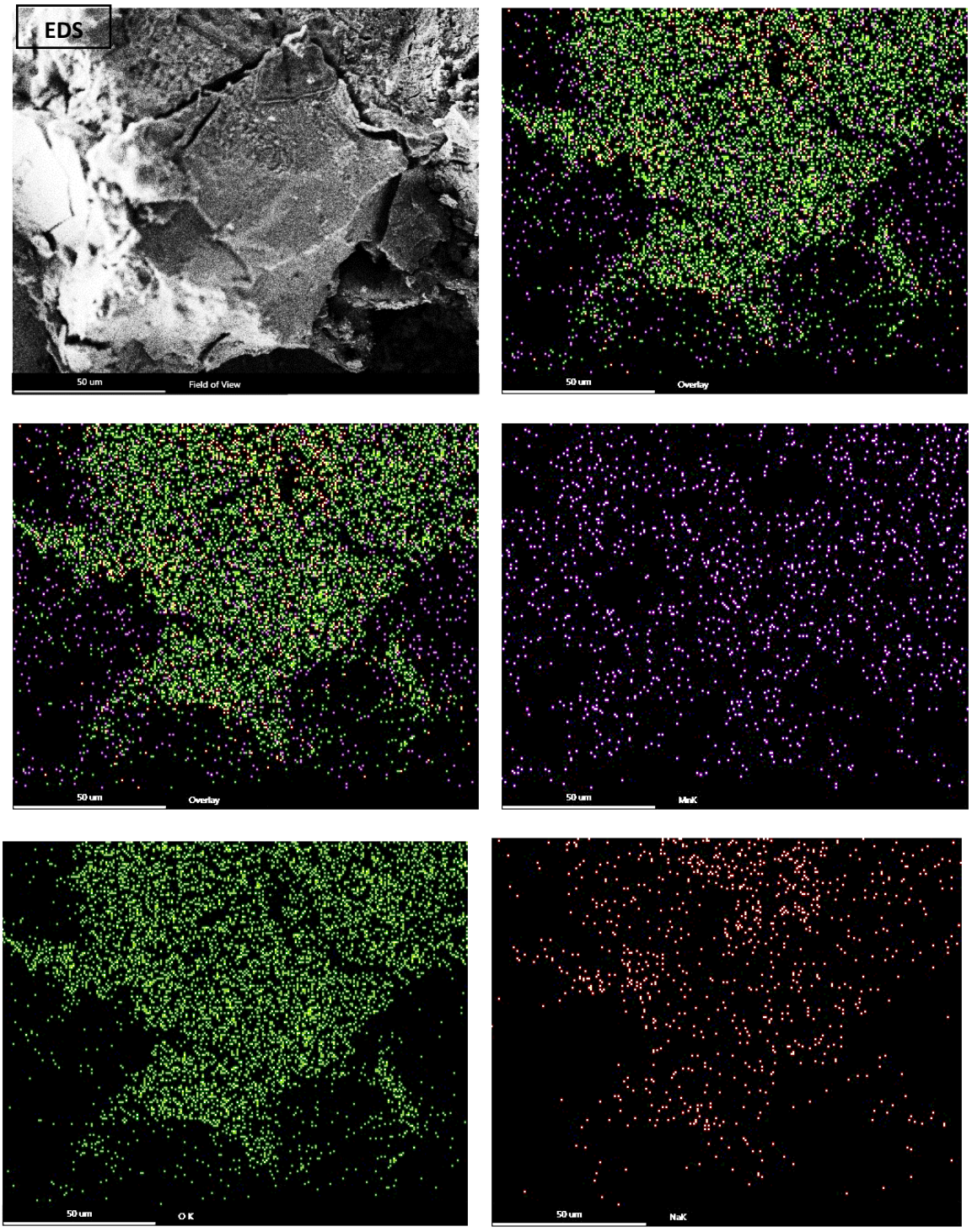

Figure 52. EDS mapping of the manganese product with a purity of 47 wt.% generated during the nitric acid washing procedure.

5.7.2 Nickel characterization

The 14 wt.% nickel sample produced through precipitating the raffinate solution of the Cyanex 272 solvent extraction process was also subjected to SEM-EDS analyses to gain insightful information. The product is mostly composed of sodium (Na) at a weight percentage of 23.70%. With a significant percentage of 15.67%, oxygen (O) is probably linked to silicates or oxides. The sample may also contain sulfides or chlorides, as indicated by the presence of sulfur (S) at 7.90 wt% and chlorine (Cl) at 27.05 wt%. The presence of 4.57 wt% nickel linked to the 15.67% oxygen suggests the presence of nickel silicates such as garnierite in the sample.

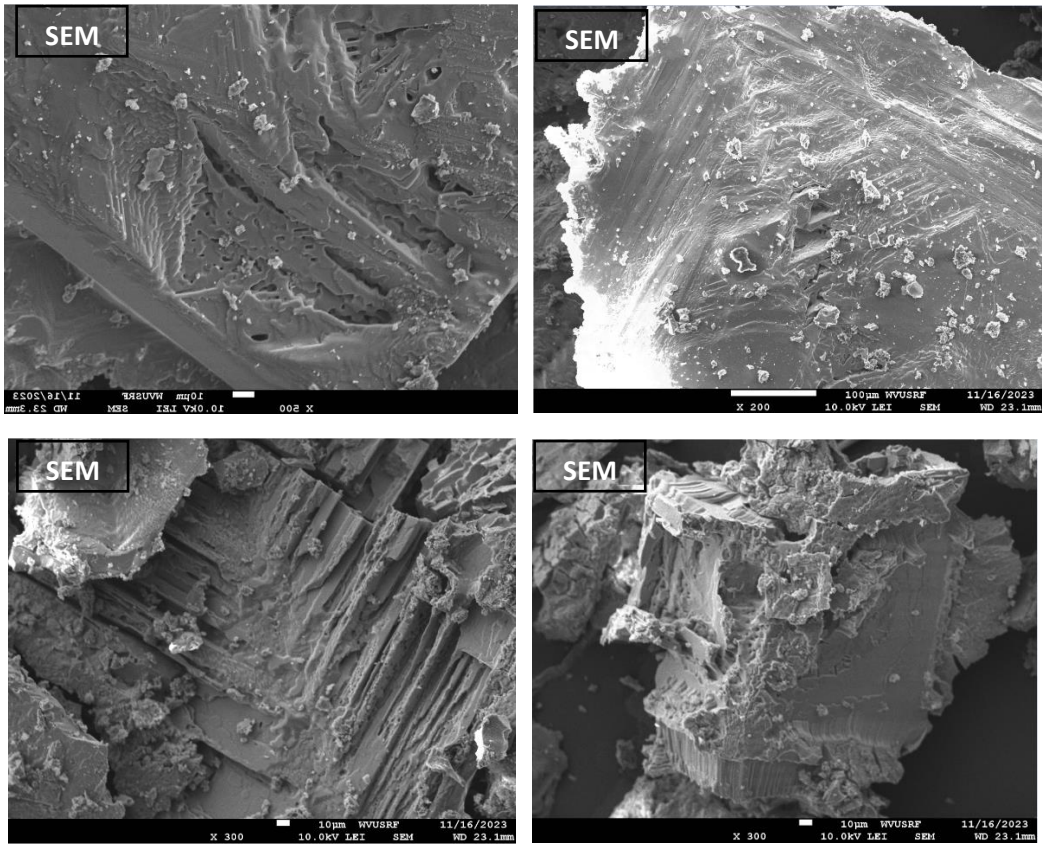

Figure 53. SEM characterization of Ni concentrates (14 wt.% purity) generated in Solvent extraction.

Table 41. Semi-Quantitative EDS analysis results of the Ni product with a purity of 14 wt.%.

Element	Weight %	Atomic %
C	21.12	36.21
O	15.67	20.17

Ni	4.57	1.60
Na	23.70	21.23
S	7.90	5.07
Cl	27.05	15.71

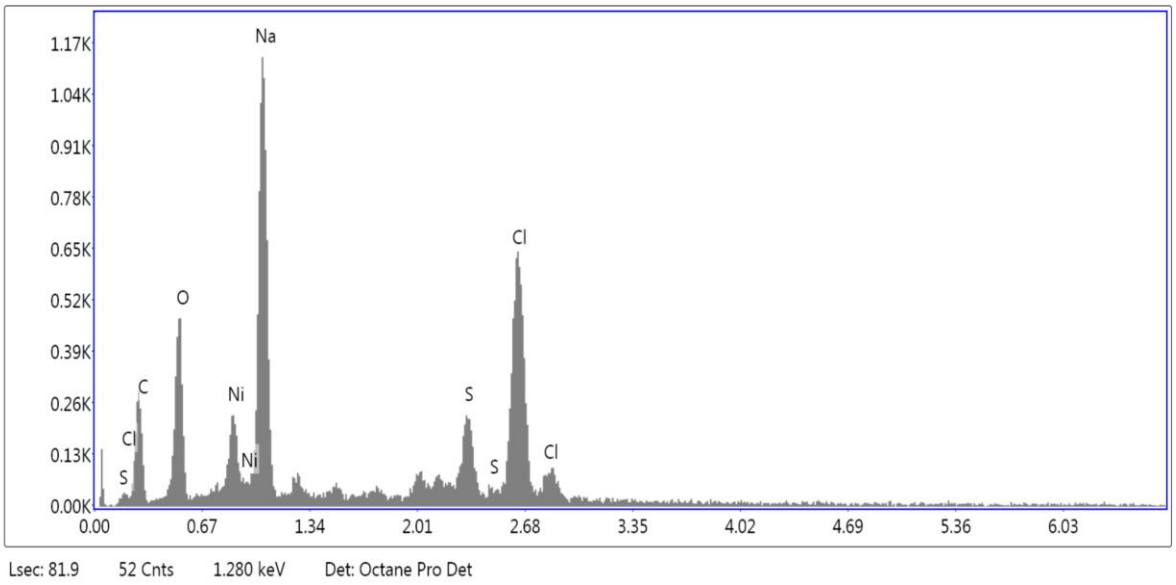

Figure 54. EDS spectrum of the Ni product with a purity of 14 wt.%

formed during the precipitation process performed in the SX-raffinate solution.

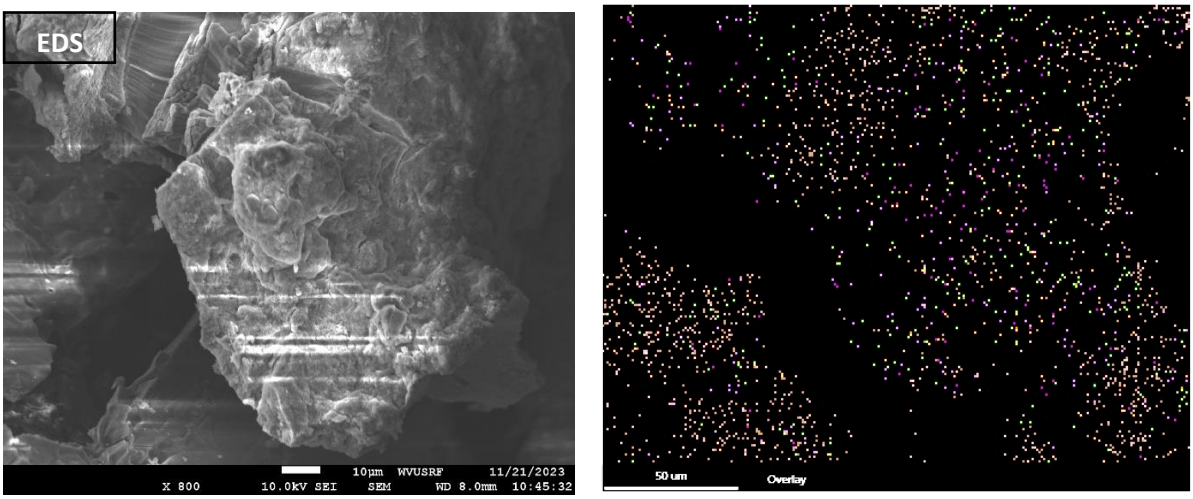

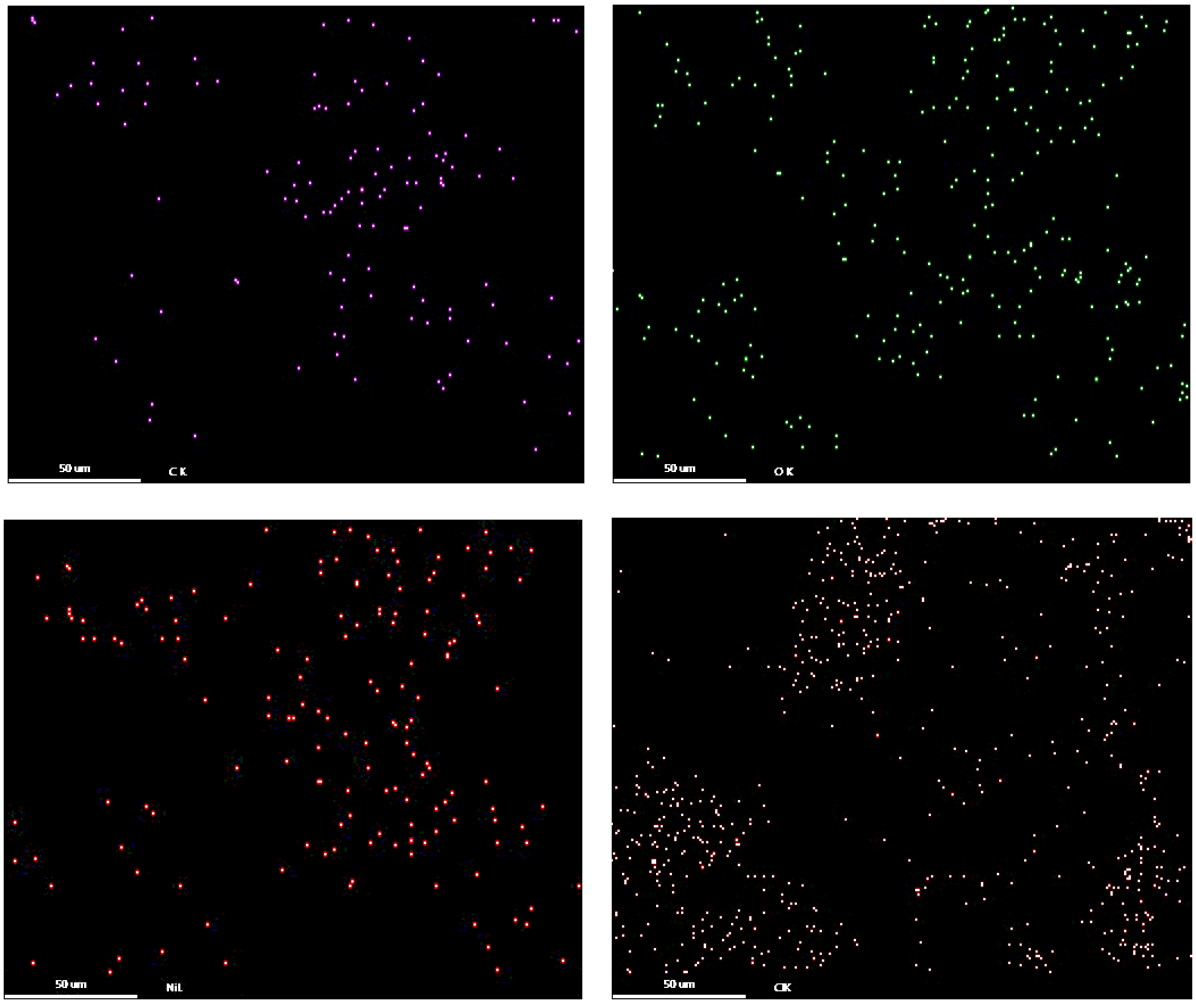

Figure 55. EDS mapping of the Ni product with a purity of 14 wt% formed during the precipitation process performed in the SX-raffinate solution.

6. SUMMARY, CONCLUSIONS AND SUGGESTIONS

6.1 Summary and conclusions

As mentioned at the beginning of this research, the main objective was to produce multiple critical minerals from the REE solvent extraction raffinate when an AMD treatment sludge was initially used as the feedstock. Initial characterization of all the unit process streams generated from REE extraction was conducted to identify the process stream with the highest concentrations of critical minerals, which was then used as the feedstock for the continuous extraction of manganese, cobalt, and nickel. The feedstock used throughout the study was the SX raffinate solution generated from REE solvent extraction with Di(2-ethylhexyl) phosphoric acid (DEHPA). By employing hydrometallurgical separation techniques, a process to selectively extract manganese, cobalt, and nickel was developed to achieve the target objectives of the research. The primary challenges identified in the study were the removal of impurities and their separation from critical minerals. The issue of handling impurities such as aluminum and iron has emerged in the process due to the efficiency and purity of the extraction processes being significantly impacted by the presence of these contaminant elements. On the other hand, the separation of different critical minerals was another significant challenge due to the fact that their chemical compositions are similar to each other. Cobalt, manganese, and nickel have similar reaction behaviors; therefore, they tend to group together in the extraction process. However, by combining detailed sample characterization with targeted separation techniques and process optimization, the impurities associated with critical minerals could be substantially reduced while enhancing the purity of the CMs. Thus, the selective extraction of manganese, cobalt, and nickel could be achieved.

To summarize the protocol established for recovering different CMs, the process began with staged NaOH precipitation, separating aluminum and iron at pH 5 followed by cobalt, manganese, and nickel separation at pH 10. The CM pre-concentrate was then washed to produce a high-purity manganese product, while cobalt and nickel were dissolved into a nitric acid solution. Subsequent staged precipitation with Na2S separated cobalt and nickel from the remaining manganese and magnesium by targeting three pH setpoints, i.e., pH 5, 10, and 12. Co-Ni solids obtained at pH 5 underwent HCl redissolution, and the dissolved solution was subjected to the solvent extraction process. Using 0.5M saponified Cyanex 272 in kerosene, cobalt was separated from nickel and impurities. The raffinate solution underwent Na2S precipitation to yield a solid nickel product. Simultaneously, the organic solution was stripped with 2M H2SO4 to remove cobalt, followed by a second Na2S precipitation for a solid cobalt product. The final products generated by the research were a manganese precipitate with a purity of 46.9 wt.%, a cobalt-nickel co-precipitate with a purity of 9.92 wt.% and 10.94 wt.%, respectively, and a Ni product with a purity of 13.94 wt.%. Additionally, other critical minerals were also obtained from the developed process, including 10.12 wt.% of aluminum, 27.6 wt.% of magnesium, and a secondary manganese product with a purity of 20.2 wt.%. Overall, the results and conclusions are summarized as follows:

1. Selective precipitation with sodium hydroxide (NaOH) is an efficient method for the separation of impurities such as aluminum, iron, and phosphorus from critical minerals, including manganese, cobalt, and nickel. However, a selective recovery of these elements is not feasible with this methodology.

2. Nearly 99% of aluminum, iron, and phosphorus in the raffinate solution were removed using 2M sodium hydroxide (NaOH) at pH 5. The solids precipitated at this pH had an aluminum purity of 10.12 wt.%, which, while classified as an impurity in this study, is a critical mineral according to the United States Geological Survey.

3. At pH 10, the recovery of manganese, cobalt, and nickel reached around 99%, generating a bulk concentrate of these elements, suitable for selective recovery of each element.

4. Nitric acid (HNO3) washing generated good results by dissolving elements selectively, such as aluminum, iron, magnesium, cobalt, and nickel, where approximately 95% of these elements were dissolved, and a solid product of manganese with a purity of 46.99 wt.% was generated.

5. XRD, SEM, and EDS analyses performed on the manganese product suggested that the solids produced had a predominant mineralogy of pyrolusite (MnO2), which corresponds to a manganese mineral purity equivalent to 74.35 wt.%.

6. Sodium sulfide (Na2S) precipitation can be used as an effective methodology to remove cobalt and nickel from manganese and magnesium in the nitric solution at alkaline pH values. Nearly all cobalt and nickel, up to 12% of manganese, and 6% of magnesium were precipitated at pH 5.

7. During sodium sulfide precipitation, additional critical minerals were generated by selective precipitation. At the pH range of 5 to 10, a second manganese product was generated with a purity of 20.14 wt.%, and between pH 10 and 12, a magnesium product with a purity of 27.5 wt.% was generated.

8. The solid product generated during the precipitation of cobalt and nickel was subjected to redissolution with 4M hydrochloric acid (HCl), where a nickel and cobalt product was generated with purities of 9.92 wt. % and 10.94 wt. %, respectively. In addition, the hydrochloric dissolution process generated a solution with 490 mg/L of nickel, 243 mg/L of cobalt, and 102 mg/L of manganese suitable for the subsequent recovery of cobalt and nickel.

9. Oxidative precipitation was tested to separate cobalt from nickel by injecting ozone (O3) into the solution, targeting the precipitation of cobalt while keeping nickel in the solution. Unfortunately, the process could not separate the elements, but it provided valuable information about this process and opened a way to explore this methodology in future research.

10. As a second alternative, solvent extraction with 0.5 M Cyanex 272 was tested with the solution generated by hydrochloric dissolution, which separated cobalt from nickel. The process was able to extract 92 % of the cobalt. However, 96% of the manganese remaining in the solution was co-extracted, along with 43% of magnesium. On the other hand, the SX raffinate solution kept 90% of the nickel without the presence of major impurities.

11. The loaded organic solution with cobalt, manganese, and magnesium was subjected to stripping with 2M sulfuric acid (H2SO4), where 82% of the cobalt was stripped, but the concentration of the element decreased significantly to a value of 52 mg/L.

12. Stripping and raffinate solutions generated from previous solvent extraction were subjected to precipitation with sodium sulfide, aiming for the selective precipitation of both elements. As a result, the raffinate solution generated a nickel product with a purity of 13.94 wt.%. However, the cobalt purity obtained from precipitating the strip solution was as low as 0.4 wt.%.

13. SEM-EDS analyses were performed on the nickel product with a purity of 13.94 wt.% to obtain in-depth information on its mineralogy. Based on the results obtained along with the ICP-MS characterization, it is likely that the solid produced corresponds to garnierite (Mg, $Ni)_3Si_4O_{10}(OH)_2 \cdot nH_2O$).

6.2 Recommendations and future work

- In the pursuit of optimizing the oxidative precipitation process, a multifaceted approach is essential. After examining crucial variables, including precipitation time, ozone injection time, and media acidity, the subsequent stage of optimization requires center efforts to optimize other variables, including precipitation pH and ozone rate. Optimizing ozone mass transfer efficiency through the system and identifying the separation pH of cobalt and nickel by investigating the impact of ozone concentration and conducting kinetic studies will provide an in-depth knowledge of oxidative precipitation kinetics. By evaluating these parameters, the oxidative precipitation process can be optimized to achieve cobalt and nickel separation from the solution generated by HCl dissolution.

- Despite the solvent extraction process having success in the separation of cobalt and nickel, the coextraction of manganese and magnesium into the organic phase poses a notable challenge in achieving high-purity cobalt precipitation. Multiple approaches can be investigated to improve the process. First, optimizing the extractant concentration in the organic phase could improve extraction selectivity, potentially reducing manganese coextraction. Another alternative is to focus on the stripping process by using selective stripping agents and testing variables such as the reagent concentration and extraction time to selectively remove cobalt from the organic solution, enhancing the efficiency of the process. By performing a deeper analysis of these variables, a reliable and selective separation of cobalt and nickel while minimizing issues related to manganese coextraction could be achieved.

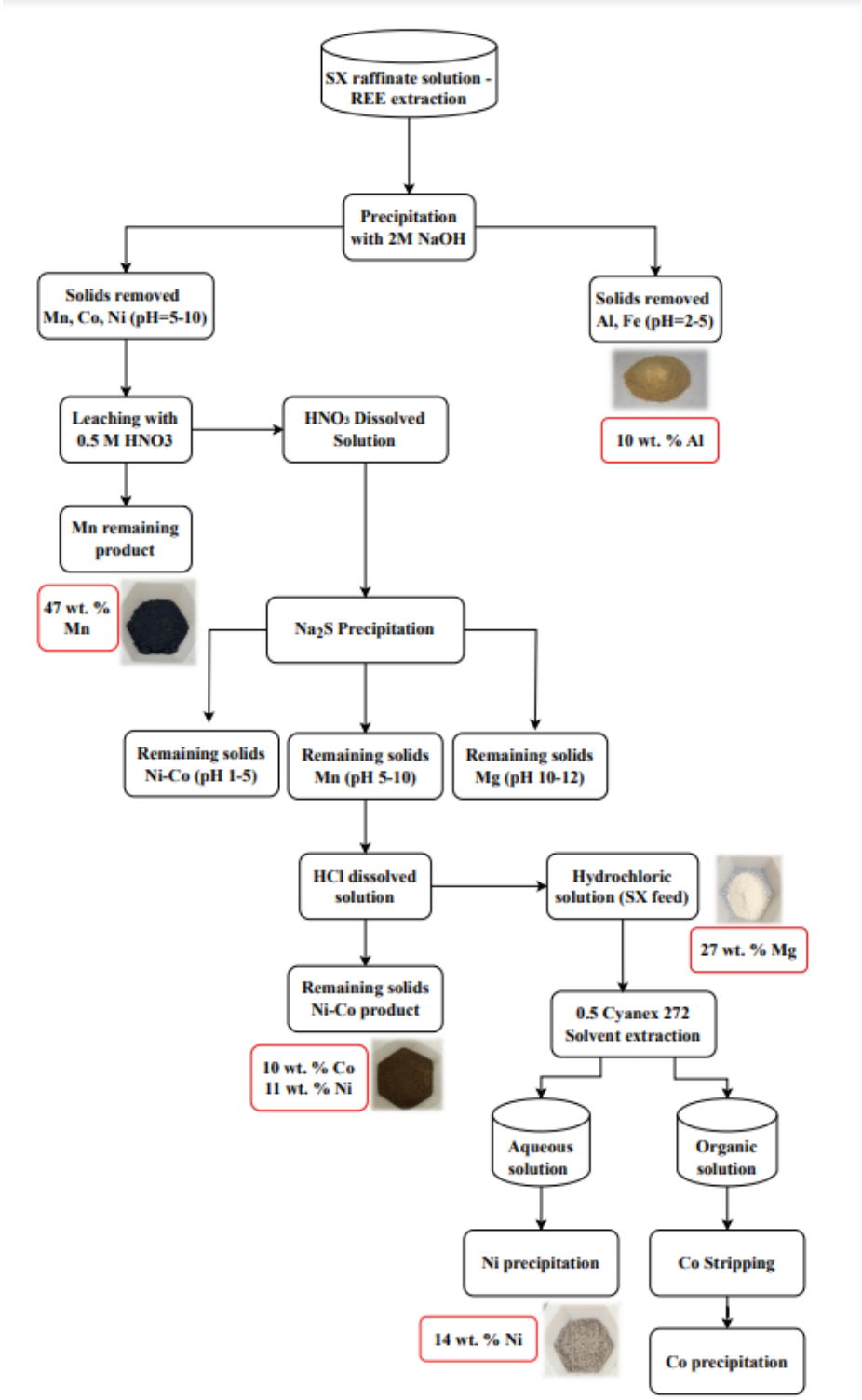

Figure 56. Experimental flowsheet designed for the selective recovery of CMs with final products included.

REFERENCES

- Alvial-Hein, G., Mahandra, H. & Ghahreman, A., 2021. Separation and recovery of cobalt and nickel from end of life products via solvent extraction technique: A review. *Journal of Cleaner Production.*

- Anon., n.d. *Atomic packing factor.* [Online] Available at: https://msestudent.com/atomic-packing-factor/

- Applegate, J. D., 2022. *2022 Final List of Critical Minerals,* s.l.: FEDERAL REGISTER.

- Barbanell, M., 2023. *World Resources Institute.* [Online] Available at: https://www.wri.org/insights/critical-minerals-us-climate-goals#:~:text=The%20country%20is%20100%25%20reliant,%25)%20and%20nickel%20(56%25).

- Basudev, S. et al., 2007. Hydrometallurgical process for recovery of cobalt from waste cathodic active material generated during manufacturing of lithium ion batteries. *Journal of Power Sources,* pp. 536-544.

- Borgohain, C., Acharyya, K., Sarma, S. & Phukan, P., 2013. A new aluminum-based metal matrix composite reinforced with cobalt ferrite magnetic nanoparticle. *Journal of Materials Science,* pp. 162-171.

- Boukerche, I. et al., 2010. Dissolution of Cobalt from CoO/Al2O3 Catalyst with Mineral Acids. *American Chemical Society,* p. 6514–6520.

- Brandt, G., 2023. *Cobalt.* [Online] Available at: https://www.britannica.com/science/cobalt-chemical-element

- Burton, J., 2022. *2022 list of critical minerals,* s.l.: USGS.

- Charles, J. A., Burroughs, C., Shewmon, P. G. & Lorig, C. H., 2023. *Britannica.* [Online] Available at: https://www.britannica.com/science/metallurgy/additional-info [Accessed 16 June 2023].

- Cheng, C. Y., 2006. Solvent extraction of nickel and cobalt with synergistic systems consisting of carboxylic acid and aliphatic hydroxy oxime.. *Hydrometallurgy,* pp. 109-117.

- Cheng, C. Y., 2006. Solvent extraction of nickel and cobalt with synergistic systems consisting of carboxylic acid and aliphatic hydroxyoxime. *Hydrometallurgy,* p. 109–117.

- Cicek, Z., Mira, A. A. & Huang, Q., 2023. Process development for the extraction of rare earth elements from an acid mine drainage treatment sludge. *Resources, Conservation and Recycling,* 198(107147).

- Cobalt-Institute, 2023. *Cobalt mining.* [Online] Available at: https://www.cobaltinstitute.org/about-cobalt/cobalt-life-cycle/cobalt-mining/#:~:text=Cobalt%20is%20mined%20across%20the,it%20into%20a%20usable%20form.

- Cobalt-Institute, 2023. *Types of deposits.* [Online] Available at: https://www.cobaltinstitute.org/about-cobalt/cobalt-deposits/

- Davey, R., 2021. *AZO life sciences.* [Online] Available at: https://www.azolifesciences.com/article/TEM-Imaging-Modes.aspx

- ELEMENTS, A., 2022. *AMERICAN ELEMENTS - The advanced materials manufacturer.* [Online] Available at: https://www.americanelements.com/cobalt-aluminum-alloy#:~:text=Primary%20applications%20include%20bearing%20assembly,step%20soldering%2C%20and%20radiation%20shielding.

- Elias, M., 2002. Nickel laterite deposits – geological overview, resources and exploitation. *Giant Ore Deposits: Characteristics, genesis and exploration,* pp. 205-220.

- Emmanuel, H., Charlène, B. & Gondia-Sokhna, S., 2021. *NICKEL IN THE ENERGY TRANSITION: WHY IS IT CALLED THE DEVIL'S METAL?.* [Online] Available at: https://www.ifpenergiesnouvelles.com/article/nickel-energy-transition-why-it-called-devils-metal

- Ewing, S., 2023. *Mineral Industry Surveys - COBALT IN JUNE 2023 ,* s.l.: USGS.

- Faraji, F., Alizadeh, A., Rashchi, F. & Mostoufi, N., 2020. Kinetics of leaching: a review. *Reviews in Chemical Engineering.*

- FUQUA, D. et al., 1986. *INVESTIGATION OF THE CHALLENGER ACCIDENT,* Washington D.C: U.S. GOVERNMENT PRINTING OFFICE.

- Garside, M., 2023. *Mine production of manganese worldwide in 2021, by country.* [Online] Available at: https://www.statista.com/statistics/1244066/global-manganese-production-volume-by-country/

- H. Sebnem Düzgün, N. L., 2018. Analysis of soma mine disaster using causal analysis based on systems theory (CAST). *Safety Science,* pp. 37-57.

- Hawkins, M., 1998. Recovering Cobalt from Primary and Secondary Sources. *Journal of Minerals, Metals and Materials Society,* pp. 46-50.

- Helmenstine, A., 2022. *Transition Metals Definition, List and Properties,* s.l.: s.n.

- Helmenstine, A. M., 2023. *What Are the Properties of the Alkaline Earth Metals?,* s.l.: s.n.

- Hitzman, M. W., Bookstrom, A. A., Slack, J. F. & Zientek, M. L., 2017. *Cobalt—Styles of Deposits and the Search for Primary Deposits,* Reston, VA: USGS.

- Hofstra, A. et al., 2021. *Deposit Classification Scheme for the Critical Minerals Mapping Initiative Global Geochemical Database,* Reston, Virginia: U.S. Geological Survey.

- Horn, S. et al., 2021. Cobalt resources in Europe and the potential for new discoveries. *Ore geology reviews,* p. Volume 131.

- Hualpa-Cutipa, E. et al., 2022. Recent trends for treatment of environmental contaminants in wastewater: An integrated valorization of industrial wastewater. *Integrated Environmental Technologies for Wastewater Treatment and Sustainable Development,* pp. 337-368.

- James Vaughan, W. H. D. W., 2011. Chemical aspects of mixed nickel-cobalt hydroxide precipitation and refining..

- Jingu Kang, G. S. J. S. S. M. S., 2010. Recovery of cobalt sulfate from spent lithium ion batteries by reductive leaching and. *Hydrometallurgy,* p. 168–171.

- Joule Bergerson, L. L., 2004. Life cycle analysis of power generation systems. *Encyclopedia of Energy,* pp. 635-645.

- Junwei Han, Y. W. X. M. X. C. H. Z. W. Q., 2022. Efficient extraction of nickel from sintered alloy by stepwise leaching: Thermodynamic and kinetic studies. *Minerals Engineering,* p. Volume 187.

- Karol Zglinicki, K. S. S. W., 2021. Critical Minerals from Post-Processing Tailing. A Case Study from Bangka Island, Indonesia. *Minerals.*

- Kim, J.-E., 2023. *Manganese Statistics and Information,* s.l.: USGS.

- Kim, J. H. & Gibb, H. J., 2006. *Cobalt and inorganic cobalt compounds,* Geneva: World health organization.

- Kislik, V. S., 2011. In: V. Kislik, ed. *Solvent Extraction: Classical and Novel Approaches.* Jerusalem: Elsevier.

- Klaus J. Schulz, L. G. W. S. W. N. R. R. S. I. N. M. P. V. W. C. a. J. L. M., 2014. *Occurrence model for magmatic sulfide-rich nickel-copper-(platinum-group element) deposits related to mafic and ultramafic dike-sill complexes,* Reston, VA: U.S. Geological Survey.

- Kuleshov, V., 2017. *Isotope geochemistry: The origin and formation of manganese rocks and ores.* Amsterdam : Elsevier Inc. .

- Li, Q. & Zhang, W., 2022. Process Development for Recovering Critical Elements from Acid Mine Drainage. Resources, Conservation & Recycling.. *Resources, Conservation and Recycling,* p. Volume 180.

- López, J., Gibert, O. & Cortina, J., 2021. Integration of membrane technologies to enhance the sustainability in the treatment of metal-containing acidic liquid wastes. An overview. *Separation and Purification Technology,* p. Volume 265.

- M. Cempel, G. N., 2006. Nickel: A Review of Its Sources and Environmental Toxicology. pp. 375-382.

- M.Hayes, S. & McCullough, E. A., 2018. Critical minerals: A review of elemental trends in comprehensive criticality studies. *Resources policy,* pp. 192-199.

- Mayerling Martineza, G. F. l. F. C. M. K. B. V. E. H., 2017. TEM analysis of the deformation microstructure of polycrystalline cobalt plastically strained in tension. *Materials Characterization,* pp. 76-83.

- McRae, M., 2023. *Nickel Statistics and Information,* s.l.: USGS.

- Michael Nicol, N. W. G. S., 2022. 4 - Solvent extraction. *Hydrometallurgy,* pp. 117-170.

- MICRESS, 2022. *MICRESS.* [Online] Available at: https://micress.rwth-aachen.de/#:~:text=MICRESS%C2%AE%2D%20the%20MICRostructure%20Evolution%20Simulation%20Software%20%2D%20is%20a%20software,transformations%2C%20especially%20in%20metallurgical%20systems.

- MRL, 2022. *MRL - Material Resources, LLC.* [Online] Available at: https://www.icmrl.net/pages/SliderPages/Slider_4HTP_MTR.html

- MSHA, 2022. *Fatality Reports,* s.l.: United States Department of Labor .

- MSHA, n.d. *DEPARTMENT OF LABOR UNITED STATES.* [Online] Available at: https://www.msha.gov/data-reports/fatality-reports/search?combine=&field_mine_category_tid=All&field_arep_fatal_date_value%5Bvalue%5D%5Byear%5D=&province=All&field_accident_classification_tid%5B%5D=24

- Mudd, G. M. & Jowitt, S. M., 2022. The New Century for Nickel Resources, Reserves, and Mining: Reassessing the Sustainability of the Devil's Metal. *Economic geology,* p. 1961–1983.

- Nanoscience, 2022. *Nanoscience Instruments.* [Online] Available at: https://www.nanoscience.com/techniques/scanning-electron-microscopy/#:~:text=A%20scanning%20electron%20microscope%20(SEM,the%20surface's%20topography%20and%20composition.

- NASA, 1986. *Rogers commission report,* Washington D.C: s.n.

- Nassar, N. T. & Fortier, S. M., 2021. *Methodology and Technical Input for the 2021 Review and Revision of the U.S. Critical Minerals List,* s.l.: U.S. Department of the Interior U.S. Geological Survey.

- Niaz Muhammad Shahani, M. J. S. I. M. J. B. U. A. R. Q., 2020. Comparative Analysis of Coal Miner's Fatalities by Fuzzy Logic. *Journal of Mining and Environment (JME),* pp. 77-87.

- Petty, T. R., 2018. *Final List of Critical Minerals 2018,* s.l.: Federal register.

- Pourret, O. & Faucon, M.-P., 2016. Cobalt. *Encyclopedia of geochemistry.*

- Project, T. M., 2020. *The Materials Project.* [Online] Available at: https://materialsproject.org/materials/mp-284

- Qasem, N. A., Mohammed, R. H. & Lawal, D. U., 2021. Removal of heavy metal ions from wastewater: a comprehensive and critical review. *Nature cities.*

- Qing-hua, T., Xue-yi, G., Yu, Y. & Zhi-hai, L., 2010. Kinetics of oxidation-precipitation of cobalt from solution by ozone. *Transactions of Nonferrous Metals Society of China,* pp. 42-45.

- R.E. Smallman, A. N., 2014. Characterization and Analysis. *Modern Physical Metallurgy,* pp. 159-250.

- R.W.Gaikwad, 2007. Acid Mine Drainage (AMD) Management. *Industrial Pollution Control,* pp. 285-297.

- Rodrigues, I. R., Deferm, C., Binnemans, K. & Riaño, S., 2022. Separation of cobalt and nickel via solvent extraction with Cyanex-272: Batch experiments and comparison of mixer-settlers and an agitated column as contactors for continuous counter-current extraction. *Separation and Purification Technology.*

- Roy, S., 1988. Manganese metallogenesis: A review. *Ore Geology Reviews,* pp. 155-170.

- Roy, S., 1992 . Environments and processes of manganese deposition. *Economic Geology,* pp. 1218-1236.

- Sadeghi, S. M., Helena, J. J. & Soares, M., 2020. A critical updated review of the hydrometallurgical routes for recycling zinc and manganese from spent zinc-based batteries. *Waste Management,* pp. 342-350.

- Savinova, E. et al., 2023. Will global cobalt supply meet demand? The geological, mineral processing, production and geographic risk profile of cobalt. *Resources, Conservation and Recycling.*

- Shedd, K., 2023. *Cobalt Statistics and Information,* s.l.: USGS.

- Skousen, J. et al., 2017. Review of Passive Systems for Acid Mine Drainage Treatment. *Mine Water Environment,* pp. 133-153.

- SOLVAY, 2017. *CYANEX® 272 Extractant,* s.l.: SOLVAY SA.

- Sun, S., Wang, S., Ye, Y. & Pan, B., 2019. Highly efficient removal of phosphonates from water by a combined Fe(III)/UV/co-precipitation process. *Water Research,* pp. 21-28.

- Talan, D., Huang, Q., Liang, L. & Song, X., 2022. Conceptual Process Development for the Separation of Thorium, Uranium, and Rare Earths from Coarse Coal Refuse. *MINERAL PROCESSING AND EXTRACTIVE METALLURGY REVIEW.*

- Teh C. Lo, M. B., 2003. Solvent Extraction. *Encyclopedia of Physical Science and Technology (Third Edition),* pp. 341-362.

- *The Challenger disaster.* 2013. [Film] Directed by James Hawes. s.l.: s.n.

- USGS, 2022. *MCS2022-Manganese,* s.l.: U.S. Geological Survey, Mineral Commodity Summaries.

- Venditti, B., 2022. [Online] Available at: https://www.visualcapitalist.com/the-50-minerals-critical-to-u-s-security/

- Venditti, B., 2022. *The 50 Minerals Critical to U.S. Security.* [Online] Available at: https://www.visualcapitalist.com/the-50-minerals-critical-to-u-s-security/

- Venditti, B., 2022. *Visual capitalist.* [Online] Available at: https://www.visualcapitalist.com/the-50-minerals-critical-to-u-s-security/#

- Venegas, E. L., Vilches Arenas, L. F., Fernandez Baco, C. & Arroyo Torralvo, F., 2023. Potential for water and metal recovery from acid mine drainage by combining hybrid membrane processes with selective metal precipitation. *Resources, Conservation & Recycling.*

- Wang, D.-Y.et al., 2010. Synthesis of Organo Cobalt-Aluminum Layered Double Hydroxide via a Novel Single-Step Self-Assembling Method and Its Use as Flame Retardant Nanofiller in PP. *American Chemical Society,* p. 14162–14169.

- Wensheng Zhang, C. Y. C., 2007. Manganese metallurgy review. Part II: Manganese separation and recovery from solution. *Hydrometallurgy,* pp. 160-177.

- Xin Sun, H. H. Z. L. F. Z., 2020. Insights into the global flow pattern of manganese. *Resources policy.*

- Xingfei Zhang, L. Z. Y. W. J. T. J. W. W. S. H. H. Y. Y., 2023. Selective separation of metals from wastewater using sulfide precipitation: A critical review in agents, operational factors and particle aggregation. *Journal of Environmental Management* .

- Xingxing Wang, A. W. W. Z. D. Z. C. W., 2022. Analysis of international nickel flow based on the industrial chain. *Resources Policy.*

- Youssef, G., 2022. Characterization of polymers. *Applied Mechanics of Polymers,* pp. 273-299.

- You, Z. et al., 2015. Extraction of manganese from iron rich MnO2 ores via selective sulfation roasting with SO2 followed by water leaching. *Hydrometallurgy,* pp. 225-231.

- Yuan, L. et al., 2022. Inhibition Role of Solvation on the Selective Extraction of Co(II): Toward Eco-Friendly Separation of Ni and Co. *ACS Sustainable Chem. Eng,* p. 1160–1171.

- Z.T Ichlas, M. M. A. M. J. V. A. S., 2020. Processing mixed nickel-cobalt hydroxide precipitate by sulfuric acid leaching followed by selective oxidative precipitation of cobalt and manganese. *Hydrometallurgy,* p. 105185.

- Zhang, W. & Cheng, C. Y., 2007. Manganese metallurgy review. Part I: Leaching of ores/secondary materials and recovery of electrolytic/chemical manganese dioxide. *Hydrometallurgy,* pp. 137-159.

- Zhang, W. & Honaker, R., 2020. Process development for the recovery of rare earth elements and critical. *Minerals Engineering.*

- Zheng, J. et al., 2022. Post-transition metal electrodes for sensing heavy metal ions by stripping voltammetry. *Advanced Materials Technologies.*

- Zhou, J. et al., 2020. Leaching kinetics of potassium and aluminum from phosphorus-potassium associated ore in HCl-CaF2 system. *Separation and Purification Technology,* p. Volume 253.

7. APPENDIX

Table 42. ICP-Ms characterization of the solution produced in the Oxidative precipitation with HCl and H_2SO_4.

H_2SO_4 dissolution			**HCl dissolution**		
Element	**Concentration (mg/l)**		**Element**	**Concentration (mg/l)**	
	Initial	**Final**		**Initial**	**Final**
Na	2422.2	20642	**Na**	2292.6	12274.8
Mg	310.4	230.8	**Mg**	297.8	283.8
Al	45.8	15.6	**Al**	34.8	12.6
Si	153.8	158	**Si**	150.2	151.2
P	2.2	2.2	**P**	1.8	1.4
K	5.8	15.4	**K**	5.4	9.6
Ca	18.2	23	**Ca**	20.4	17.8
Sc	0.004	0.004	**Sc**	0.004	0
Ti	0.2	0	**Ti**	0	0
V	0	0	**V**	0	0
Cr	0	0	**Cr**	0	0
Fe	1.6	0.8	**Fe**	1.6	1
Mn	208.8	120.2	**Mn**	191.8	158.4
Co	41.8	27.6	**Co**	39.4	32.8
Ni	66.6	44	**Ni**	62.8	47.6
Cu	0.4	89.2	**Cu**	0.4	1
Zn	51	50.4	**Zn**	47.2	38.2

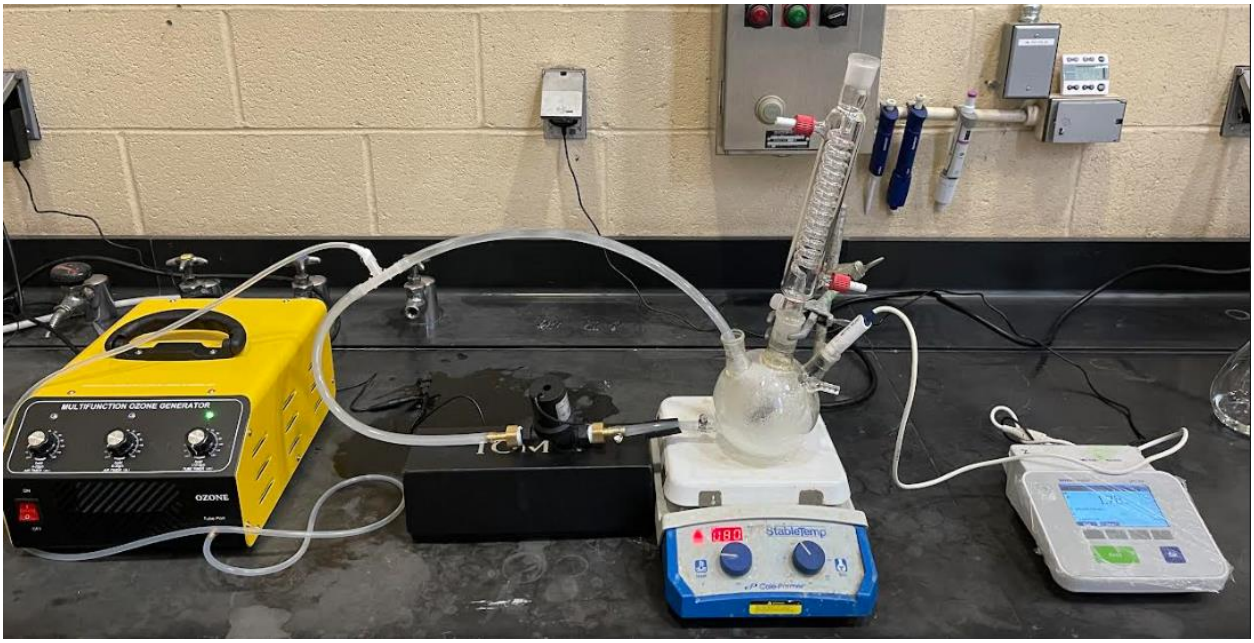

Figure 57. Set up for oxidative precipitation with ozone.